A STUDY OF ELECTRON SCATTERING MECHANISMS IN LEAD SULPHIDE AT LOW TEMPERATURES

A Thesis

presented by

Yet Chong Chan, B.Sc.

to the

University of St. Andrews

in application for the Degree

of Doctor of Philosophy

DECLARATION

I hereby certify that this thesis has been composed by me, and is a record of work done by me, and has not previously been presented for a Higher Degree.

The research was carried out in the Physical Laboratory of St. Salvator's College, in the University of St. Andrews, under the supervision of Dr. D.M. Finlayson.

(Yet Chong Chan)

CERTIFICATE

I certify that Yet Chong Chan, B.Sc., has spent nine terms at research work in the Physical Laboratory of St. Salvator's College, University of St. Andrews, under my direction, that she has fulfilled the conditions of Ordinance No. 16 (St. Andrews) and that she is qualified to submit the accompanying thesis in application for the Degree of Doctor of Philosophy.

Research Supervisor

CAREER

I first matriculated in the University of St. Andrews in October 1963. I studied Mathematics and Natural Philosophy, and obtained a 2nd Class 1st Division B.Sc. Honours in Natural Philosophy in 1966.

In October 1966, following the award of a University Research Scholarship, I was enrolled as a research student under Ordinance 12, and was transferred to Ordinance 16 in October 1967 as a candidate for the degree of Ph.D.

ACKNOWLEDGEMENTS

I wish to express my sincere thanks to my supervisor Dr. D.M. Finlayson for his patient guidance, encouragement and advice which greatly enhanced my understanding. I am also very grateful to Professor J.F. Allen, FRS for providing research facilities and his help and encouragement during my years in St. Andrews. My thanks are also due to the technical staff of the Physics Department, in particular to Mr. J. McNab for his help and co-operation in technical matters.

I would like to express my gratitude to St. Andrews University for a University Research Scholarship.

Abstract

This thesis reports a study of electron scattering mechanisms in lead sulphide by means of resistivity, thermoelectric and thermomagnetic effect measurements.

In Chapter I some general theory on transport phenomena in solids is discussed. In Chapter II, the theory of thermomagnetic and thermoelectric effects which are relevant to our measurements are summarized with emphasis on a discussion of scattering mechanisms for the Nernst effect measurements. In Chapter III we examine Kondo's theory of scattering by spin-spin interaction which gives rise to a ln T dependence of resistivity. Detailed derivations of the resistivity formulae are included to elucidate various points. The third and fourth chapters deal with the experimental details including calibration of thermometers.

The sixth and seventh chapters present and discuss the experimental results obtained. From these results we have found the following:

1. For low concentration n type PbS, Kondo type spin-spin interaction exists at temperature below about 30°K.
2. Both resistivity and Nernst effect measurements show that ionized impurity scattering is not the main scattering mechanism in the low temperature region.
3. Resistivity, thermoelectric power and Nernst effect measurements show that at temperatures above say 40°K acoustic lattice vibrations provide the major scattering mechanism.
4. A rapid change of thermoelectric power with temperature observed in some samples is attributed to phonon drag effects.

CONTENTS

CHAPTER V

Experimentation II - Measurements on Resistivity, Thermoelectric and Thermomagnetic Effects

CHAPTER VI

Discussion of Resistivity Measurements

CHAPTER I

Transport Phenomena in Solid

1.1 Introduction

In this chapter we want to discuss some general theory on transport phenomena in solids. Firstly we will review various relevant phenomena and then we will go on to consider the Boltzmann transport equation and its application to the quantitative study of electrical, thermoelectric and thermomagnetic effects. A short review of various scattering mechanisms is also included in this chapter.

1.2 Thermoelectric and Thermomagnetic Phenomena

1.2.1 Thermoelectricity: When a temperature gradient is applied to a conductor, this produces not only an energy flow (i.e. the heat flow) but also an electric current. There are several macroscopic phenomena within the scope of thermoelectricity. I only mention those related to my measurements.

(1) Seebeck effect, and thermoelectric power

Take two different kinds of conductors to form a circuit as shown in Fig. 1-1. If we maintain the two junctions at temperature T_o and T_o+T, then there will be a current flow if the circuit is closed. If the voltage across CD is V, then

$$\lim_{T \to o} \frac{V}{T} = \left(\frac{V}{T}\right)_{\text{at } T=0} = \textcircled{H}_{1,2}$$

defines the thermoelectric power (or differential Seebeck e.m.f.) of the pair of conductors I and II.

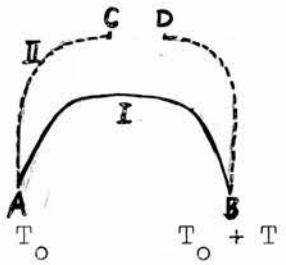

Fig. 1-1

The absolute thermoelectric power of a single material is defined as (from Fig 1-2) $\textcircled{H} = {}^{\Delta V}/_{\Delta T}$.

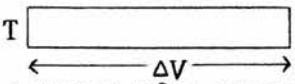

Fig. 1-2

It was found that the thermoelectric power of a super-conductor is zero. So to find the absolute thermoelectric power of a conductor, we can use a superconducting material II together with the material I for which we want to find the thermopower. The thermopower of a semi-conductor is usually much greater than that of a metal, so that in practice we use a metal and the semiconducting material which we want to investigate to form the circuit.

Consider the circuit in Fig. 1-1 (p.1) to be formed by a material II which has zero thermopower and conduction in I is by electrons. Then if B is at higher temperature than A, electrons will tend to diffuse from B to A. After some time the electron concentration at A will be greater than that at B, and so an electric field is set up directed from B to A to prevent electrons from further diffusion. It is this field which gives the potential difference across CD. If CD is shorted, electrons would flow from A via CD back to B (i.e. current i from D to C). Thus with negative charged carriers the hot junction becomes positive and the cold junction negative. We say that the thermoelectric power has a negative sign when this polarity is observed.

(2) Thermal Conductivity

Thermal conductivity is a measure of the transport of energy when a temperature gradient is set up. If the quantity of heat ω flows through a unit cross section in unit time when a temperature gradient dT/dX is applied, the thermal conductivity λ is given by $\omega = \lambda \frac{dT}{dX}$.

The heat flux is contributed by:

1. the part carried by the electrons or holes and

2. the part carried by lattice vibrations, usually the accoustic phonons.

In pure semiconductors, the major contribution to the thermal conductivity comes from phonons. For heavily doped or impure semiconductors both contributions may be comparable in magnitude.

1.2.2 Thermomagnetic effects : These are effects which appear in metals or semiconductors when a temperature gradient and a magnetic field are applied to the materials at the same time. Thermomagnetic effects are similar to magnetoelectric phenomena. There are several named effects.

1. Nernst Effect

Set up a temperature gradient in the X direction and a magnetic field in the z direction, (there being no temperature gradient in the y direction or electric current in any direction), then

(a) The transverse Nernst effect is the appearance of a potential difference in the y direction. To see the physical origin of this effect, we examine Fig. 1-3. Suppose the current carriers are electrons, then electrons with a drift velocity V_x will move along the negative x direction from A to B. The two ends of the sample are not electrically connected. Therefore after the transient period, the number of hot electrons drifting from the hot to the cold end is equal to the number of cold

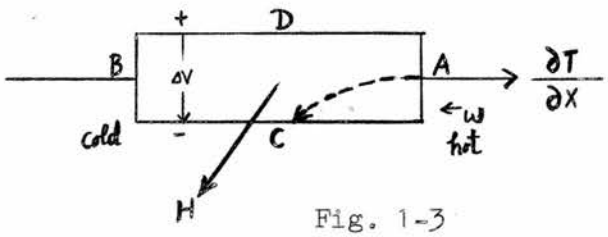

Fig. 1-3

electrons drifting from the cold to the hot end, so that a dynamical equilibrium is set up and the current $I_x = 0$. By this time, there should be accumulation of electrons on the surface C due to the deflection of the unbalanced drift of electrons caused by the magnetic field before $I_x = 0$. Now after the steady state with $I_x = 0$ has been established, we still have both hot and cold electrons drifting in opposite directions along the crystal and hence they are deflected by the magnetic field. But there are as many cold electrons deflected to one side as there are hot electrons deflected to the other side. Hence no further net accumulation of charges on any of the two sides of the crystal occurs. Furthermore the electrons already accumulated on surface C during the transient period would disappear as well because there seems to be nothing to balance their mutual electrostatic repulsion. However it is an experimental fact that there is potential difference between C and D. It is apparent that there must be something wrong with the above argument. The error in the above argument lies in the fact that the amount of deflection of an individual electron is not solely determined by its drift velocity, i.e. not solely determined by the Lorentz force. It also depends on the length of time the electron is subjected to the force. This time may be taken to be the relaxation time τ of the electron. The relaxation time is energy dependent. This means that hot electrons will have a τ_{hot} different from τ_{cold} of cold electrons. Hence although they have the same drift velocity, they are deflected by different amounts depending on the scattering mechanism and so a net accumulation of charge on one side would therefore appear. This explains the

appearance of the transverse Nernst effect.

The transverse Nernst coefficient $Q^{\perp}$ is defined as

$$E_y = Q^{\perp} H_z \frac{\partial T}{\partial X}$$

The sign of the effect is chosen as follows: Using a right-hand system of coordinates, a transverse effect is regarded as positive if a positive temperature gradient along the x axis and a magnetic field along the z axis produce an electric field E_y along the y axis. The sign of the transverse Nernst effect is independent of the carrier sign.

(b) The longitudinal Nernst effect is the change of thermo-electric power in a magnetic field from the zero field value. The longitudinal Nernst coefficient Q^{11} is defined as

$$E_x(H) - E_x(0) = E_x = -\frac{\partial V}{\partial X} = [\textcircled{H}(H) - \textcircled{H}(0)]\frac{\partial T}{\partial X} = Q^{11}\frac{\partial T}{\partial X}$$

The effect is positive if the absolute value of the thermoelectric field $E_x(0)$ increases in a magnetic field, i.e. $|E_x(H)| - |E_x(0)| > 0$.

2. Ettingshausen Effect

A temperature gradient is applied along the x direction of the sample. If we pass an electric current through the sample in the same direction and apply a magnetic field in the z direction, then it is found that a heat flow is set up in the y direction; if the faces are thermally insulated, a temperature gradient is set up. This is called the Ettingshausen effect.

It is found that the temperature gradient dT/dy is linearly proportional to H_z and I_x, and the Ettingshausen coefficient P is defined by $dT/dy = P H_z I_x$

1.3 Boltzmann Transport Equation and its Applications

The method of dealing with transport problem is in general to set up the transport equation and solve for the distribution function f before we can find out the current flow or heat flow. The Boltzmann transport equation under electric field $\underline{E}$ and magnetic field $\underline{H}$ is given by

$$\underline{V}_k \cdot \nabla f + e[\underline{E} + \frac{1}{c}(\underline{V}_k \times \underline{H})] \nabla_p f = [\frac{\partial f}{\partial t}]_{\text{scattering}} \quad (1\text{-}3\text{-}1)$$

Scattering changes the $\underline{k}$ value of carriers and causes transition from $\underline{k}$ to $\underline{k}'$ and conversely from $\underline{k}'$ to $\underline{k}$. The rate of change of the distribution function $f_{\underline{k}}$ is given by

$$[\frac{\partial f_{\underline{k}}}{\partial t}]_{\text{scattering}} = \int \{ f_{\underline{k}'}(1 - f_{\underline{k}}) - f_{\underline{k}}(1 - f_{\underline{k}'}) \} \, Q(\underline{k}\,\underline{k}') d^3\underline{k}' \quad (1\text{-}3\text{-}2)$$

where $Q(\underline{k}\,\underline{k}')$ is the transition probability measuring the transition rate when $\underline{k}$ is occupied and $\underline{k}'$ empty and vice versa.

If we assume that the external forces do not greatly alter the equilibrium distribution function $f_{\underline{k}}^{\circ}$ i.e. $f_{\underline{k}} - f_{\underline{k}}^{\circ} \ll f_{\underline{k}}^{\circ}$ where $f_{\underline{k}}$ is the perturbed distribution function and $\underline{V}_k$ is the velocity of electron in state $\underline{k}$, then a relaxation time τ can be defined to be

$$[\frac{\partial f}{\partial t}]_{\text{scattering}} = - \frac{(f - f^{\circ})}{\tau(\underline{k})}$$

we also assume that the change of the distribution function is of form

$$f - f^{\circ} = \underline{V}_k \cdot \chi(\underline{r}, \underline{k}) \quad (1\text{-}3\text{-}3)$$

where χ defined by this equation, gives the departure of the system from equilibrium. So $[\frac{\partial f}{\partial t}]_{\text{scattering}} = - \frac{f - f^{\circ}}{\tau(\underline{k})} = - \frac{\underline{V}_k \cdot \chi}{\tau(\underline{k})}$ (1-3-4)

The transport equation (1-3-1) becomes

$$\underline{V}_k \cdot \nabla f + e[\underline{E} + 1/C\ (\underline{V}_k \times \underline{H})] \nabla_{\underline{P}} f = -(f - f^\circ)/\tau \qquad (1\text{-}3\text{-}5)$$

Substituting equation (1-3-3) into (1-3-5) with

$$f = 1/(e^{\frac{\varepsilon_k - \mu}{kT}} + 1) \text{ and } \underline{V}_k = (1/\hbar)\frac{\partial \varepsilon(\underline{k})}{\partial k} = \underline{P}/m$$

and neglecting the small quantities $\underline{E} \cdot \chi$, $\nabla T \chi$ and $\nabla \mu \chi$, we obtain an equation for χ

$$\chi + (e\tau/C)(H \times m^{-1}\chi) = \chi_o \qquad (1\text{-}3\text{-}6)$$

where $$\chi_o = \{-e\underline{E} + (T\frac{\partial}{T}(\frac{\mu}{T}) + \varepsilon)\nabla T\}\tau \frac{\partial f^\circ}{\partial \varepsilon}$$

m is the effective mass, μ is the chemical potential.

The solution for equation (1-3-6) with spherical energy surface ($\varepsilon = P^2/2m$) is

$$\chi = -\frac{\chi_o + \beta(\chi_o \times \underline{H}_o) + \beta^2 \underline{H}_o(\chi_o \cdot \underline{H}_o)}{1 + \beta^2} \qquad (1\text{-}3\text{-}7)$$

where $$\underline{H}_o = \underline{H}/H \;,\; \beta = e\tau H/mc$$

The electric current j and heat flow W_e are given by

$$j = e\int \underline{v}\, dn, \qquad W_e = \int \varepsilon \underline{v}\, dn$$

where dn is the number of carriers per unit volume in coordinate space given by $dn = f(2/h^3)dP$, where $(2/h^3)dP$ is the no of states per unit volume in momentum space, and from equation (1-3-3) we have

$$j = (2e/h^3)\int \underline{V} f\, dP = (2e/h^3)\int \underline{V}(\underline{V} \cdot \underline{\chi})\, d\,P \qquad (1\text{-}3\text{-}8)$$

$$W_e = (2/h^3)\int \varepsilon \underline{V} f\, dP = (2/h^3)\int \varepsilon \underline{V}(\underline{V} \cdot \underline{\chi})\, dP \qquad (1\text{-}3\text{-}9)$$

f° being the distribution function in equilibrium which has no contribution to j or W_e. Substituting the value of χ in (1-3-7) into (1-3-8) and (1-3-9) we obtain the general expression for current and heat flow.

$$j = e^2 I_{10}\underline{E}' - eI_{11}\nabla \ln T + \{(e^2 I_{20}\underline{E}' - eI_{21}\nabla \ln T) \times \underline{H}_o\}$$
$$+ \underline{H}_o\{(e^2 I_{30}\underline{E}' - eI_{31}\nabla \ln T)\,\underline{H}_o\} \qquad (1\text{-}3\text{-}10)$$

$$W_e = e I_{11}\underline{E}' - I_{12}\nabla \ln T + \left\{(e I_{21}\underline{E}' - I_{22}\nabla \ln T)\times \underline{H}_o\right\} + \underline{H}_o\left\{(e I_{31}\underline{E}' - I_{32}\nabla \ln T)\underline{H}_o\right\} \quad (1\text{-}3\text{-}11)$$

where $\underline{E}' = \underline{E} - (T/e)\nabla(\mu/T)$ (1-3-12)

$$I_{ij} = \frac{8\pi}{3h^3}\left(\frac{eH}{C}\right)^{i-1}\int_0^\infty P^3\left(\frac{\tau}{m}\right)^i \varepsilon^j \frac{df_o}{dP}\frac{dP}{1+\beta^2} \qquad i=1,2,3. \quad (1\text{-}3\text{-}13)$$

with $\beta = e\tau H/mC$

Now let us interpret various terms appearing in the above equation (1-3-10)

(1). The first term $e^2 I_{10}\underline{E}'$ is the current along the direction of $\underline{E}'$, produced by the electric field $\underline{E}$ and the chemical potential gradient. From equation (1-3-12)

$$\nabla(\mu/T) = \mu\nabla(1/T) + 1/T(\nabla\mu) = -(\mu/T^2)\nabla T + 1/T(\nabla\mu)$$

The chemical potential gradient is usually very small in practice and also the temperature gradient inside the sample is negligible if no external temperature gradient is applied. Then $\underline{E}' = \underline{E}$ which is the external electric field, and $e^2 I_{10}$ will just be the usual conductivity σ in the absence of magnetic field

$$\sigma = e^2 I_{10} = e^2\frac{8\pi}{3h^3}\int_0^\infty P^3\left(\frac{\tau}{m}\right)\frac{df_o}{dP}\,dP = e^2\frac{8\pi}{3h^3}\int_0^\infty P^4\left(\frac{\tau}{m^2}\right)\frac{df_o}{d\varepsilon}\,dP$$

$$= \frac{8\pi e^2}{3h^3}\int v_{\underline{k}}^2\tau\frac{df_o}{d\varepsilon}\frac{dP_x dP_y dP_z}{4\pi} = \frac{e^2}{12\pi^3}\int v_{\underline{k}}^2\tau\frac{df_o}{d\varepsilon}\,d^3k \quad (1\text{-}3\text{-}14)$$

(2). The second term $e I_{11}\nabla \ln T = e I_{11}(1/T)\nabla T$ is the thermoelectric current along the temperature gradient. Without magnetic field, it gives the usual Seebeck thermoelectric current. When a magnetic field is applied, it then just gives the longitudinal Nernst effect.

(3). The third term $(e^2 I_{20}\underline{E}' - eI_{21}\nabla \ln T)\times \underline{H}_o$ where $\underline{H}_o = \underline{H}/H$ represents the Hall and the Nernst-Ettingshausen current flowing at right angles to the electric and magnetic field or temperature gradient and magnetic field. To examine the behaviour in a magnetic field, we write down the coefficients I_{20} and I_{21}

$$I_{20} = \frac{8\pi}{3h^3}\left(\frac{eH}{C}\right)\int_0^\infty P^3\left(\frac{\tau}{m}\right)^2 \frac{df_o}{dP}\,\frac{dP}{1+(e\tau H/mC)^2}\quad ;$$

$$I_{21} = \frac{8\pi}{3h^3}\left(\frac{eH}{C}\right)\int_0^\infty P^3\left(\frac{\tau}{m}\right)^2 \varepsilon\,\frac{df_o}{dP}\,\frac{dP}{1+(e\tau H/mC)^2}$$

If magnetic field is weak, we may neglect $\beta = e\tau H/mC$ in the integrals. Then the bracket terms increase linearly with H. In the strong magnetic field case, $\beta \gg 1$, we may write $1+(e\tau H/mC)^2 \approx (e\tau H/mC)^2$. Hence the bracket term decreases as $1/H$.

(4). The fourth term $\underline{H}_o\left\{(e^2 I_{30}\underline{E}' - eI_{31}\nabla \ln T)\right\}\underline{H}_o$ is the current along the magnetic field; it disappears when the magnetic field is normal to the electric field and the temperature gradient. From the coefficients I_{30} and I_{31}, it is proportional to H^2 in weak field and approaches a fixed limit under strong magnetic field.

From equations (1-3-10) and (1-3-11), both j and W_e are linearly dependent on the temperature gradient ∇T. This is consistent with the phenomenological law which states that the flux, eg the current j, is linearly proportional to the force (for example temperature gradient ∇T etc.) But this result was obtained under two assumptions:

〈1〉 The temperature gradient ∇T is not too great, so that in the calculation of j and W_e, the products involving ∇T and small quantities

such as χ can be neglected.

(2) The temperature gradients are assumed to be constant and that the sample is uniform.

1.4 Scattering Mechanism

Deviations of the distribution function from the equilibrium value gives rise to transport phenomena. Internal collisions between the electrons and lattice or atoms tend to retore equilibrium, and the time involved in this process is called the relaxation time. There are several types of scattering mechanism which are characterised by their different energy dependence on relaxation time or temperature dependence on mobility.

One may theoretically calculate the transition probability for various scattering mechanisms. The corresponding rate of change of the distribution function may then be found from equation (1-3-2). Equating this to $-(f-f^\circ)/\tau$, we can finally obtain the relaxation time.

So from a theoretical point of view, the main job is the calculation of the transition probability due to a particular scattering. This is given by quantum theory to be

$Q_{PP'} = (2\pi/h) \mid V_{PP'} \mid^2 \delta(\mathcal{E}_{P'} - \mathcal{E}_P)$ where $V_{PP'} = \int \psi_P U \psi_{P'} d\tau$

and ψ_P , $\psi_{P'}$ are electron wave functions respectively in state P and P' and U is the scattering potential which characterises the scattering; the δ function is defined by

$$\delta(x-a) = 0 \quad \text{for } x \neq a$$

$$\int_{-\infty}^{\infty} f(x)\,\delta(x-a)\,dx = f(a)$$

In what follows we shall quote some of the relevant formulae for a few common scattering mechanisms.

1.4.1 Lattice Scattering

The study of lattice vibrations may be approached by regarding the crystal as a homogeneous continuum rather than a discrete periodic structure. Then any disturbance in this continuum will generate a wave which propagates through the material. This is the so-called lattice wave whose magnitude in classical theory represents the deviation of the corresponding point in the material from the equilibrium position.

In analogy to the concept of quantization of electromagnetic waves which leads to the fact that the electromagnetic wave possesses discrete packets of energy, each being called a photon, one can also quantize the lattice wave in a similar fashion. One then obtains the result that lattice waves are composed of packets of energy. Each packet is called a phonon. One can ascribe momentum $\hbar\underline{q}$ as well as energy $\hbar\omega\underline{q}$ to a phonon as in the case of a photon. The idea of quantizing a wave field will be mentioned in greater detail in chapter III. The interaction between the lattice and electrons may be formulated in terms of the interaction between the phonons and the electrons and it is this interaction which constitutes the lattice scattering. During the interaction, a phonon may be emitted or absorbed as a whole. An electron transition from state $\underline{P}$ to state $\underline{P} + \hbar\underline{q}$ or state $\underline{P} - \hbar\underline{q}$ is always accompanied by a transition of a phonon with a wave vector $\underline{q}$. The transition probability for lattice vibration is found to be for

phonon emission: $Q(P, P-\hbar\underline{q}) = \frac{4\pi}{9} \frac{c^2 q}{NMV} (N_{\underline{q}} + 1) \delta (\mathcal{E}_{\underline{P}-\hbar\underline{q}} - \mathcal{E}_{\underline{P}+\hbar\omega\underline{q}})$

for phonon absorption: $Q(P,P+\hbar\underline{q}) = \frac{4\pi}{9} \frac{c^2 q}{NMV} N_{\underline{q}} \delta(\mathcal{E}_{\underline{P}+\hbar\underline{q}} - \mathcal{E}_{\underline{P}-\hbar\omega\underline{q}})$

where N= no. of unit cells in the crystal; M = mass of atom;

V = velocity of sound (= velocity of propagation of longitudinal wave);

$N_{\underline{q}}$ = no of phonons; $\underline{q}$ = phonon wave vector (= $2\pi/\lambda$);

C = is called the Bloch constant which is characteristic of the interaction between electron and lattice and it is found to be approximately proportional to the Debye temperature of a crystal.

Substituting Q into equation (1-3-2) together with equation (1-3-3) and (1-3-4) the relaxation time τ is found to be

$$\tau_a = \frac{q\pi\hbar^4 V^2 M}{4\sqrt{2}\, a^3 C^2 (mkT)^{3/2}} \left(\frac{\mathcal{E}}{kT}\right)^{-\frac{1}{2}}$$

and the mobility

$$\mu_a = \frac{3\pi^{\frac{1}{2}} \hbar^4 V^2 e M}{2^{\frac{1}{2}} a^3 C^2 m^{5/2}} (kT)^{-3/2}$$ where a is the lattice constant

1.4.2 Ionized Impurity Scattering

This is one of the important scattering mechanisms for electrons at low temperature. The transition probability for scattering by impurity ions is calculated by the following assumptions:

(1) The masses of the scattering ions are assumed to be much greater than the electron mass. (2) Collisions are elastic (no change of energy of electron) and (3) Impurity ions are distributed at random and they scatter electrons independently. The relaxation time τ_i is found to be

$$\frac{1}{\tau_i} = \frac{2\pi N_i m e^4}{\alpha^2 P^3} \left\{ \ln(1+b) - \frac{b}{1+b} \right\}$$

with $b = \alpha K TP^2/\pi e^2 h^2 n$

where Ni - number of ions per unit volume;

$\varkappa$ = electrical permittivity

n = density of conduction electrons

and the mobility

$$\mu_i = \frac{2^{7/2}\,\varkappa^2\,(kT)^{3/2}}{\pi^{3/2}\,m^{\frac{1}{2}}\,N_i\,e^3\left\{\ln(1+b)-\frac{b}{1+b}\right\}}$$

1.4.3 Scattering on Neutral Impurities

At low temperatures many of the impurities in a semiconductor may not be ionized and these will have a different scattering effect on an electron. The relaxation time for scattering by neutral impurities is found to be independent of temperature and carrier energy, but it is inversely proportional to the electrical permittivity $\varkappa$ of the crystal

$$\tau = \frac{m^2 e^2}{20\hbar^3 \varkappa N_n}$$ where N_n is the concentration of neutral impurities.

The above three kinds of scattering are the main mechanisms responsible for scattering in semiconductors. The relaxation time has an energy dependence of the form

$$\tau = \tau_o(T)\ (\mathcal{E}/kT)^{r-\frac{1}{2}}$$

where $\tau_o(T)$ and r are governed by the actual scattering mechanism. For lattice scattering, ionized impurity scattering and neutral impurity scattering r is respectively equal to 0, 2 and $\frac{1}{2}$.

There are still some other kinds of scattering mechanisms apart from these three kinds mentioned, for example spin-spin interaction between electrons and impurity atoms which we shall discuss in detail in chapter III.

CHAPTER II

Thermomagnetic and Thermoelectric Effects

2.1 Introduction

In this chapter only those theories needed in the analysis of our experimental results will be reviewed. Formulae will be quoted without derivation, emphasis will be given to qualitative aspects.

2.2 Nernst Effects

The Nernst effect arises when a longitudinal temperature gradient along the x direction and a magnetic field in the z direction or any direction in the xz plane are applied. The effect may occur under either isothermal or adiabatic conditions. The isothermal condition is represented by $\partial T/\partial y = \partial T/\partial z = 0$, ie there are no transverse temperature gradients along the y and z directions. The adiabatic condition means that there is no heat flow along the y and z direction, ie $\omega_y = \omega_z = 0$.

It is found for many materials that the difference in magnitude of the Nernst effect under isothermal and adiabatic condition is negligible. Thus it is convenient to use isothermal formulae even though experiments were carried out under adiabatic conditions, as the isothermal formalae are much simpler. Hence in what follows we shall only discuss the isothermal case.

2.2.1 The Transverse Nernst Effect

From equation (1-3-10) with $j = 0$, we obtained an expression for the transverse Nernst field

$$E_y = \frac{I_{11}I_{20} - I_{10}I_{21}}{\ell (I_{10}^2 + I_{20}^2)} \sin\theta \frac{\partial \ln T}{\partial x} \qquad (2\text{-}2\text{-}1)$$

where I_{ij} are given by equation (1-3-13). From the expressions for I_{ij}, one can show that the transverse Nernst field is an odd function of magnetic field $\underline{H}$

$$\text{ie} \quad E_y(\underline{H}) = - E_y(-\underline{H})$$

In the case where $\theta = \frac{\pi}{2}$, ie magnetic field H is perpendicular to the temperature gradient; and the energy dependent relaxation time τ may be written in the form of $\tau \alpha (\frac{\varepsilon}{kT})^{r-\frac{1}{2}}$, the formula may be simplified in the two limiting cases of weak and strong magnetic field. In the weak field case, ie when $(\frac{\mu H}{C})^2 \ll 1$

$$E_y = (\tfrac{1}{2}-r) A_r \frac{k}{e} \frac{\mu H}{C} \frac{\partial T}{\partial x} \qquad (2\text{-}2\text{-}2)$$

In the strong field case, ie when $(\frac{\mu H}{C})^2 \gg 1$

$$E_y = (\tfrac{1}{2}-r)\, C_r \frac{k}{e} (\frac{\mu H}{C})^{-1} \frac{\partial T}{\partial x} \qquad (2\text{-}2\text{-}3)$$

where μ is the carrier mobility ; and

$$A_r = \frac{3\sqrt{\pi}}{4} \frac{\Gamma(\frac{3}{2} + 2r)}{\Gamma^2(2 + r)} \; ; \quad C_r = \frac{16}{9\pi} \Gamma(3-r)\, \Gamma(2+r)$$

$$\Gamma(n) = \int_0^\infty x^{n-1} e^{-x} dx$$

Measurement of the transverse Nernst field will enable us either to find out the mobility if the type of scattering mechanism (ie r) is known, or to calculate the value of r and hence to investigate the scattering mechanism provided the mobility is obtained from other sources, eg resistivity measurements.

In fact without knowing the mobility, it should be possible to determine whether r is greater or smaller than $\frac{1}{2}$ from the sign of the effect alone. As we have already mentioned in Chapter I, different r

represents different scattering mechanism. Hence we can estimate the predominant mechanism by the sign of the effect.

We may elucidate the situation by examining the following physical picture. Consider a crystal in which a temperature gradient is set up along the positive x direction. Under the action of an applied magnetic field in the positive z direction, an electron hotter than average moving from right to left is deflected downward making an angle Θ_1 with the x axis. From the following diagram we see that $\Theta_1 \propto \tau_{hot}$

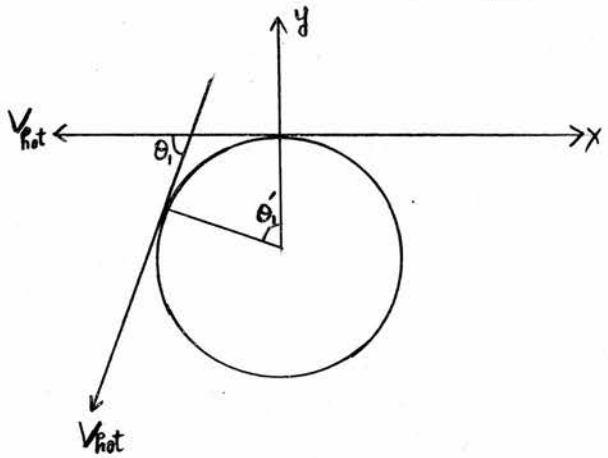

(After a time interval τ , taking

τ = mean free time between collision)

The sphere radius R, which is the trajectory of a free electron in the magnetic field H

$$R = \frac{m V_{hot}}{e H}$$

$$\Theta_1 = \Theta_1' = \frac{V_{hot} \tau_{hot}}{R} = \frac{e H \tau_{hot}}{m}$$

Similarly a cold electron travelling from left to right is deflected upward at an angle $\Theta_2 \propto \tau_{cold}$. Schematically we have

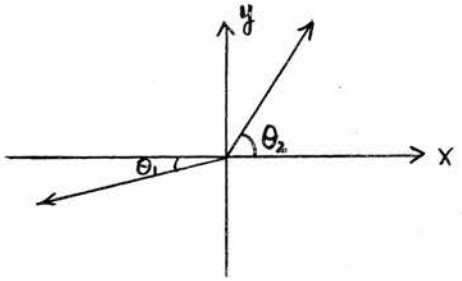

We further assume $\tau \propto \varepsilon^{r-\frac{1}{2}}$

Now if the scattering mechanism is such that $\theta_2 > \theta_1$, this implies $\tau_{cold} > \tau_{hot}$, and an electric field will be set up directed along positive y direction. This will give a transverse Nernst field with positive sign. As the hot electron has higher energy ε than the cold electron, so we must have $r < \frac{1}{2}$ in order to satisfy $\tau_{cold} > \tau_{hot}$. Therefore r = 0 which represents acoustic lattice scattering leads to a positive E_y. On the other hand if the scattering mechanism is such that $\theta_2 < \theta_1$, then $\tau_{cold} < \tau_{hot}$ and it gives rise to a negative Nernst field, r must be greater than $\frac{1}{2}$. Hence r = 2 which represents ionized impurity scattering gives a negative E_y. Vanishing of the Nernst field ($E_y = 0$) implies that $r = \frac{1}{2}$, ie scattering by neutral impurities.

Unlike the Hall effect, the sign of the transverse Nernst effect cannot be used to determine the type of current carriers, since the effect of a temperature gradient on the motion of charge carriers is independent of the sign of their charge. As the magnetic field deflects electrons and holes in opposite directions and they themselves move in opposite directions consequently the transverse Nernst field has the same direction for both electrons and holes.

Now we consider the dependence of the transverse Nernst effect on the intensity of magnetic field. In weak magnetic field, E_y is proportional to $\mu H/C$ whereas in strong field, it is proportional to $(\mu H/C)^{-1}$. Consequently in field of intermediate strength ie when $\frac{\mu H}{C} \approx 1$, the function $E(\frac{\mu H}{C})$ should have at least one maximum. The transverse Nernst coefficient Q^1 is defined to be $E_y = Q^1 H \frac{\partial T}{\partial x}$, we see that Q^1 is independent of H in the weak field case and proportional to H^{-2} in the strong field case.

2.2.2 The Longitudinal Nernst Effect

From the general expression of the longitudinal Nernst field E_x, it may be shown that E_x is an even function of magnetic field

$$\text{ie} \quad E_x(\underline{H}) = E_x(-\underline{H})$$

Now we consider the case when the magnetic field is perpendicular to the temperature gradient. Again simplified results are obtained for weak and strong field cases.

When $(\frac{\mu H}{C})^2 \ll 1$

$$E_x = (1-2r)\left(b_r - \frac{A_r^2}{2}\right)\frac{k}{e}\left(\frac{\mu H}{C}\right)^2 \frac{\partial T}{\partial x} \qquad (2\text{-}2\text{-}4)$$

when $(\frac{\mu H}{C})^2 \gg 1$

$$E_x = (\tfrac{1}{2}-r)\frac{k}{e}\frac{\partial T}{\partial x} \qquad (2\text{-}2\text{-}5)$$

where $$b_r = \frac{9\pi}{16}\frac{\Gamma(1+3r)}{\Gamma^3(2+r)}$$

In a weak magnetic field there is a quadratic dependence of E_x on the parameter $(\frac{\mu H}{C})$, while in a strong field E_x is independent of magnetic field. It therefore tends to a saturation value. Hence

equation (2-2-5) can be used to determine the r value.

Now we consider the relation between the longitudinal field E_x and this scattering mechanism qualitatively. Application of a magnetic field changes the thermoelectric field along the x-axis. We can visualize this by the following consideration. Deflection of electrons by magnetic field reduces their mean velocity in x direction. The greater the deflection the greater the change in the thermoelectric field will result. Suppose in the absence of magnetic field the thermoelectric field is directed along the negative x direction due to a temperature gradient along positive x direction. Now in the presence of a magnetic field for the case $r < \frac{1}{2}$, cold electrons moving from left to right will have a longer relaxation time than the hot ones moving in the opposite direction, and hence bigger deflection. Consequently a field E_x appears in the negative direction of x ($E_x < 0$) ie in the same direction as the primary thermoelectric field and the absolute value of the thermoelectric power increases. If $r > \frac{1}{2}$, E_x is directed in the positive x direction ($E_x > 0$) and the absolute value of thermoelectric power decreases. When $r = \frac{1}{2}$, $E_x = 0$ ie the magnetic field does not change the thermoelectric power. The direction of E_x for holes is opposite to that for electrons. Notice the effect has the same sign independent of whether carriers are electrons or holes. Now as may be done in the transverse case, we define a non-dimensional field $\mathcal{E}_x = \dfrac{E_x}{\frac{k}{e}\frac{\partial T}{\partial x}}$,

then for both electrons and holes, $\mathcal{E}_x$ is positive if $r < \frac{1}{2}$ and $\mathcal{E}_x$

is negative if $r > \frac{1}{2}$. The sign of $\mathcal{E}_x$ is consistent with the sign convention we adopted in Chapter 1. The effect is positive if absolute thermoelectric power increases and negative if it decreases. A positive $\mathcal{E}_x$ is thus always associated with a positive transverse Nernst effect which in most cases represent lattice scattering. A negative $\mathcal{E}_x$ is associated with a negative E_y which means that impurity scattering is most likely predominant.

The r value can be readily found from equation (2-2-5) in the strong field case without knowing the mobility. In the weak field case the easiest way to find the r is by considering the ratio

$$\frac{\mathcal{E}_y^2}{\mathcal{E}_x} = \frac{(\frac{1}{2} - r) A_r^2}{2b_r - A_r^2} \qquad (2\text{-}2\text{-}6)$$

We can put in various trial values for r and compare the calculated ratio with the experimental value. The r which gives the best fit will be the right one.

2.3 Thermoelectric Power

If a simple scattering process in which the relaxation time can be expressed as a power of the energy is assumed, then the thermoelectric power of both the degenerate and non-degenerate electron gas for an impurity semiconductor is given by

$$\Theta = \pm \frac{k}{e} \left[\frac{r+2}{r+1} \frac{F_{r+1}(\mu^*)}{F_r(\mu^*)} - \mu^*\right] \qquad (2\text{-}3\text{-}1)^*$$

where $F_r(\mu^*)$ is the Fermi integral $F_r(\mu^*) = \int_0^\infty \frac{x^r\, dx}{1+\exp(x-\mu^*)}$

* see Wright (1951), Johnson (1956)

μ^* is the reduced chemical potential $(\frac{\mu}{kT})$; k is the Boltzmann constant.

In the case of a non-degenerate electron gas, the thermoelectric power has the form

$$\textcircled{H} = -\frac{k}{e}\left[(2+r) + \ln \frac{2(2\pi m^* kT)^{3/2}}{h^3 n}\right] \qquad (2\text{-}3\text{-}2)$$

If the effective mass m^*, the electron concentration n and r are all independent of temperature, then equation (2-3-2) becomes

$$\textcircled{H} = -\frac{3}{2}\frac{k}{e} \ln T + \text{const}$$

Therefore a plot of $\textcircled{H}$ against ln T in the non-degenerate range gives a straight line with slope equal to $\frac{3}{2}\frac{k}{e}$. If the scattering mechanism is known ie r is known, we can find the effective mass from the thermoelectric power measurement. Suppose the effective mass is not independent of temperature, we shall not obtain a straight line. We rewrite equation (2-3-2) in the following form

$$\textcircled{H} = -\frac{k}{e}\left[(2+r) + \frac{3}{2}\ln\frac{m^*}{m_o} + \frac{3}{2}\ln T - \ln n + \ln \frac{2(2\pi m_o k)^{3/2}}{h^3}\right]$$

where m_o is the free electron mass. The dependence of $\frac{m^*}{m_o}$ on temperature can be easily found from experimental data of $\textcircled{H}$ at different temperature.

For the degenerate region, the thermoelectric power $\textcircled{H}$ can be found directly from equation (2-3-1) provided r and μ^* are known. But in general we want to obtain information about μ^* and hence the effective mass from thermoelectric power measurements. As the carrier density n is given by

$$n = 4\pi \left(\frac{2m^*kT}{h^2}\right)^{3/2} F_{\frac{1}{2}}(\mu^*) \qquad (2\text{-}3\text{-}3)$$

We have, from (2-3-3)

$$\frac{m^*}{m_o} = \frac{h^2}{2m_o kT} \left(\frac{n}{4\pi}\right)^{2/3} F_{\frac{1}{2}}^{-2/3}(\mu^*) \qquad (2\text{-}3\text{-}4)$$

Hence the effective mass ratio can be found from μ^* which is known from the value of thermoelectric power (M).

Thermoelectric power is often employed to study the effective mass of the carriers. It is also found convenient to investigate the scattering mechanism through the measurements of thermoelectric power.

2.4 Phonon Drag

The expressions for Nernst effect and thermoelectric power given in Section 2.2 and 2.3 were derived with the assumption that the phonons are in an equilibrium distribution, ie the lattice is not significantly perturbed by the temperature gradient. In practice the presence of a temperature gradient produces an anisotropy in the propagation of lattice vibrations. In some materials especially at low temperatures, the mutual interactions between phonons are insufficient to re-establish the lattice equilibrium. Then a pushing of the charge carriers from hot to cold ends owing to the asymmetrical distribution of phonon motions occurs. This "dragging" of the electrons because of the non-equilibrium distribution of phonons is what is known as the phonon drag effect. Herring (1954) showed that only longwavelength phonons are effective in the "dragging" effect. The effect is proportional to the strength of the electron-phonon coupling and to the relaxation time for the randomization of the motions of the long-wave length phonons with which the carriers interact. At low temperatures phonon drag may be more

important than at high temperature since mutual collisions between phonons are less frequent and therefore the time taken to re-establish the equilibrium state is longer. One may assume the phonon distribution function and electron distribution function to be independent of each other. Then the thermoelectric power, the Nernst field and other thermoelectric and thermomagnetic coefficients can be represented as sums of electron and phonon contributions.

The phonon drag gives rise to an additional term in the thermoelectric power. The direction of the thermoelectric field caused by phonon drag is such as to increase the magnitude of the thermoelectric power. The phonon contribution to the thermoelectric power Θ_{ph} has been estimated by Herring (1954), Frederikse (1953), Johnson (1956) to be

$$\Theta_{ph} = \frac{\omega^2 \tau_{ph}}{\mu T} = \frac{\omega l_{ph}}{\mu T} \qquad (2\text{-}4\text{-}1)$$

where ω is the velocity of sound, l_{ph} is the mean free path of those phonons which interact with the carriers, τ_{ph} is the phonon relaxation time and μ is the mobility of carriers.

Gurevich and Obraztsor (1957) discussed the influence of phonon drag on the Nernst effects in semiconductors. Tsidil'kovskii (1962) discussed the problem in more detail and found that the effect of phonon drag on the thermomagnetic phenomena is governed primarily by the nature of the dependence of the phonon mean free path on its wave vector. By assuming that phonon mean free path l_{ph} is independent of wave vector $\underline{q}$, formulae for transverse and longitudinal Nernst field due to phonon drag are obtained for weak and strong magnetic field cases as follows.

$$\left(\frac{\mu H}{C}\right)^2 \ll 1 \qquad (E_y)_{ph} = \left(\frac{3\pi}{8} - 1\right) \left|\textcircled{H}_{ph}\right| \frac{\mu H}{C} \frac{\partial T}{\partial x} \qquad (2\text{-}4\text{-}2)$$

$$\left(\frac{\mu H}{C}\right)^2 \gg 1 \qquad (E_y)_{ph} \alpha \left(\frac{\mu H}{C}\right)^{-1} \qquad (2\text{-}4\text{-}3)$$

Longitudinal Nernst field

$$\left(\frac{\mu H}{C}\right)^2 \ll 1 \qquad (E_x)_{ph} = \frac{9\pi}{16}\left(1 - \frac{\pi}{4}\right) \textcircled{H}_{ph} \left(\frac{\mu H}{C}\right)^2 \frac{\partial T}{\partial x} \qquad (2\text{-}4\text{-}4)$$

$$\left(\frac{\mu H}{C}\right)^2 \gg 1 \qquad (E_x)_{ph} = \left(\frac{32}{9\pi} - 1\right) \textcircled{H}_{ph} \frac{\partial T}{\partial x} \qquad (2\text{-}4\text{-}5)$$

where $\textcircled{H}_{ph}$ is the thermoelectric power due to phonon drag and is given by (2-4-1). If the dependence of the $\textcircled{H}_{ph}$ on temperature and temperature dependence of mobility are known, then the dependence of the Nernst field due to phonon drag on temperature can be found. Calculation of Gurevich showed that $(\mathcal{E}_y)_{ph}$ and $(\mathcal{E}_x)_{ph}$ are both $\alpha\ T^{-5}$.

It was pointed out by Herring et al (1958) that even if phonon contribution to thermoelectric power $\textcircled{H}_{ph}$ is only a fraction of electron contribution $\textcircled{H}_e$, the phonon contribution to the Nernst field will be bigger than or of the order of electron contribution.

CHAPTER III

Theory of Kondo Effect

3.1 Introduction

Experimental measurements of resistivity of the semiconductor PbS revealed a logarithmic dependence of resistivity on temperature at low temperatures. It is found for PbS with low carrier concentrations that the resistivity decreases logarithmically from about 1°K with increasing temperatures, and after passing through a minimum value, increases with temperature. A lowering of the resistance due to the application of a magnetic field at low temperature, i.e. the negative magnetoresistance, has also been observed in these crystals.

The phenomena mentioned above are similar to those observed in dilute magnetic alloys. By assuming that the resistivity minimum in metal alloy is a direct consequence of the spin-spin interaction between localized magnetic impurities and the conduction electrons, Kondo was able to derive the logarithmic temperature dependence of resistivity.

We note that the work of Cape and Hake (Phys. Rev. 139A 142 (1965)) indicates that there is no necessary correlation between a resistance minimum and the presence of localised magnetic states. However we observe a logarithmic temperature dependence of resistivity and a very good correlation between resistance minimum and negative magneto-resistance so that in our case the resistance minimum is almost certainly associated with localised moments. A Kondo type theory therefore seems the most appropriate for our purpose although in its original form it may not be strictly applicable to semiconductors.

Section 3.2 summarizes the required quantum theory so as to clarify the notation subsequently used. The material of this section can be found in any standard text book and may be omitted.

3.2 Quantum Field Theory

3.2.1 Introduction

In studying a system of many particles, we may attempt to generalize our usual Schrödinger equation for a single particle into a Schrödinger equation for many particles. However it is found that such extension is not satisfactory because

(1) a many particle Schrödinger equation is mathematically very difficult to solve due to the increase in the number of variables.

(2) in high energy physics where annihilation and creation of particles takes place, the Schrödinger equation is unable to describe the phenomena, so a "quantum field theory" has been invented to deal with a many particle system.

The concept of classical fields is well known. A classical field is described by a function $\psi(\underline{r},t)$ of space-time whose behaviour is determined by the classical field equation which may be derived from a Lagrangian by the Lagrangian equation.

The idea that a classical field may be thought of as being made up by particles in a certain sense originates from the photo electric effect. In the photo electric effect, experimental evidence leads to the inevitable conclusion that the energy of an electromagnetic wave of a given frequency cannot take on arbitrarily continuous values.

Instead, it can just assume discrete values which are integral multiples of $h\nu$. So one is led to the idea that at least under certain experimental conditions the electromagnetic wave, as a classical field with its apparent continuity, may be regarded as being composed of particles - the photons, with each quantum of energy associated with one photon. This crude physical picture is sufficient to explain the photo electric effect. A rigorous quantum formalism has also been developed to put the particle concept into a well defined quantitative theory, based on concepts of quantum mechanics. The scheme of the theory is (1) Set up the classical field theory by the Hamiltonian formalism. That is first to find the Lagrangian so that the field equation may be derived from the Lagrangian by the Lagrangian equation. From the Lagrangian one defines the momentum of the field and hence obtains the Hamiltonian as being the energy of the field. The whole set up is similar to the Hamiltonian formalism of classical mechanics of particles.

(2) In analogy to the formalism of quantum mechanics, we postulate in the new theory that the field and its momentum are to be replaced by operators satisfying certain commutation relations. Alternatively, one may decompose the field into Fourier series and regard the coeffients of the series as operators satisfying the corresponding commutation relations. As a result, the Hamiltonian is an operator.

(3) The energy of the field is postulated to be represented by the Hamiltonian operator in the sense that the only measurable

energy values of the field are the eigenvalues of the Hamiltonian operator. One is then able to compute the energy by solving the eigenvalue equation for the Hamiltonian. The Hamiltonian eigenvalues are usually discrete. The physical interpretation is therefore that each eigenvalue is a quantum of energy and the corresponding eigenfunction is the wave function for the corresponding quantum, or field particle.

The last two steps are called the quantization of the field which bring out the particle concept from a continuous field by way of giving discrete eigenvalues for the Hamiltonian.

So one obtains a quantum theory of the electromagnetic field. However the idea is proved to be so fruitful that it has been extended to quantize other fields, such as the field of sound waves in a continuum. People even go one step further to quantize a field, this has no apparent classical meaning as in the case of the electromagnetic field. The only justification then rests solely on the validity of its quantitative predictions as compared with experimental results. The one that concerns us is the formulation of a quantum field theory for the "electron field." In quantum mechanics, an electron is described by a function of space $\underline{r}$ and time t, say $\psi(\underline{r},t)$. $\psi(\underline{r},t)$ itself has no direct physical meaning as in the case of the electromagnetic wave. Despite this, one regards the wave function $\psi(\underline{r},t)$ formally as the "electron field" with the Schrödinger equation as the field equation in as much as the electromagnetic field is considered as the photon field with Maxwell equations as field equations. Once this is done, one may then proceed to quantize

the "electron field" in exactly the same way as one would do with the electromagnetic field. Since our Schrödinger equation is obtained by quantizing our classical system, our present procedure of quantizing the wave function again is also called the theory of second quantization. We will discuss this theory in more detail now.

3.2.2 Quantization of the "Electron Field"

We proceed according to the procedure just mentioned

I. Set up a classical Lagrangian and Hamiltonian formalism

We want to find a function $\mathcal{L}$ such that the field equation (Schrödinger equation for electron system) may be obtained from it. It is found that $\mathcal{L} = i\hbar\phi^*\dot{\phi} - \frac{\hbar^2}{2m}(\nabla\dot{\phi})(\nabla\phi^*)$ is the required Lagrangian, i.e. the Lagrangian equation obtained will be the Schrödinger equation.

We define Momentum density $\pi = \frac{\partial\mathcal{L}}{\partial\dot{\phi}} = i\hbar\phi^*$ and Hamiltonian density $\mathcal{H} = \pi\dot{\phi} - \mathcal{L} = (\hbar^2/2m)(\nabla\phi)(\nabla\phi^*)$.

The total Hamiltonian which is regarded as the total energy of the field is given by $H = \int d^3r\,\mathcal{H} = \int d^3r(\hbar^2/2m)(\nabla\phi^*)(\nabla\phi)$

II. We expand our field variable $\phi(\underline{r},t)$ by means of a complex Fourier Series

Suppose our field is enclosed in a cubic box of side L. It is well known that the set of functions $u_{\underline{k}} = \frac{1}{\sqrt{v}} e^{i\underline{k}\cdot\underline{r}}$ where $\underline{k} = \frac{2\pi}{L}(n_1, n_2, n_3)$ and $v = L^3$ = volume of the box forms a complete orthonormal set, which means that

(1) Orthonormality: $\int_v d^3x\, u_{\underline{k}}^*(\underline{x})\, u_{\underline{k}'}(\underline{x}) = \delta_{\underline{k}\underline{k}'}$

(2) Completeness: any function $f(\underline{x})$ defined within the box may be expressed as a linear combination of $u_{\underline{k}}(\underline{x})$ i.e. $f(\underline{x}) = \sum_{\underline{k}} c_{\underline{k}} u_{\underline{k}}(\underline{x})$

with $c_{\underline{k}} = \int_V d^3x\, u_{\underline{k}}^*(\underline{x})\, f(\underline{x})$ by the orthonormality of $u_{\underline{k}}(x)$

So we may write $\phi(\underline{r},t) = \sum_{\underline{k}} a_{\underline{k}}\, u_{\underline{k}} = \frac{1}{\sqrt{V}} \sum_{\underline{k}} a_{\underline{k}}\, e^{i\underline{k}\cdot\underline{r}}$ with

$a_{\underline{k}} = \int d^3r\, u_{\underline{k}}^*\, \phi(\underline{r},t)$.

We then postulate that $\phi(\underline{r},t)\ \pi(\underline{r},t)$ should be operators which satisfy the following commutation relations:

$[\phi(\underline{r},t), \phi(\underline{r}',t)] = 0$; $[\pi(\underline{r},t), \pi(\underline{r}',t)] = 0$;

$[\phi(\underline{r},t), \pi(\underline{r}',t)] = i\hbar\, \delta(\underline{r},\underline{r}')$

$a_{\underline{k}}$ and $a_{\underline{k}}^*$ are also operators and it may be shown that $a_{\underline{k}}$, $a_{\underline{k}'}^*$ satisfy the following commutation relations

$[a_{\underline{k}}, a_{\underline{k}'}] = 0$; $[a_{\underline{k}}^*, a_{\underline{k}'}^*] = 0$; $[a_{\underline{k}}, a_{\underline{k}'}^*] = \delta_{\underline{k}\underline{k}'}$

These commutation relations completely determine the properties of operator $a_{\underline{k}}$, $a_{\underline{k}}^*$, and hence the properties of $\phi(\underline{r},t)$ and H.

III. Energy of the system

To find the eigenvalues of the energy operator H

$$H = (\hbar^2/2m) \int d^3r\, \nabla\phi^* \cdot \nabla\phi = (\hbar^2/2m) \int d^3r \Big[\sum_{\underline{k}} -i\underline{k}\, a_{\underline{k}}^*\, u_{\underline{k}}^*(\underline{r})\Big]\Big[\sum_{\underline{k}'} i\underline{k}'\, a_{\underline{k}'}\, u_{\underline{k}'}(\underline{r})\Big]$$

$$= (\hbar^2/2m) \sum_{\underline{k}\underline{k}'} \underline{k}\cdot\underline{k}'\, a_{\underline{k}}^*\, a_{\underline{k}'} \int d^3r\, u_{\underline{k}}^*(\underline{r})\, u_{\underline{k}}(\underline{r}) = \sum_{\underline{k}} \hbar\, \omega_{\underline{k}}\, a_{\underline{k}}^*\, a_{\underline{k}}$$

with $\omega_{\underline{k}} = (\hbar/2m)\underline{k}^2$

It can be shown purely mathematically using the commutation relations of $a_{\underline{k}}$ and $a_{\underline{k}}^*$ that:

(1) The eigenvalues of H are $n\hbar\,\omega_{\underline{k}}$ with $n = 0, 1, 2, \ldots$ i.e. let $|n_{\underline{k}}\rangle$ denote the corresponding eigenfunction, then

$H|n_{\underline{k}}\rangle = n\hbar\omega_{\underline{k}}|n_{\underline{k}}\rangle$. Let $|0\rangle$ represent the lowest eigenstate with lowest energy eigenvalue 0. This state is called the vacuum state, and $H|0\rangle = 0$.

(2) It may be shown that eigenfunctions belonging to different eigenvalues are orthogonal to each other, i.e. $\langle \underline{k}|\underline{k}'\rangle = 0$ unless $\underline{k} = \underline{k}'$ in Dirac notation. We can normalize the eigenfunction so that $\langle \underline{k}|\underline{k}\rangle = 1$, so we have $\langle \underline{k}|\underline{k}'\rangle = \delta_{\underline{k}\underline{k}'}$.

(3) If $|n_{\underline{k}}\rangle$ is the eigenfunction of H with eigenvalue $n\hbar\omega_{\underline{k}}$, then

(A) $a^*|n_{\underline{k}}\rangle$ will be the eigenfunction of H with eigenvalue $(n+1)\hbar\omega_{\underline{k}}$ i.e. $H\, a^*_{\underline{k}}|n_{\underline{k}}\rangle = (n+1)\hbar\omega_{\underline{k}}\, a^*_{\underline{k}}|n_{\underline{k}}\rangle$

Compare with $H|(n+1)_{\underline{k}}\rangle = (n+1)\hbar\omega_{\underline{k}}|(n+1)_{\underline{k}}\rangle$ so $a^*_{\underline{k}}|n_{\underline{k}}\rangle = |(n+1)_{\underline{k}}\rangle$

Hence $a^*_{\underline{k}}$ is interpreted as the creation operator for particle with energy $\hbar\omega_{\underline{k}}$. In particular we may prove that $a^*_{\underline{k}}$ acting on the vacuum state will create a state with energy $\hbar\omega_{\underline{k}}$, i.e. $H(a^*_{\underline{k}}|0\rangle) = \hbar\omega_{\underline{k}}(a^*_{\underline{k}}|0\rangle)$ so we say $a^*_{\underline{k}}$ creates a particle with energy $\hbar\omega_{\underline{k}}$ on operating on the vacuum state. The one particle state is denoted by $|\underline{k}\rangle$,i.e. $a^*_{\underline{k}}|0\rangle = |\underline{k}\rangle$

(B) $a_{\underline{k}}|n_{\underline{k}}\rangle$ will be the eigenfunction of H with eigenvalue $(n-1)\hbar\omega_{\underline{k}}$, i.e. $H\, a_{\underline{k}}|n_{\underline{k}}\rangle = (n-1)\hbar\omega_{\underline{k}}\, a_{\underline{k}}|n_{\underline{k}}\rangle$ also

$H|(n-1)_{\underline{k}}\rangle = (n-1)\hbar\omega_{\underline{k}}|(n-1)_{\underline{k}}\rangle$ so $a_{\underline{k}}|n_{\underline{k}}\rangle = |(n-1)_{\underline{k}}\rangle$

Hence $a_{\underline{k}}$ is interpreted as annihilation operator. In particular one can show that $a_{\underline{k}}|0\rangle = 0$ i.e. $a_{\underline{k}}$ annihilates the vacuum.

IV. Interaction Hamiltonian

The Hamiltonian we discuss above is only for free field without interaction. For a field with interaction energy V,

The Lagrangian $\mathcal{L} = i\hbar \phi^* \dot{\phi} - (\hbar^2/2m) \nabla\phi^* - \phi^* V \phi$

Momentum density $\pi = \frac{\partial \mathcal{L}}{\partial \dot{\phi}} = i\hbar \phi^*$

$$\mathcal{H} = \pi \dot{\phi} - \mathcal{L} = \frac{\hbar^2}{2m} \nabla\phi^* \cdot \nabla\phi + \phi^* V \phi = \mathcal{H}_0 + \mathcal{H}_{int}$$

$$\mathcal{H}_{int} = \phi^* V \phi$$

The total energy operator is $H = \int d^3r \, \mathcal{H}_0 + \int d^3r \, \mathcal{H}_{int}$

V. Pauli Exclusion Principle and Quantum Field Theory

In the above quantization scheme there is no restriction as to the number of particles allowed in a particular state. So the system of particles described by the above quantum theory does not obey the Pauli exclusion principle. It is therefore a system obeying Bose-Einstein statistics. For our system of electrons obeying Pauli exclusion principle, we must have a theory which allows at most one particle in each state. It can be rigorously shown that such a theory may be obtained by changing our previous commutation relations to anticommutation relations. That is by requiring the operators to satisfy the following relation:

$$\{\phi(\underline{r},t)\ \phi(\underline{r}',t)\} = \phi(\underline{r},t)\phi(\underline{r}',t) + \phi(\underline{r}',t)\phi(\underline{r},t) = 0 ;$$

$$\{\pi(\underline{r},t)\ \pi(\underline{r}',t)\} = 0 ; \quad \{\phi(\underline{r},t)\ \pi(\underline{r}',t)\} = i\hbar\, \delta(\underline{r},\underline{r}')$$

These are equivalent to:

$$\{a_{\underline{k}}, a_{\underline{k}'}\} = a_{\underline{k}} a_{\underline{k}'} + a_{\underline{k}'} a_{\underline{k}} = 0; \quad \{a^*_{\underline{k}}, a^*_{\underline{k}}\} = 0; \quad \{a_{\underline{k}}, a^*_{\underline{k}'}\} = \delta_{\underline{k}\underline{k}'}$$

The above so-called anticommutation relations will give the following new properties to the operators

(1) $H = \sum_{\underline{k}} \hbar\omega_{\underline{k}} a^*_{\underline{k}} a_{\underline{k}}$ as before

(2) $H\, a^*_{\underline{k}} |0\rangle = \hbar\omega_{\underline{k}}\, a^*_{\underline{k}} |0\rangle$ i.e. $a^*_{\underline{k}}$ may again be interpreted as creation operator which can create a particle state from vacuum. But with the anticommutation relation it may be shown that

(A) $a^*_{\underline{k}} |\underline{k}\rangle = 0$ i.e. $a^*_{\underline{k}}\, a^*_{\underline{k}} |0\rangle = 0$

(B) the Hamiltonian eigenvalues for a particular $\underline{k}$ state is either 0 or $\hbar\omega_{\underline{k}}$. No eigenvalues of $n\hbar\omega_{\underline{k}}$ exist.

Hence the physical result that we cannot put two particles in the same state.

(C) The $a_{\underline{k}}$ has the usual properties of annihilation operators, i.e. $a_{\underline{k}} |\underline{k}\rangle = 0$; $a_{\underline{k}} |0\rangle = 0$.

So we have finally obtained a quantum field theory for electrons obeying Pauli exclusion principle and it is this theory that we shall use for our discussion of the Kondo effect.

3.2.3 Quantum Theory of Spin

I. Quantum Mechanical Treatment of Spin

In elementary quantum mechanics in which one just considers particles without spin, the state is described by a wave function of space and time $\psi(\underline{r},t)$. The easiest way of extending the theory to accommodate spin is to assume that a particle with spin $\frac{1}{2}$ should be described by a two-component wave function, i.e. $\psi(\underline{r},t) = \begin{pmatrix} \psi_{\frac{1}{2}}(\underline{r},t) \\ \psi_{-\frac{1}{2}}(\underline{r},t) \end{pmatrix}$

with $\left|\psi_{\frac{1}{2}}(\underline{r},t)\right|^2 d\tau$, $\left|\psi_{-\frac{1}{2}}(\underline{r},t)\right|^2 d\tau$ being interpreted as the probability

of finding the particle in volume $d\tau$ at $\underline{r}, t$ with z-component of spin equal to $\frac{1}{2}\hbar$ (i.e. spin up) and z-component of spin equal to $-\frac{1}{2}\hbar$ (i.e. spin down) respectively.

Alternatively, one may still formally retain the one-component appearance of the wave function by introducing the concept of spin coordinate and spin functions. Firstly one introduces a new variable ζ which takes only two values $\pm \frac{1}{2}$. Then one defines a one-component wave function of $\underline{r}, t$ and ζ by

$$\psi(\underline{r}, t, \zeta) = \psi_{\frac{1}{2}}(\underline{r}, t) \quad \text{if } \zeta = \tfrac{1}{2}$$
$$\psi_{-\frac{1}{2}}(\underline{r}, t) \quad \text{if } \zeta = -\tfrac{1}{2}$$

i.e. $\psi(\underline{r}, t, \frac{1}{2}) = \psi_{\frac{1}{2}}(\underline{r}, t)$; $\psi(\underline{r}, t, -\frac{1}{2}) = \psi_{-\frac{1}{2}}(\underline{r}, t)$

The variable ζ, introduced just for the sake of spin, is called spin variable. So we see that $\psi(\underline{r}, t, \zeta)$ contains the same information about the particle as the original two-component wave function. This may be made even clearer if we define two more functions of the variable ζ only in the following way. We define

$\alpha(\zeta)$ by $\alpha(\zeta) = 1$ if $\zeta = \frac{1}{2}$; $= 0$ if $\zeta = -\frac{1}{2}$ and $\beta(\zeta)$ by $\beta(\zeta) = 0$ if $\zeta = \frac{1}{2}$; $= 1$ if $\zeta = -\frac{1}{2}$

Then we can immediately verify that $\psi(\underline{r}, t, \zeta) = \psi_{\frac{1}{2}}(\underline{r}, t)\alpha(\zeta) + \psi_{-\frac{1}{2}}(\underline{r}, t)\beta(\zeta)$ and $\alpha(\zeta)$, $\beta(\zeta)$ being functions of the spin coordinate ζ only are called spin functions. One can show that $\alpha(\zeta)$, $\beta(\zeta)$ are eigenfunctions of the z-component spin operators S_z with eigenvalues $\frac{1}{2}\hbar$ and $-\frac{1}{2}\hbar$ respectively, i.e. $S_z\alpha(\zeta) = \frac{1}{2}\hbar\alpha(\zeta)$; $S_z\beta(\zeta) = -\frac{1}{2}\hbar\beta(\zeta)$

It can be shown that:

1. The spin operators S_x, S_y, S_z may be represented by the following matrices

$$S_x = \tfrac{1}{2}\hbar\begin{pmatrix}0 & 1\\ 1 & 0\end{pmatrix}; \quad S_y = \tfrac{1}{2}\hbar\begin{pmatrix}0 & -i\\ i & 0\end{pmatrix}; \quad S_z = \tfrac{1}{2}\hbar\begin{pmatrix}1 & 0\\ 0 & -1\end{pmatrix}$$

and $\alpha(\zeta)$, $\beta(\zeta)$ may be represented by column matrices

$$\alpha(\zeta) = \begin{pmatrix}1\\ 0\end{pmatrix}; \qquad \beta(\zeta) = \begin{pmatrix}0\\ 1\end{pmatrix}$$

2. $S_x\alpha(\zeta) = \tfrac{1}{2}\hbar\beta(\zeta)$ $\qquad S_x\beta(\zeta) = \tfrac{1}{2}\hbar\alpha(\zeta)$

$S_y\alpha(\zeta) = \tfrac{i}{2}\hbar\beta(\zeta)$ $\qquad S_y\beta(\zeta) = -\tfrac{i}{2}\hbar\alpha(\zeta)$

3. The set of spin functions are orthonormal with each other in the sense that

$$\sum_{\zeta}\alpha(\zeta)\,\alpha(\zeta) = 1; \quad \sum_{\zeta}\beta(\zeta)\,\beta(\zeta) = 1; \quad \sum_{\zeta}\alpha(\zeta)\,\beta(\zeta) = 0$$

4. There are 2 operators in spin theory corresponding more or less to the creation and annihilation operators. They are

$$S_+ = S_x + i\,S_y \qquad \text{and} \qquad S_- = S_x - i\,S_y$$

One can show that:

A. S_+ operating on a state with z-component spin $-\frac{1}{2}\hbar$ will create a state with z-component spin $\frac{1}{2}\hbar$

$$S_+\beta(\zeta) = (S_x + i\,S_y)\beta(\zeta) = S_x\beta(\zeta) + i\,S_y\beta(\zeta) = \hbar\alpha(\zeta)$$

so S_+ may be interpreted as "spin flip up" operator.

B. S_- operating on a state with z-component spin $+\frac{1}{2}\hbar$ will create a state with z-component spin $-\frac{1}{2}\hbar$

$$S_-\alpha(\zeta) = (S_x - i\,S_y)\alpha(\zeta) = \hbar\beta(\zeta)$$

so S_- may be interpreted as "spin flip down" operator.

We so far only consider 2 special spin functions of a single conduction electron, $\alpha(\zeta)$ and $\beta(\zeta)$, which have z-component spin $+\frac{1}{2}\hbar$ and

$-\frac{1}{2}\hbar$. Now if we consider the more general case, say the spin of an atom, then the z-component of spin of the atom may take values other than $\pm\frac{1}{2}\hbar$. If the maximum z-component of spin of atom is $j \geq \frac{1}{2}$, then it may be shown that the other possible z-component of spin will be $m = j, j-1, \cdots\cdots, -j$, and the spin state is denoted by $|j,m\rangle$. j, the maximum z-component of spin value of the atom and the actual value of z-component of spin of the state m. And $S_z |j,m\rangle = m\hbar |j,m\rangle$.

A perturbation which causes the spin to change will be represented by the spin flip operator S_+ and S_-. It can be proved mathematically that

$$S_+ |j,m\rangle = \sqrt{(j-m)(j+m+1)}\,\hbar\, |j, m+1\rangle$$

$$S_- |j,m\rangle = \sqrt{(j+m)(j-m+1)}\,\hbar\, |j, m-1\rangle$$

One sees that when the "spin flip up" and "spin flip down" operators act on the state $|j,m\rangle$, we obtain state $|j, m+1\rangle$ and $|j, m-1\rangle$ with different coefficients. The difference in coefficients implies that the physical effect in the 2 processes are not the same. They are not symmetrical processes. In particular, if the particle is already in its lowest spin state, then one can see that the "spin flip down" operator operating on it will not give another state

$$\therefore\ S_- |j,m\rangle = \sqrt{(j+m)(j-m+1)}\,\hbar\, |j, m-1\rangle = 0 \quad \text{for } m = -j$$

and in general processes $S_+ S_- \neq S_- S_+$

For electron with $j=\frac{1}{2}$, we have

$$S_+ \alpha(\zeta) = S_+ \left|\tfrac{1}{2},\tfrac{1}{2}\right\rangle = 0; \qquad S_- \beta(\zeta) = S_- \left|\tfrac{1}{2}, -\tfrac{1}{2}\right\rangle = 0$$

Note: There is another definition of spin operators as used by Landau in his book Quantum Mechanics. That is to represent spin operator by

$S_x = \frac{1}{2}\begin{pmatrix} 0 & 1 \\ 1 & 0 \end{pmatrix}$; $S_y = \frac{1}{2}\begin{pmatrix} 0 & -i \\ i & 0 \end{pmatrix}$; $S_z = \frac{1}{2}\begin{pmatrix} 1 & 0 \\ 0 & -1 \end{pmatrix}$

In this convention the eigenvalues of S_z will be $\pm\frac{1}{2}$ instead of $\pm\frac{1}{2}\hbar$, and all our formulae will again be valid if we just drop the $\hbar$. Following Kondo, we will use this convention in our calculation later on.

II. Quantum Field Treatment of Spin

To obtain a quantum field theory of electron with spin, we should now quantize the electron field specified by our new wave function $\phi(\underline{r},t,\zeta)$. We know that

$$\phi(\underline{r},t,\zeta) = \phi_{\frac{1}{2}}(\underline{r},t)\,\alpha(\zeta) + \phi_{-\frac{1}{2}}(\underline{r},t)\beta(\zeta) = \sum_s \phi_s(\underline{r},t)\alpha_s(\zeta)$$

where $S = \pm\frac{1}{2}$; $\alpha_{\frac{1}{2}}(\zeta) = \alpha(\zeta)$; $\alpha_{-\frac{1}{2}}(\zeta) = \beta(\zeta)$

$\phi_s(\underline{r},t)$ being function of $\underline{r},t$ only may again be expanded in terms of Fourier series,

$$\phi_s(\underline{r},t) = \sum_{\underline{k}} a_{\underline{k}s}\, U_{\underline{k}} = \sum_{\underline{k}} a_{\underline{k}s}\, \frac{1}{\sqrt{V}}\, e^{i\underline{k}\cdot\underline{r}}$$

with $$a_{\underline{k}s} = \int d^3r\, \frac{1}{\sqrt{V}}\, e^{-i\underline{k}\cdot\underline{r}}\, \phi_s(\underline{r},t)$$

so $$\phi(\underline{r},t,\zeta) = \sum_{\underline{k}s} a_{\underline{k}s}\, U_{\underline{k}}\, \alpha_s(\zeta) = \sum_{\underline{k}s} a_{\underline{k}s}\, U_{\underline{k}s}\,(\underline{r},\zeta)$$

where $$U_{\underline{k}s}\,(\underline{r},\zeta) = U_{\underline{k}}(\underline{r})\,\alpha_s(\zeta)$$

The quantization procedure is done by requiring the $a_{\underline{k}s}$ to satisfy the following anticommutation relations:

$$\{a_{\underline{k}s}, a_{\underline{k}'s'}\} = 0 \;;\quad \{a^*_{\underline{k}s}, a^*_{\underline{k}'s'}\} = 0 \;;\quad \{a_{\underline{k}s}, a^*_{\underline{k}'s'}\} = \delta_{\underline{k}\underline{k}'}\delta_{ss'}$$

The free field Hamiltonian may be shown to be

$$H = \sum_{\underline{k}s} \hbar\,\omega_{\underline{k}}\, a^*_{\underline{k}s}\, a_{\underline{k}s} \qquad \text{where } \omega_{\underline{k}} = \frac{1}{2m}\hbar\,\underline{k}^2$$

The properties of operators $a_{\underline{k}s}$ and $a^*_{\underline{k}s}$ are the same as before and hence they have the same physical interpretation, e.g. $a^*_{\underline{k}s}$ = creation operator for a particle with energy $\hbar\omega_s$ and z-component spin S. In particular, the Pauli exclusion principle is satisfied.

References for Quantum Field Theory

1. Introduction to Quantum Field Theory (Mandl)

2. Quantum Mechanics (Schiff)

3. Quantum Mechanics (Landau and Lifshitz)

3.3 Kondo's Theory of Logarithmic Temperature Dependence of Resistivity

This chapter follows the treatment given by Kondo (Prog. Theor. Physics, 32, p. 37, 1964), but the steps of the calculation are given in considerably greater detail. In chapter 6 we consider the modifications necessary to adapt the Kondo theory to the semiconductor case.

3.3.1 Basic Assumption of Kondo's Theory

As mentioned before, Kondo assumed that the resistivity minimum found in dilute magnetic alloys is due to the spin-spin interaction between localized magnetic impurity atoms and the conduction electrons. This may be formulated quantitatively using quantum field theory.

Let the impurity atoms be fixed at positions $\underline{R}_n$ with spin represented by the operator S_n. Assume that spin-spin interaction between the conduction electrons and the impurities may be represented by an interaction Hamiltonian density

$$\mathcal{H}_{int}(\underline{r}, \zeta) = \phi^*(\underline{r}, \zeta) V(\underline{r}) \phi(\underline{r}, \zeta) \quad \text{with} \quad V(\underline{r}) = -\sum_n g\, \delta(\underline{r}-\underline{R}_n)\, \underline{\sigma}\cdot\underline{S}_n$$

where $\underline{\sigma}$ is spin operator for electron; $\underline{\sigma}\cdot\underline{S}_n = \sigma_x S_{nx} + \sigma_y S_{ny} + \sigma_z S_{nz}$; $\delta(\underline{r}-\underline{R}_n)$ is the Dirac δ-function; g is a constant called the coupling constant whose value indicates the strength of the interaction; the negative sign is a convention only as the g may be positive or negative. Note that with the spin coordinate appearing in $\mathcal{H}_{int}$, the total Hamiltonian is obtained by summing over the spin coordinate as well as the usual integration over the volume, i.e.

$$H_{int} = \sum_\zeta \int d^3\underline{r}\, \mathcal{H}_{int} = -\sum_\zeta \int d^3\underline{r}\, \phi^*(\underline{r}, \zeta) g \sum_n \delta(\underline{r}-\underline{R}_n)\, \underline{\sigma}\cdot\underline{S}_n\, \phi(\underline{r}, \zeta)$$

Recall $$\phi(\underline{r}) = \sum_{\underline{k}s} \frac{e^{i\underline{k}\cdot\underline{r}}}{\sqrt{V}}\, a_{\underline{k}s}\, \alpha_s(\zeta)$$

$$H_{int} = -g \sum_{\zeta} \sum_{n} d^3\underline{r} \sum_{\underline{k}'s'} \frac{e^{-i\underline{k}'\underline{r}}}{\sqrt{V}}\, a^*_{\underline{k}'s'} \alpha_{s'}(\zeta)\, \delta(\underline{r}-\underline{R}_n)\, \underline{\sigma}\cdot\underline{S}_n \sum_{\underline{k}s} \frac{e^{i\underline{k}\cdot\underline{r}}}{\sqrt{V}}\, a_{\underline{k}s}\alpha_s(\zeta)$$

$$= -\frac{g}{V} \sum_{n} \sum_{\substack{\underline{k}'s' \\ \underline{k}s \\ \zeta}} e^{i(\underline{k}-\underline{k}')\underline{R}_n}\, \alpha_{s'}(\zeta)\, \underline{\sigma}\cdot\underline{S}_n\, \alpha_s(\zeta)\, a^*_{\underline{k}'s'}\, a_{\underline{k}s}$$

Introduce a new set of notations α_+, α_-, $a_{\underline{k}+}$, $a_{\underline{k}-}$, $a^*_{\underline{k}+}$, $a^*_{\underline{k}-}$ for brevity

let $\alpha_+(\zeta) = \alpha_{\frac{1}{2}}(\zeta) = \alpha(\zeta)$; $\alpha_-(\zeta) = \alpha_{-\frac{1}{2}}(\zeta) = \beta(\zeta)$;

$$a_{\underline{k}+} = a_{\underline{k}\frac{1}{2}}\ ; \quad a_{\underline{k}-} = a_{\underline{k}-\frac{1}{2}}\ ; \quad a^*_{\underline{k}+} = a^*_{\underline{k}\frac{1}{2}}\ ; \quad a^*_{\underline{k}-} = a^*_{\underline{k}-\frac{1}{2}}\ ;$$

The state of an electron with energy $\hbar\omega_{\underline{k}}$ and spin up is represented by $|\underline{k}+\rangle$ (and $|\underline{k}-\rangle$ for spin down).

Consider $$\sum_{ss'\zeta} \alpha_{s'}(\zeta)(\sigma_x S_{nx} + \sigma_y S_{ny} + \sigma_z S_{nz})\alpha_s(\zeta)\, a^*_{\underline{k}'s'} a_{\underline{k}s} = \sum_{ss'\zeta} [① + ② + ③]$$

$$\sum_{ss'\zeta} ① = \sum_{ss'\zeta} \alpha_{s'}\sigma_x S_{nx}\alpha_s\, a^*_{\underline{k}'s'} a_{\underline{k}s} = \sum_{ss'\zeta} \alpha_{s'}\sigma_x\, \alpha_s\, S_{nx}\, a^*_{\underline{k}'s'} a_{\underline{k}s}$$

$$= \sum_{\zeta} [\alpha_+\sigma_x\alpha_+ S_{nx}\, a^*_{\underline{k}'+} a_{\underline{k}+} + \alpha_-\sigma_x\alpha_- S_{nx}\, a^*_{\underline{k}'-} a_{\underline{k}-} + \alpha_+\sigma_x\alpha_- S_{nx}\, a^*_{\underline{k}'+} a_{\underline{k}-}$$
$$+ \alpha_-\sigma_x\alpha_+ S_{nx}\, a^*_{\underline{k}'-} a_{\underline{k}+}]$$

$$= \sum_{\zeta} [\alpha_+(\tfrac{1}{2}\alpha_-) S_{nx}\, a^*_{\underline{k}'+} a_{\underline{k}+} + \alpha(\tfrac{1}{2}\alpha_+) S_{nx}\, a^*_{\underline{k}'-} a_{\underline{k}-} + \alpha_+(\tfrac{1}{2}\alpha_+) S_{nx}\, a^*_{\underline{k}'+} a_{\underline{k}-}$$
$$+ \alpha_-(\tfrac{1}{2}\alpha_-) S_{nx}\, a^*_{\underline{k}'-} a_{\underline{k}+}]$$

$= \frac{1}{2} S_{nx}\, a^*_{\underline{k}'+} a_{\underline{k}-} + \frac{1}{2} S_{nx}\, a^*_{\underline{k}'-} a_{\underline{k}+}$ by the orthonormality of the spin functions. Similarily

$$\sum_{ss'\zeta} ② = \sum_{ss'\zeta} \alpha_{s'}\sigma_y\, \alpha_s\, S_{ny}\, a^*_{\underline{k}'s'} a_{\underline{k}s} = -\frac{i}{2} S_{ny}\, a^*_{\underline{k}'+} a_{\underline{k}-} + \frac{i}{2} S_{ny}\, a^*_{\underline{k}'-} a_{\underline{k}+}$$

$$\sum_{ss'\xi} ③ = \sum_{ss'\xi} \alpha_{s'}\delta_z \alpha_s S_{nz} a^*_{\underline{k}'s'} a_{\underline{k}s} = \tfrac{1}{2} S_{nz} a^*_{\underline{k}'+} a_{\underline{k}+} - \tfrac{1}{2} S_{nz} a^*_{\underline{k}'-} a_{\underline{k}-}$$

$$\therefore \sum_{ss'\xi} [① + ② + ③] = \tfrac{1}{2}(S_{nx} - iS_{ny}) a^*_{\underline{k}'+} a_{\underline{k}-} + \tfrac{1}{2}(S_{nx} + iS_{ny}) a^*_{\underline{k}'-} a_{\underline{k}+}$$

$$+ \tfrac{1}{2} S_{nz}(a^*_{\underline{k}'+} a_{\underline{k}+} - a^*_{\underline{k}'-} a_{\underline{k}-})$$

$$= \tfrac{1}{2}[(a^*_{\underline{k}'+} a_{\underline{k}+} - a^*_{\underline{k}'-} a_{\underline{k}-}) S_{nz} + a^*_{\underline{k}'+} a_{\underline{k}-} S_{n-} + a^*_{\underline{k}'-} a_{\underline{k}+} S_{n+}]$$

So finally

$$H_{int} = -\frac{g}{V} \tfrac{1}{2} \sum_{n\underline{k}\,\underline{k}'} e^{i(\underline{k}-\underline{k}')R_n} [(a^*_{\underline{k}'+} a_{\underline{k}+} - a^*_{\underline{k}'-} a_{\underline{k}-}) S_{nz} + a^*_{\underline{k}'+} a_{\underline{k}'-} S_{n-}$$

$$+ a^*_{\underline{k}'-} a_{\underline{k}+} S_{n+}]$$

let $\frac{1}{2}\frac{g}{V} = \frac{J}{N}$ where N is the total number of atoms in the crystal

$J = \frac{1}{2} g \frac{N}{V}$ being proportional to g, is a measure of the coupling strength.

$$H_{int} = H' = -(\frac{J}{N}) \sum_{nkk'} e^{i(\underline{k}-\underline{k}')R_n} [(a^*_{\underline{k}'+} a_{\underline{k}+} - a^*_{\underline{k}'-} a_{\underline{k}-}) S_{nz} + a^*_{\underline{k}'+} a_{\underline{k}-} S_{n-} +$$

$$a^*_{\underline{k}'-} a_{\underline{k}+} S_{n+}] \qquad (3\text{-}3\text{-}1\text{-}1)$$

In order to find the resistivity ρ ie to find conductivity σ which involves a relaxation time τ, we have to find the energy dependence on τ. This τ can be obtained if we know the transition probability.

So first of all we have to calculate the transition probability. The transition probability per unit time from the initial state "a" to the final state "b" is given to the second Born approximation by

$$W(a \to b) = \frac{2\pi}{\hbar} \delta(\mathcal{E}_a - \mathcal{E}_b)[H'_{ab} H'_{ba} + \sum_{c \neq a} (H'_{ac} H'_{cb} H'_{ba} + c.c.)/(\mathcal{E}_a - \mathcal{E}_c)]$$

where c.c. denote complex conjugate; (3-3-1-2)

a,b,c denote states of the system and $\mathcal{E}_a$, $\mathcal{E}_b$, $\mathcal{E}_c$ are their energies and

H'_{ab} is the matrix element of $H' = H_{int}$ between the two states. We shall not derive this transition probability W, but we want to say a few things about it.

(1) The appearance of the δ-function implied $W(a \to b)=0$ unless $\varepsilon_a = \varepsilon_b$, and this implies that our scattering process is an elastic one, ie. the energy of the incoming particle is equal to the energy of the outgoing particle after collision (energy conserved).

But at $\varepsilon_a = \varepsilon_b$, $\delta(\varepsilon_a - \varepsilon_b) = \infty$. Should $W(a \to b)$ go to infinity? It should not! The reason is as follows: All physical measurements are performed within a finite time interval, according to the uncertainty principle, $\Delta\varepsilon\, \Delta t \geq \frac{\hbar}{2}$. This implies that all energy levels are not absolutely sharp, and hence the physically measured transition probability $W(a \to b)$ is actually for transition from ε_a to a group of final states with energy around ε_b. So we need to integrate the above expression and this will then eliminate the singular behaviour of the δ function.

(2) We shall assume that the contribution due to the interaction between the spin of the impurities themselves is very small and may be neglected.

3.3.2 Calculation of Matrix Elements and Transition Probability in the First Order Born Approximation

The first order Born approximation involves only matrix elements H'_{ab} and H'_{ba}, so it is interpreted as the contribution due to direct transitions from state "a" to state "b". We shall show that this process only gives a temperature independent term to the resistivity.

We consider the following transitions:

Case I Transition of electron from $|\bar{k}+\rangle$ to $|\bar{k}'+\rangle$ without change of spin

The wave function of the system consists of wave functions of the impurity and the electron $\Phi = |\underline{k}+\rangle \Psi_{imp}$

We assume that impurity is spatially fixed so it may be represented by its spin function only. Let its maximum z-component spin be denoted by j, then its spin function may be written as $|j, M_n\rangle$ describing the n^{th} impurity with z-component spin M_n. So, $\Phi = |\underline{k}+\rangle |j, M_n\rangle$ or simply $\Phi = |\underline{k}+; j M_n\rangle$. Matrix elements $H'_{\underline{k}+M_n, \underline{k}'+M_n} = \langle \underline{k}+; j M_n | H' | \underline{k}'+; j M_n \rangle$ (the impurity spin is unchanged).

Now substitute the expression for H' given in equation (3-3-1-1) into it, we have

$$H'_{\underline{k}+,\underline{k}'+} = \sum_n H'_{\underline{k}+M_n, \underline{k}'+M_n} = -\left(\frac{J}{N}\right)\sum_n [① + ② + ③ + ④]$$

① = contribution from the first term in H'

$$= \sum_{\underline{k}\underline{k}'\bar{n}} e^{i(\underline{k}-\underline{k}')R_{\bar{n}}} \langle \underline{k}+; jM_n | a^*_{\underline{k}'+} a_{\underline{k}+} S_{\bar{n}z} | \underline{k}'+; j M_n \rangle$$

$$= \sum_{\underline{k}'} e^{i(\underline{k}'-\underline{k}')R_n} \langle \underline{k}+; j M_n | a^*_{\underline{k}'+} M_n | 0; jM_n \rangle = e^{i(\underline{k}'-\underline{k})R_n} M_n$$

$\because$ $S_{\bar{n}z}|\underline{k}'+; j M_n\rangle = M_n |\underline{k}'+; jM_n\rangle$ for $\bar{n} = n$;

$= 0$ for $\bar{n} \neq n$

$a_{\underline{k}+} M_n |\underline{k}'+; j M_n\rangle = M_n |0; j M_n\rangle$ for $\underline{k} = \underline{k}'$

$= 0$ for $\underline{k} \neq \underline{k}'$

$a^*_{\underline{k}'+} M_n \left| 0;\ j\ M_n \right\rangle = M_n \left| \underline{k}'+;\ j\ M_n \right\rangle$ and by the orthonormal property of eigenfunctions ie $\left\langle \underline{\bar{k}}+;\ j\ M_n \middle|\ \underline{k}'+;\ j\ M_n \right\rangle = 1$ for $\underline{k}' = \underline{\bar{k}}$

$= 0$ for $\underline{k}' \neq \underline{\bar{k}}$

$$(2) = -\sum_{\underline{k}\underline{k}'\underline{n}} e^{i(\underline{k}-\underline{k}')\underline{R}_n} \left\langle \underline{\bar{k}}+;\ j\ M_n \middle| a^*_{\underline{k}'-} a_{\underline{k}-} S_{nz} \middle|\ \underline{\bar{k}}'+;\ j\ M_n \right\rangle = 0$$

$$(3) = \sum_{\underline{k}\underline{k}'\underline{n}} e^{i(\underline{k}-\underline{k}')\underline{R}_n} \left\langle \underline{\bar{k}}+;\ j\ M_n \middle| a^*_{\underline{k}'+} a_{\underline{k}-} S_{n-} \middle|\ \underline{\bar{k}}'+;\ j\ M_n \right\rangle = 0$$

$$(4) = \sum_{\underline{k}\underline{k}'\underline{n}} e^{i(\underline{k}-\underline{k}')\underline{R}_n} \left\langle \underline{\bar{k}}+;\ j\ M_n \middle| a^*_{\underline{k}'-} a_{\underline{k}+} S_{n+} \middle|\ \underline{\bar{k}}'+;\ j\ M_n \right\rangle$$

$\because\ S_{n+} \left|\ \underline{\bar{k}}'+;\ j\ M_n \right\rangle = \sqrt{(j-M_n)(j+M_n+1)}\ \left|\ \underline{\bar{k}}'+;\ j(M_n+1) \right\rangle$

so $(4) = \sum_{\underline{k}'} e^{i(\underline{\bar{k}}'-\underline{k}')\underline{R}_n} \sqrt{(j-M_n)(j+M_n+1)} \left\langle \underline{\bar{k}}+;\ j\ M_n \middle| a^*_{\underline{k}'-} \middle|\ 0;\ jM_n \right\rangle = 0$

so $H'_{\underline{\bar{k}}+,\underline{\bar{k}}'+} = -\left(\frac{J}{N}\right) \sum_n e^{i(\underline{\bar{k}}'-\underline{\bar{k}})\underline{R}_n} M_n$ Similarly

$$H'_{\underline{\bar{k}}'+,\underline{\bar{k}}+} = -\left(\frac{J}{N}\right) \sum_{n'} e^{i(\underline{\bar{k}}-\underline{\bar{k}}')\underline{R}_{n'}} M_{n'}$$

Hence $H'_{\underline{\bar{k}}+,\underline{\bar{k}}'+}\ H'_{\underline{\bar{k}}'+,\underline{\bar{k}}+} = \left(\frac{J}{N}\right)^2 \sum_{n=n'} M_n^{\,2} + \sum_{n\neq n'} \left(\frac{J}{N}\right)^2 e^{i(\underline{\bar{k}}-\underline{\bar{k}}')(\underline{R}_n - \underline{R}_n)} M_n M_{n'}$

The second term in the above expression may be interpreted as the contribution due to interaction between impurities indirectly through conduction electrons. As mentioned before, we assume this to be small and may be neglected.

Recall that M_n is related to j and with the assumption that the localized spins are randomly oriented, one can show by summing $M_n^{\,2}$ from -j to +j that

$$\sum_n M_n^{\,2} = \frac{1}{3}\, j\,(j+1)\, CN$$

where j is the maximum value of M_n, being either the integer or half integer.

C is the impurity concentration, which is the probability of an atom being an impurity atom.

N is total number of atoms in the crystal. Hence CN is the total number of impurity atoms.

So transition probability $W(a\rightarrow b)$ for the transition is

$$\frac{2\pi}{\hbar}\left(\frac{J}{N}\right)^2 \frac{1}{3} j(j+1)\, CN\, \delta(\mathcal{E}_{\underline{k}} - \mathcal{E}_{\underline{k}'}) = \frac{2\pi J^2 j(j+1) C}{3\hbar N}\, \delta(\mathcal{E}_{\underline{k}} - \mathcal{E}_{\underline{k}'}) \qquad (3\text{-}3\text{-}2\text{-}1)$$

which is independent of temperature, and one may expect it to contribute a constant term in resistivity as will be confirmed later.

Case II Transition of electron from $|\bar{\underline{k}}-\rangle$ to $|\bar{\underline{k}}'-\rangle$ without change of spin

By repeating the calculations of Case I, we easily obtain identical results for the first order Born transition probability. The matrix elements are the same as those in case I apart from a negative sign.

Case III Transition of electron from $|\bar{\underline{k}}+\rangle$ to $|\bar{\underline{k}}'-\rangle$ with spin flip down

Matrix element $H'_{\bar{\underline{k}}+M_n,\ \bar{\underline{k}}'-(M_n+1)} = \left\langle \bar{\underline{k}}+;\ j\ M_n \right| H' \left| \bar{\underline{k}}'-;\ j(M_n+1) \right\rangle$

Notice that conservation of spin requires the impurity spin M_n to flip up, so the final impurity state has spin M_n+1.

$$H'_{\bar{\underline{k}}+,\ \bar{\underline{k}}'-} = \sum_n H'_{\bar{\underline{k}}+M_n,\ \bar{\underline{k}}'-(M_n+1)} = -\frac{J}{N}\sum_n [\,① + ② + ③ + ④\,]$$

$$① = \sum_{\underline{k}\underline{k}'\bar{n}} e^{i(\underline{k}-\underline{k}')\underline{R}_{\bar{n}}} \left\langle \bar{\underline{k}}+;\ j\ M_n \right| a^*_{\underline{k}'}\, a_{\underline{k}+}\, S_{\bar{n}z} \left| \bar{\underline{k}}'-;\ j(M_n+1) \right\rangle = 0$$

$$② = -\sum_{\underline{k}\underline{k}'\bar{n}} e^{i(\underline{k}-\underline{k}')\underline{R}_{\bar{n}}} \left\langle \bar{\underline{k}}+;\ jM_n \right| a^*_{\underline{k}'-}\, a_{\underline{k}-}\, S_{\bar{n}z} \left| \bar{\underline{k}}'-;\ j(M_n+1) \right\rangle$$

$$= -\sum_{\underline{k}'} e^{i(\underline{\bar{k}}'-\underline{\bar{k}})\underline{R}_n} \left\langle \underline{\bar{k}}+;\ j\ M_n \right| \left. \underline{k}'-;\ j(M_n+1) \right\rangle = 0$$

$$③ = \sum_{\underline{k}\underline{k}'\underline{n}} e^{i(\underline{k}-\underline{k}')\underline{R}_n} \left\langle \underline{\bar{k}}+;\ j\ M_n \right| a^*_{\underline{k}'+}\, a_{\underline{k}-}\, S_{\underline{n}-} \left| \underline{\bar{k}}'-;\ j(M_n+1) \right\rangle$$

$$= \sum_{\underline{k}'} e^{i(\underline{\bar{k}}'-\underline{k}')\underline{R}_n} \sqrt{(j+M_n+1)(j-M_n)} \left\langle \underline{\bar{k}}+;\ j\ M_n \right| \left. \underline{k}'+;\ j\ M_n \right\rangle$$

$$= e^{i(\underline{\bar{k}}'-\underline{\bar{k}})\underline{R}_n} \sqrt{(j+M_n+1)(j-M_n)}$$

$$④ = \sum_{\underline{k}\underline{k}'\underline{n}} e^{i(\underline{k}-\underline{k}')\underline{R}_n} \left\langle \underline{\bar{k}}+;\ j\ M_n \right| a^*_{\underline{k}'-}\, a_{\underline{k}+}\, S_{\underline{n}+} \left| \underline{\bar{k}}'-;\ j(M_n+1) \right\rangle = 0$$

so $H'_{\underline{\bar{k}}+,\ \underline{\bar{k}}'-} = \sum_n H'_{\underline{\bar{k}}+M_n,\ \underline{\bar{k}}'-(M_n+1)} = -\left(\frac{J}{N}\right)\sum_n e^{i(\underline{\bar{k}}'-\underline{\bar{k}})\underline{R}_n} \sqrt{(j+M_n+1)(j-M_n)}$

Similarly $H'_{\underline{\bar{k}}'-,\underline{\bar{k}}+} = -\left(\frac{J}{N}\right)\sum_{n'} e^{i(\underline{\bar{k}}-\underline{\bar{k}}')\underline{R}_{n'}} \sqrt{(j+M_{n'}+1)(j-M_{n'})}$

$\therefore \quad H'_{\underline{\bar{k}}+,\underline{\bar{k}}'-} H_{\underline{\bar{k}}'-,\underline{\bar{k}}+} = \left(\frac{J}{N}\right)^2 \sum_n (j+M_n+1)(j-M_n) + (\text{terms with } n \neq n'$

which represents correlation between impurities and will be neglected)

Now $\sum_n (j+M_n+1)(j-M_n) = \sum_n [j^2-M_n{}^2+j-M_n] = \sum_n (j^2+j) - \sum_n M_n{}^2 - \sum_n M_n$

$= CN\left[j^2+j-\frac{1}{3}j(j+1)\right] = \frac{2}{3} CN\ j(j+1)$

Hence the contribution to the first order Born transition probability is

$$\frac{4\pi J^2 C}{3\hbar N}\ j(j+1)\ \delta(\mathcal{E}_{\underline{\bar{k}}} - \mathcal{E}_{\underline{\bar{k}}'}) \qquad (3\text{-}3\text{-}2\text{-}2)$$

Case IV Transition of electron from $|\underline{\bar{k}}-\rangle$ to $|\underline{\bar{k}}'+\rangle$ with spin flip up

Repeat calculations as in Case III. In this case, the impurity spin should flip down. So we have

$$H'_{\underline{\bar{k}}-,\underline{\bar{k}}'+} = \sum_n H'_{\underline{\bar{k}}-M_n,\ \underline{\bar{k}}'+(M_n-1)} = \left\langle \underline{\bar{k}}-;\ j\ M_n \right| H' \left| \underline{\bar{k}}'+;\ j(M_n-1) \right\rangle$$

$$= -\left(\frac{J}{N}\right)\sum_{n} e^{i(\bar{k}-\bar{k}')R_n} \sqrt{(j-M_n+1)(j+M_n)}$$

Similarly

$$H_{\bar{k}'+,\bar{k}-} = -\left(\frac{J}{N}\right)\sum_{n} e^{i(\bar{k}'-\bar{k})R_n} \sqrt{(j-M_n+1)(j+M_n)}$$

$$\therefore \quad H'_{\bar{k}-,\bar{k}'+} H'_{\bar{k}'+,\bar{k}-} = \left(\frac{J}{N}\right)^2 \sum_{n} (j-M_n+1)(j+M_n) = \frac{2}{3}CN\, j(j+1)$$

Hence the contribution to first order Born transition probability is the same as in Case III.

3.3.3 Calculations of Matrix Elemements and Transitions Probability due to Second Order Born Approximation

This contains the products of matrix elements $H'_{ac}H'_{cb}$ with sum over $|c\rangle$. The natural interpretation is that it represents the transition from $|a\rangle \rightarrow |b\rangle$ in 2 steps with $|c\rangle$ as intermediate state, ie $|a\rangle \rightarrow |c\rangle \rightarrow |b\rangle$. Since it sums over all possible $|c\rangle$, we must enumerate all physically possible transitions from $|a\rangle$ to $|b\rangle$ by the 2 steps process. We now consider the following transitions as in 1st order Born transitions.

Case I $|\bar{k}+\rangle \rightarrow |\bar{k}'+\rangle$ transition

There are four possible processes:

Process 1: Electron in state $|\bar{k}+\rangle$ scattered to $|q+\rangle$, then to $|\bar{k}'+\rangle$, ie $|\bar{k}+\rangle \rightarrow |q+\rangle \rightarrow |\bar{k}'\rangle$. This process is physically possible only if $|q+\rangle$ is unoccupied and this has a probability $(1 - f^{\circ}_{q})$. The 2nd order Born transition probability term may be written as

$$\frac{2\pi}{\hbar}\,\delta(\mathcal{E}_{\bar{k}} - \mathcal{E}_{\bar{k}'}) \sum_{q} [H'_{\bar{k}+,q+}H'_{q+,\bar{k}'+} + H'_{\bar{k}'+,\bar{k}+} + c.c.]\,(1-f^{\circ}_{q})/(\mathcal{E}_{\bar{k}} - \mathcal{E}_{q}) \quad (A)$$

The calculations of matrix elements are the same as in 1st order term, so we immediately write out the expressions for matrix elements using the results obtained previously.

$$H'_{\bar{k}+,\bar{q}+} = -(\frac{J}{N})\sum_{n} e^{i(\bar{q}-\bar{k})R_{n}} M_{n} \quad , \quad H'_{\bar{q}+,\bar{k}'+} = -(\frac{J}{N})\sum_{n'} e^{i(\bar{k}'-\bar{q})R_{n'}} M_{n'}$$

$$H'_{\bar{k}+,\bar{k}+} = -(\frac{J}{N})\sum_{n''} e^{i(\bar{k}-\bar{k}')R_{n''}} M_{n''}$$

$$H'_{\bar{k}+,\bar{q}+} H'_{\bar{q}+,\bar{k}'+} + H'_{\bar{k}'+,\bar{k}+} = -(\frac{J}{N})^{3} \sum_{nn'n''} e^{i[(\bar{q}-\bar{k})R_{n}+(\bar{k}'-\bar{q})R_{n'}+(\bar{k}-\bar{k}')R_{n''}]} M_{n} M_{n'} M_{n''}$$

$$= -(\frac{J}{N})^{3}\sum_{n} M_{n}^{3} + (\text{terms with } n\neq n'\neq n'' \text{ represent correlation between impurities and are neglected})$$

so (A) becomes

$$+2\,\frac{2\pi}{\hbar}\,(-\frac{J}{N})^{3}\,\delta(\varepsilon_{\bar{k}}-\varepsilon_{\bar{k}'})\sum_{n} M_{n}^{3} \sum_{\bar{q}} \frac{1-f^{\circ}_{\bar{q}}}{\varepsilon_{\bar{k}}-\varepsilon_{\bar{q}}} \qquad (A')$$

(extra factor 2 comes from the complex conjugate terms)

Process 2: One of the electrons in state $|\bar{q}+\rangle$ is first scattered to $|\bar{k}'+\rangle$, and then the electron in state $|\bar{k}+\rangle$ fills up the state $|\bar{q}+\rangle$ which is now empty.

$$|\bar{q}+\rangle \rightarrow |\bar{k}'+\rangle$$
$$|\bar{k}+\rangle \rightarrow |\bar{q}+\rangle$$

This process is possible if $\bar{q}+$ state is occupied and it has a probability $f^{\circ}_{\bar{q}}$.

The second order Born transition term may be written as

$$\frac{2\pi}{\hbar}\,\delta(\varepsilon_{\bar{k}}-\varepsilon_{\bar{k}'})\sum_{\bar{q}} [H'_{\bar{q}+,\bar{k}'+} H'_{\bar{k}+,\bar{q}+} H'_{\bar{k}',\bar{k}} + C.C.]\, f^{\circ}_{\bar{q}} \Big/ (\varepsilon_{\bar{k}'}-\varepsilon_{\bar{q}}) \qquad (B)$$

The calculation of the matrix elements is the same as in process 1, which gives

$$-2\,\frac{2\pi}{\hbar}\,(-\frac{J}{N})^{3}\,\delta(\varepsilon_{\bar{k}}-\varepsilon_{\bar{k}'})\sum_{n} M_{n}^{3} \sum_{\bar{q}} f^{\circ}_{\bar{q}} \Big/ (\varepsilon_{\bar{q}}-\varepsilon_{\bar{k}'}) \qquad (B')$$

Process 3: During the process of transition, the sign of the spin may

be changed in the intermediate state. Electron in state $|\underline{\bar{k}}+\rangle$ is first scattered to state $|\underline{q}-\rangle$ while the z-component of spin of the n^{th} atom is increased by 1 from $M_n \rightarrow M_n+1$ due to conservation of spin. Then the electron is again scattered to $|\underline{\bar{k}}'+\rangle$ and the z-component of spin of the n^{th} atom returns to M_n.

$$\begin{array}{ccccc} |\underline{\bar{k}}+\rangle & & |\underline{q}-\rangle & & |\underline{\bar{k}}'+\rangle \\ |j,M_n\rangle & \longrightarrow & |j,(M_n+1)\rangle & \longrightarrow & |j,M_n\rangle \end{array}$$

In this process, the second order Born approximation may be written as

$$\frac{2\pi}{\hbar}\delta(\mathcal{E}_{\underline{\bar{k}}}-\mathcal{E}_{\underline{\bar{k}}'})\sum_{\underline{q}n}[H'_{\underline{\bar{k}}+M_n,\underline{q}-(M_n+1)}H'_{\underline{q}-(M_n+1),\underline{\bar{k}}'+M_n}H'_{\underline{\bar{k}}'+M_n,\underline{\bar{k}}+M_n}+C.C.](1-f^{\circ}_{\underline{q}})\Big/(\mathcal{E}_{\underline{\bar{k}}}-\mathcal{E}_{\underline{q}}) \quad (C)$$

The matrix elements can be written out immediately using results obtained in the first order term

$$H'_{\underline{\bar{k}}+M_n,\underline{q}-(M_n+1)} = -\left(\frac{J}{N}\right) e^{i(\underline{q}-\underline{\bar{k}})\underline{R}_n} \sqrt{(j+M_n+1)(j-M_n)}$$

$$H'_{\underline{q}-(M_n+1),\underline{\bar{k}}'+M_n} = -\left(\frac{J}{N}\right) e^{i(\underline{\bar{k}}'-\underline{q})\underline{R}_{n'}} \sqrt{(j+M_n+1)(j-M_n)}$$

$$H'_{\underline{\bar{k}}'+M_n,\underline{\bar{k}}+M_n} = -\left(\frac{J}{N}\right) e^{i(\underline{\bar{k}}-\underline{\bar{k}}')\underline{R}_{n''}} M_n$$

$$H'_{\underline{\bar{k}}+M_n,\underline{q}-(M_n+1)}H'_{\underline{q}-(M_n+1),\underline{\bar{k}}'+M_n}H'_{\underline{\bar{k}}'+M_n,\underline{\bar{k}}+M_n}$$

$$= -\left(\frac{J}{N}\right)^3 e^{i[(\underline{q}-\underline{\bar{k}})\underline{R}_n + (\underline{\bar{k}}'-\underline{q})\underline{R}_{n'} + (\underline{\bar{k}}-\underline{\bar{k}}')\underline{R}_{n''}]} M_n(j+M_n+1)(j-M_n)$$

$$= -\left(\frac{J}{N}\right)^3 M_n\,(j-M_n)(j+M_n+1).$$

so the 2nd order Born term (C) becomes

$$2\,\frac{2\pi}{\hbar}\,\delta(\mathcal{E}_{\underline{\bar{k}}}-\mathcal{E}_{\underline{\bar{k}}'})\left(-\frac{J}{N}\right)^3\sum_n M_n(j-M_n)(j+M_n+1)\sum_{\underline{q}}(1-f^{\circ}_{\underline{q}})/(\mathcal{E}_{\underline{\bar{k}}}-\mathcal{E}_{\underline{q}}) \quad (C')$$

the factor 2 comes from the c.c. terms.

Process 4 One of the electrons in state $|\underline{q}-\rangle$ is first scattered to the state $|\underline{\bar{k}}'+\rangle$ while the impurity atom spin is decreased by 1 from $M_n \longrightarrow M_n-1$. Then the electron with $|\underline{\bar{k}}+\rangle$ fills the state $|\underline{q}-\rangle$ and the z component of spin of the impurity atom is increased by 1 from $(M_n-1) \longrightarrow M_n$.

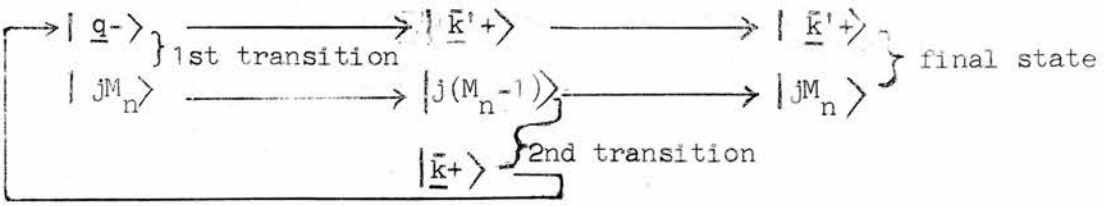

The second order Born approximation in this process can be written as

$$\frac{2\pi}{\hbar}\,\delta(\mathcal{E}_{\underline{\bar{k}}}-\mathcal{E}_{\underline{\bar{k}}'})\sum_{\underline{q}n}[H'_{\underline{q}-M_n,\underline{\bar{k}}'+(M_n-1)}\,H'_{\underline{\bar{k}}+(M_n-1),\underline{q}-M_n}$$

$$H'_{\underline{\bar{k}}'+M_n,\underline{\bar{k}}+M_n}+\text{c.c.}]\,f^{\circ}_{\underline{q}}\,/\,(\mathcal{E}_{\underline{\bar{k}}'}-\mathcal{E}_{\underline{q}}) \qquad (D)$$

The matrix elements can be written out immediately using results obtained in the 1st order term:

$$H'_{\underline{q}-M_n,\underline{\bar{k}}'+(M_n-1)} = -(\frac{J}{N})\,e^{i(\underline{q}-\underline{\bar{k}}')R_n}\sqrt{(j-M_n+1)(j+M_n)}$$

$$H'_{\underline{\bar{k}}+(M_n-1),\underline{q}-M_n} = -(\frac{J}{N})\,e^{i(\underline{\bar{k}}-\underline{q})R_{n'}}\sqrt{(j-M_n+1)(j+M_n)}$$

So equation (D) becomes

$$2\,\frac{2\pi}{\hbar}\,\delta(\mathcal{E}_{\underline{\bar{k}}}-\mathcal{E}_{\underline{\bar{k}}'})\,(-\frac{J}{N})^3\sum_n M_n(j+M_n)(j-M_n+1)\sum_{\underline{q}} f^{\circ}_{\underline{q}}\,/\,(\mathcal{E}_{\underline{q}}-\mathcal{E}_{\underline{\bar{k}}'}) \qquad (D')$$

So the total contribution due to these 4 processes is given by (A') + (B') + (C') + (D'), apart from the common factor $\frac{2\pi}{\hbar}\,\delta(\mathcal{E}_{\underline{\bar{k}}}-\mathcal{E}_{\underline{\bar{k}}'})$,

$$2(-\frac{J}{N})^3\sum_{\underline{n}} M_n^3\sum_{\underline{q}}(1-f^{\circ}_{\underline{q}})/(\mathcal{E}_{\underline{\bar{k}}}-\mathcal{E}_{\underline{q}}) - 2(-\frac{J}{N})^3\sum_n M_n^3\sum_{\underline{q}} f^{\circ}_{\underline{q}}/(\mathcal{E}_{\underline{q}}-\mathcal{E}_{\underline{\bar{k}}'})$$

$$+2\left(-\frac{J}{N}\right)^3 \sum_n M_n(j-M_n)(j+M_n+1) \sum_{\underline{q}} (1-f^\circ_{\underline{q}})/(\mathcal{E}_{\underline{k}} - \mathcal{E}_{\underline{q}}) -$$

$$2\left(-\frac{J}{N}\right)^3 \sum_n M_n(j+M_n)(j-M_n+1) \sum_{\underline{q}} f^\circ_{\underline{q}}/(\mathcal{E}_{\underline{q}} - \mathcal{E}_{\underline{k}'}) \qquad (3\text{-}3\text{-}3\text{-}1')$$

The first and second terms in (3-3-3-1′) were obtained originally with the help of the Fermi distribution function, eg the first term is possible only if state $|\underline{q}+\rangle$ has a probability of being unoccupied, that is $(1-f^\circ_{\underline{q}}) \neq 0$. Hence the expression involves $f^\circ_{\underline{q}}$. Combining these 2 terms and noting that $\mathcal{E}_{\underline{k}} = \mathcal{E}_{\underline{k}'}$, we obtain

$$2\left(-\frac{J}{N}\right)^3 \sum_n M_n^3 \sum_{\underline{q}} \frac{1}{\mathcal{E}_{\underline{k}} - \mathcal{E}_{\underline{q}}}$$

This expression does not involve the Fermi distribution function $f^\circ_{\underline{q}}$, that is it ignores the Pauli Principle. Remember that these 2 processes do not involve spin flip. This situation is usually encountered when the perturbing system has no internal degree of freedom. They are of the same nature as the corresponding direct transitions in the first order Born terms, so we expect it to contribute a constant term to resistivity. However, this comes from the 2nd order Born approximation which means that its constant contribution to resistivity must be much smaller than the constant contribution due to the first order Born terms. So we shall neglect it.

For the same reason we shall discard the terms which do not involve $f^\circ_{\underline{q}}$ in the third and fourth term of (3-3-3-1′), and we only keep those terms containing $f^\circ_{\underline{q}}$, and so, (3-3-3-1′) becomes

$$4\left(\frac{J^3}{N^3}\right) \sum_n M_n^2 \sum_{\underline{q}} f^\circ_{\underline{q}}/(\mathcal{E}_{\underline{q}} - \mathcal{E}_{\underline{k}}) \text{ with } \sum_n M_n^2 = \frac{1}{3}j(j+1)CN \qquad (3\text{-}3\text{-}3\text{-}1'')$$

Remember the 3rd and 4th terms in (3-3-3-1') involve "spin flip" in the intermediate states. In the 3rd process, the z-component of a localized spin was first increased and then decreased whereas in the 4th process, it was first decreased and then increased. As we stressed before the spin flip operators S+, S- do not have an identical effect and in particular $S+S- \neq S-S+$. It is this non-symmetrical flip of localized spins that give rise to the temperature dependence of resistivity.

Let $$g(\mathcal{E}) = \frac{1}{N} \sum_{\underline{q}} f^{\circ}_{\underline{q}} / (\mathcal{E}_{\underline{q}} - \mathcal{E}) \qquad (3\text{-}3\text{-}3\text{-}1''')$$

then equation (3-3-3-1") becomes

$$4 \frac{J^3}{N} \frac{1}{3} j(j+1) C \, g(\mathcal{E})$$

so the 2nd order Born terms in this transition become (from (3-3-1-2))

$$W(\underline{k}+ \rightarrow \underline{k}'+) = \{2\pi J^2 \, j(j+1) C / 3\hbar N\} \, 4J \, g(\mathcal{E}_{\underline{k}}) \, \delta(\mathcal{E}_{\underline{k}} - \mathcal{E}_{\underline{k}'}) \qquad (3\text{-}3\text{-}3\text{-}1)$$

Case II $|\underline{k}-\rangle \rightarrow |\underline{k}'-\rangle$ transition

There is nothing physically new in this case. One only needs to repeat all the calculations and it turns out that an identical result is obtained for the transition probability.

Case III $|\underline{k}+\rangle \rightarrow |\underline{k}'-\rangle$ transition

In this process in which the electron with $|\underline{k}+\rangle$ is scattered to the state $|\underline{k}'-\rangle$ while the n^{th} spin of the impurity atom increases its z-component by unity from M_n to M_n+1. The transition may also be achieved by the following four processes.

Process 1 The state of the electron is first changed from $|\underline{k}+\rangle$ to $|\underline{q}-\rangle$, the z-component spin of the n^{th} impurity atom being increased from M_n to M_n+1, and then the electron is scattered from $|\underline{q}-\rangle$ to $|\underline{k}'-\rangle$, while the impurity spin remains unchanged in the last transition.

$$\begin{array}{ccccc} |\underline{k}+\rangle & \longrightarrow & |\underline{q}-\rangle & \longrightarrow & |\underline{k}'-\rangle \\ |j,M_n\rangle & & |j,(M_n+1)\rangle & & |j,(M_n+1)\rangle \end{array}$$

Process 2 One of the occupied states, denoted by $|\underline{q}-\rangle$ is changed to $|\underline{k}'-\rangle$ with the z-component of the localized spin being unchanged. Then the electron with $|\underline{k}+\rangle$ fills up the empty state $|\underline{q}-\rangle$, while the z-component localized spin is increased by unity.

$$\begin{array}{ccccc} |\underline{q}-\rangle & \longrightarrow & |\underline{k}'-\rangle & \longrightarrow & |\underline{k}'-\rangle \\ |j,M_n\rangle & \longrightarrow & |j,M_n\rangle & \longrightarrow & |j,(M_n+1)\rangle \\ & & |\underline{k}+\rangle & & \end{array}$$

(1st transition: $|\underline{q}-\rangle \to |\underline{k}'-\rangle$, $|j,M_n\rangle \to |j,M_n\rangle$; 2nd transition: $|j,M_n\rangle \to |j,(M_n+1)\rangle$, $|\underline{k}+\rangle \to |\underline{q}-\rangle$; final state: $|\underline{k}'-\rangle$, $|j,(M_n+1)\rangle$)

Process 3 The electron with $|\underline{k}+\rangle$ is scattered to the unoccupied state $|\underline{q}+\rangle$, all the z-component of the localized spin being unchanged, and then to the state $|\underline{k}'-\rangle$, M_n being increased by unity.

$$\begin{array}{ccccc} |\underline{k}+\rangle & \longrightarrow & |\underline{q}+\rangle & \longrightarrow & |\underline{k}'-\rangle \\ |j,M_n\rangle & & |j,M_n\rangle & & |j,(M_n+1)\rangle \end{array}$$

Process 4 One of the occupied states $|\underline{q}+\rangle$ is changed to state $|\underline{k}'-\rangle$ M_n being increased by unity. Then the electron with $|\underline{k}+\rangle$ is scattered to the empty state $|\underline{q}+\rangle$, all the z-component of the localized spin being unchanged.

$$\begin{array}{ccccc} |\underline{q}+\rangle & \xrightarrow[\text{1st transition}]{} & |\underline{k}'-\rangle & \longrightarrow & |\underline{k}'-\rangle \\ |j,M_n\rangle & \longrightarrow & |j,(M_n+1)\rangle & \longrightarrow & |j,(M_n+1)\rangle \\ & & |\underline{k}+\rangle & & \end{array}$$

(2nd transition: $|j,(M_n+1)\rangle \to |j,(M_n+1)\rangle$, $|\underline{k}+\rangle \to |\underline{q}+\rangle$; final state: $|\underline{k}'-\rangle$, $|j,(M_n+1)\rangle$)

The total transition probability for all these processes is calculated by summing over all the impurities in exactly the same way as before and found to be

$$W(\bar{k}+\rightarrow\bar{k}'-) = \{4\pi J^2 j(j+1)\, C/3\hbar N\}\, 4J\, g(\varepsilon_{\underline{k}})\, \delta(\varepsilon_{\bar{k}} - \varepsilon_{\bar{k}'}) \quad (3\text{-}3\text{-}3\text{-}2)$$

The transition probability in this case is twice that of case I.

Case IV $|\bar{k}-\rangle \rightarrow |\bar{k}'+\rangle$ transition

Similar calculations give the total transition probability which is the same as in case III.

3.3.4 A Summary of Results

We have calculated the transition probability up to the 2nd order Born approximation. Replace the notation j by S, $\bar{k}$ by $\underline{k}$ and $\bar{k}'$ by $\underline{k}'$ in equation (3-3-2-1), (3-3-3-1) and (3-3-2-2), (3-3-3-2) to give the same form as the Kondo equation. For transition without spin flip (Case I or II in 3.3.2 and 3.3.3)

$$W(\underline{k}\pm\rightarrow\underline{k}'\pm) = 2\pi J^2 S(S+1)C/3\hbar N[1+4J\, g(\varepsilon_{\underline{k}})]\, \delta(\varepsilon_{\underline{k}} - \varepsilon_{\underline{k}'}) \quad (3\text{-}3\text{-}4\text{-}1)$$

For transition with spin flip (Case III or IV in 3.3.2 and 3.3.3)

$$W(\underline{k}\pm\rightarrow\underline{k}'\mp) = 4\pi J^2 S(S+1)C/3\hbar N\,[1+4J\, g(\varepsilon_{\underline{k}})]\, \delta(\varepsilon_{\underline{k}} - \varepsilon_{\underline{k}'}) \quad (3\text{-}3\text{-}4\text{-}2)$$

3.3.5 Calculation for the Temperature Dependence of Resistivity

When the state $\underline{k}\pm$ is occupied and $\underline{k}'\pm$ is empty, the rate of change of distribution function $f^{\pm}_{\underline{k}}$ due to scattering is given by equation (1-3-2)

$$\left(\frac{\partial f^{\pm}_{\underline{k}}}{\partial t}\right)_{coll} = \sum_{\underline{k}'} [f^{\pm}_{\underline{k}'}(1-f^{\pm}_{\underline{k}}) - f^{\pm}_{\underline{k}}(1-f^{\pm}_{\underline{k}'})]\, W(\underline{k}\pm\rightarrow\underline{k}'\pm)$$

$$+ \sum_{\underline{k}'} \left[f^{\pm}_{\underline{k}'} \left(1 - f^{\mp}_{\underline{k}}\right) - f^{\mp}_{\underline{k}} \left(1 - f^{\pm}_{\underline{k}'}\right) \right] W\left(\underline{k}\,\pm \rightarrow \underline{k}'\,\mp\right)$$

$$= \sum_{\underline{k}'} \left(f^{\pm}_{\underline{k}'} - f^{\pm}_{\underline{k}} \right) W\left(\underline{k}\,\pm \rightarrow \underline{k}'\,\pm\right) + \sum_{\underline{k}'} \left(f^{\mp}_{\underline{k}'} - f^{\pm}_{\underline{k}} \right) W\left(\underline{k}\,\pm \rightarrow \underline{k}'\,\mp\right) \quad (3\text{-}3\text{-}5\text{-}1)$$

When the electric field E is applied along x' direction, $f^{\pm}_{\underline{k}}$ may be expressed by

$$f^{\pm}_{\underline{k}} = f^{\circ}_{\underline{k}} - E\, \mathbf{k}_{x'}\, \Phi\left(\mathcal{E}_{\underline{k}}\right)$$

As mentioned before, the transition is possible only if $\mathcal{E}_{\underline{k}} = \mathcal{E}_{\underline{k}'}$

hence $$f^{\circ}_{\underline{k}} = f^{\circ}_{\underline{k}'} = 1 \Big/ \left(e^{\frac{\mathcal{E}_{\underline{k}} - \mathcal{E}_F}{kT}} + 1 \right)$$

consider 1st term in (3-3-5-1)

$$\sum_{\underline{k}'} W\left(\underline{k}\,\pm \rightarrow \underline{k}'\,\pm\right) \left(f^{\pm}_{\underline{k}'} - f^{\pm}_{\underline{k}} \right) = \sum_{\underline{k}'} W\left(\underline{k}\,\pm \rightarrow \underline{k}'\,\pm\right) \left(f^{\pm}_{\underline{k}'} - f^{\circ}_{\underline{k}} + f^{\circ}_{\underline{k}} - f^{\pm}_{\underline{k}} \right)$$

$$= -\sum_{\underline{k}'} W\left(\underline{k}\,\pm \rightarrow \underline{k}\,\pm\right) \left(f^{\pm}_{\underline{k}} - f^{\circ}_{\underline{k}} \right) + \sum_{\underline{k}'} W\left(\underline{k}\,\mp \rightarrow \underline{k}'\,\pm\right) \left(f^{\pm}_{\underline{k}'} - f^{\circ}_{\underline{k}} \right)$$

But the 2nd term in the above equation

$$\sum_{\underline{k}'} W\left(\underline{k}\,\pm \rightarrow \underline{k}'\,\pm\right) \left(f^{\pm}_{\underline{k}'} - f^{\circ}_{\underline{k}} \right) = \sum_{\underline{k}'} W\left(\underline{k}\,\pm \rightarrow \underline{k}'\,\pm\right) \left(f^{\circ}_{\underline{k}'} - E\, \mathbf{k}_{x'}\, \Phi\left(\mathcal{E}_{\underline{k}'}\right) - f^{\circ}_{\underline{k}} \right)$$

$$= -\sum_{\underline{k}'} W\left(\underline{k}\,\pm \rightarrow \underline{k}'\,\pm\right) E\, \mathbf{k}_{x'}\, \Phi\left(\mathcal{E}_{\underline{k}'}\right) = 0$$

The reason is: (1) for each $\mathbf{k}_{x'}$, there is an $-\mathbf{k}_{x'}$

(2) Transition probability $W\left(\underline{k}\,\pm \rightarrow \underline{k}'\,\pm\right) = W\left(\underline{k}\,\pm \rightarrow -\underline{k}'\,\pm\right)$

(3) $\mathcal{E}_{k'} \propto \left(-\underline{k}'\right)^2 = k'^2$

Therefore 1st term in (3-3-5-1) becomes

$$-\sum_{\underline{k}'} W\left(\underline{k}\,\pm \rightarrow \underline{k}'\,\pm\right) \left(f^{\pm}_{\underline{k}} - f^{\circ}_{\underline{k}} \right)$$

Similarly for 2nd term in (3-3-5-1), so (3-3-5-1) becomes

$$\left(\frac{\partial f_{\underline{k}}^{\pm}}{\partial t}\right)_{coll} = -(f_{\underline{k}}^{\pm} - f_{\underline{k}}^{\circ}) \sum_{\underline{k}'} [W(\underline{k}^{\pm} \rightarrow \underline{k}'^{\pm}) + W(\underline{k}^{\pm} \rightarrow \underline{k}'^{\mp})] \quad (3\text{-}3\text{-}5\text{-}2)$$

Now from general theory of scattering mechanism, ie equation (1-3-4)

we have $$\left(\frac{\partial f_{\underline{k}}^{\pm}}{\partial t}\right)_{coll} = -\frac{f_{\underline{k}}^{\pm} - f_{\underline{k}}^{\circ}}{\tau_{\underline{k}}}$$

so $$\frac{1}{\tau_{\underline{k}}} = \sum_{\underline{k}'} [W(\underline{k}^{\pm} \rightarrow \underline{k}'^{\pm}) + W(\underline{k}^{\pm} \rightarrow \underline{k}'^{\mp})]$$

gives the value for the relaxation time $\tau_{\underline{k}}$. Substitute equation (3-3-4-1) and (3-3-4-2) for transition probability

$$\frac{1}{\tau_{\underline{k}}} = \frac{6\pi J^2 S(S+1)C}{3\hbar N} [1 + 4J\, g(\mathcal{E}_{\underline{k}})] \sum_{\underline{k}'} \delta(\mathcal{E}_{\underline{k}} - \mathcal{E}_{\underline{k}'})$$

$$= \frac{6\pi J^2 S(S+1)C}{3\hbar N_o} [1 + 4J\, g(\mathcal{E}_{\underline{k}})] \frac{1}{V} \sum_{\underline{k}'} \delta(\mathcal{E}_{\underline{k}} - \mathcal{E}_{\underline{k}'})$$

where N_o is the number of atoms per unit volume; V is the volume of the crystal. Consider

$$\frac{1}{V} \sum_{\underline{k}'} \delta(\mathcal{E}_{\underline{k}} - \mathcal{E}_{\underline{k}'}) = \frac{1}{(2\pi)^3} \int_0^{\infty} \delta(\mathcal{E}_{\underline{k}} - \mathcal{E}_{\underline{k}'}) d^3k'$$

$$= \frac{4\pi}{(2\pi)^3} \int_0^{\infty} \delta\left[\frac{\hbar^2}{2m}(k^2 - k'^2)\right] k'^2\, dk'$$

$$= \frac{1}{2\pi^2} \frac{2m}{\hbar^2} \int_0^{\infty} \delta(k^2 - k'^2) k'^2\, dk' \quad (\because \delta(\lambda x) = \tfrac{1}{\lambda}\delta(x) \text{ for } \lambda > 0)$$

$$= \frac{m}{\pi^2\hbar^2} \frac{1}{2k} \int_0^{\infty} [\delta(k-k') + \delta(k+k')] k'^2 dk' \quad (\because \delta(a^2 - x^2) = \tfrac{1}{2a}[\delta(a-x) + \delta(a+x)] \text{ for } a > 0)$$

$$= \frac{m}{2\pi^2\hbar^2 k} k^2 = \frac{mk}{2\pi^2\hbar^2}$$

$$(\because \int_0^{\infty} k'^2 \delta(k-k') dk' = k^2 \quad \text{and}$$

$\int_0^\infty k'^2\,\delta(k+k')dk' = \int_0^\infty k'^2\,\delta[k'-(-k)]dk' = 0$ as k' is positive, so it $\neq -k$)

$$\therefore \frac{1}{\tau_{\underline{k}}} = \frac{\pi W^2 S(S+1)C}{\hbar} \frac{mk}{N_o \pi^2 \hbar^2} [1+4J\, g(\mathcal{E}_{\underline{k}})]$$

Let z = number of conduction electrons per atom = n/N_o

where n = number of conduction electrons per unit volume = $\frac{(2m)^{3/2}}{3\pi^2\hbar^3}\mathcal{E}_F^{3/2} = \frac{2}{3}\frac{k_o^3}{2\pi^2}$

As the majority of conduction electrons are at the Fermi surface, we can replace k by k_o; then

$$\frac{mk_o}{N_o \pi^2 \hbar^2} = \frac{2m}{N_o k_o \hbar^2}\frac{k_o^3}{2\pi^2} = \frac{3n}{2N_o \mathcal{E}_F} = \frac{3z}{2\mathcal{E}_F}$$

finally $$\frac{1}{\tau_{\underline{k}}} = \frac{3\pi z J^2 S(S+1)C}{2\mathcal{E}_F \hbar}[1 + 4J\, g(\mathcal{E}_{\underline{k}})] \qquad (3\text{-}3\text{-}5\text{-}3)$$

where $g(\mathcal{E}_{\underline{k}})$ is a function of energy given by equation (3-3-3-1"')

We shall now examine the limiting case of $g(\mathcal{E}_{\underline{k}})$ when temperature T is at absolute zero, and hence investigate the dependence of the transition probability on the energy of the initial state $\mathcal{E}_{\underline{k}}$, which is entirely contained in the function $g(\mathcal{E}_{\underline{k}})$

At $T = 0$, $f^\circ_{\underline{q}} = 1$ for $\underline{q} < \underline{k}_o$ and $f^\circ_{\underline{q}} = 0$ for $\underline{q} > \underline{k}_o$

then equation (3-3-3-1"') becomes

$$g(\mathcal{E}_{\underline{k}}) = \frac{1}{N} \sum_{\substack{\text{sum up to} \\ \underline{q} = \underline{k}_o}} \frac{1}{\mathcal{E}_{\underline{q}} - \mathcal{E}_{\underline{k}}}$$

Assuming free electron $\mathcal{E}$-$\underline{k}$ relationship $\mathcal{E}_{\underline{k}} = \frac{\hbar^2 k^2}{2m}$

$$g(\varepsilon_{\underline{k}}) = \frac{1}{N_o}\left(\frac{1}{V}\sum_{\underline{q}}^{k_o} \frac{1}{\underline{q}^2 - \underline{k}^2}\right)\frac{2m}{\hbar^2}$$

Considering the V to be large, we see that $\underline{q}$ may be regarded as a continuous variable and the summation may be replaced by an integral by the well known procedure: $\frac{1}{V}\sum_{\underline{q}} \rightarrow \frac{1}{(2\pi)^3}\int d^3\underline{q}$

$$g(\varepsilon_{\underline{k}}) = \frac{2m}{N_o\hbar^2}\frac{1}{(2\pi)^3}\int_o^{k_o} \frac{1}{\underline{q}^2-\underline{k}^2} d^3q = \frac{2m}{N_o\hbar^2}\frac{1}{(2\pi)^3} 4\pi\int_o^{k_o} \frac{q^2\,dq}{q^2-k^2}$$

$$= \frac{m}{\pi^2 N_o\hbar^2}\left(k_o + \frac{k}{2}\ln\left|\frac{k-k_o}{k+k_o}\right|\right) = \frac{mk_o}{\pi^2 N_o\hbar^2}\left(1 + \frac{k}{2k_o}\ln\left|\frac{k-k_o}{k+k_o}\right|\right)$$

$$= \frac{k_o^3}{2\pi^2 N_o\varepsilon_F}\left(1+\frac{k}{2k_o}\ln\left|\frac{k-k_o}{k+k_o}\right|\right) = \frac{3}{2}\frac{n}{N_o\varepsilon_F}\left(1 + \frac{k}{2k_o}\ln\left|\frac{k-k_o}{k+k_o}\right|\right)$$

$$= \frac{3}{2}\frac{z}{\varepsilon_F}\left(1 + \frac{k}{2k_o}\ln\left|\frac{k-k_o}{k+k_o}\right|\right) \qquad \text{for } T=0 \qquad (3\text{-}3\text{-}5\text{-}4)$$

The function $g(\varepsilon_{\underline{k}})$ has a logarithmic singularity at $k = k_o$. This is introduced by taking the step function as the distribution function at T=0, and so $g(\varepsilon_{\underline{k}})$ diverges when $\varepsilon_{\underline{k}}$ appraoches ε_F. This divergence arises from neglecting the energy of the localized magnetic impurity system. Therefore when considering s-d interaction at or near absolute zero, the exchange interaction between the localized impurity spins and the anisotropy energy for the direction of the spin relative to the crystalline axes needs to be taken into account. However, when we consider interaction for a temperature range somewhat higher than absolute zero, equation (3-3-3-1"') will not cause divergence trouble.

We can still see from equation (3-3-5-4) and the expressions for the transition probability (3-3-4-1) and (3-3-4-2) that if the interaction coupling strength J is negative, the transition probability W increases when an electron approaches the Fermi surface, since the average of $|k-k_0|$ for thermally excited electrons is proportional to T for $T \neq 0$. We can see that at finite temperature the transition probability will be proportional to ln T, and so we expect resistivity due to spin-spin interaction should have a term proportional to ln T.

From the standard theory, the conductivity is given by equation (1-3-14)

$$\sigma = -\frac{e^2}{12\pi^3}\int \tau_{\underline{k}} v_{\underline{k}}^2 \frac{df_{\underline{k}}^{\circ}}{d\varepsilon_{\underline{k}}} d^3k$$

The resistivity is the inverse of σ

$$\rho = \frac{1}{\sigma} = -\frac{12\pi^3}{e^2} \frac{1}{\int \tau_{\underline{k}} v_{\underline{k}}^2 \frac{df_{\underline{k}}}{d\varepsilon_{\underline{k}}} d^3k}$$

$\tau_{\underline{k}}$ is given by equation (3-3-5-3)

$$\tau_{\underline{k}} = \left[\frac{3\pi z J^2 S(S+1) C}{2\varepsilon_F \hbar}\right]^{-1} (1+4J\, g(\varepsilon_{\underline{k}}))^{-1} \approx \left[C\rho_M \frac{e^2 z}{m} \frac{N}{V}\right]^{-1} (1-4Jg(\varepsilon_{\underline{k}}))$$

$$= \left[C\rho_M \frac{e^2 n}{m}\right]^{-1} (1-4J\, g(\varepsilon_{\underline{k}}))$$

where $z = n/(\frac{N}{V})$; $\qquad \rho_M = \frac{3\pi m J^2 S(S+1)}{2e^2\hbar\varepsilon_F} \frac{V}{N}$ (3-3-5-5)

$$\therefore \rho \approx -\frac{C\rho_M 12\pi^3 n}{m} \frac{1}{\int (1-4J\, g(\varepsilon_{\underline{k}})) v_{\underline{k}}^2 \frac{df_{\underline{k}}}{d\varepsilon_{\underline{k}}} d^3k}$$

$$= -C\rho_M \frac{12\pi^3 n}{m} \frac{1}{A - 4J\int v_{\underline{k}}^2 g(\varepsilon_{\underline{k}}) \frac{df_{\underline{k}}}{d\varepsilon_{\underline{k}}} d^3k}$$

$$= -c\rho_M \frac{12\pi^3 n}{m} \frac{1}{A}\left[\frac{1}{1-(4J/A)\int v_{\underline{k}}^2 g(\varepsilon_{\underline{k}}) \frac{df_{\underline{k}}}{d\varepsilon_{\underline{k}}} d^3k}\right] \text{ where } A = \int v_{\underline{k}}^2 \frac{df_{\underline{k}}}{d\varepsilon_{\underline{k}}} d^3k$$

$$\approx -c\rho_M \frac{12\pi^3 n}{m} \frac{1}{A}\left[1+(4J/A)\int v_{\underline{k}}^2 g(\varepsilon_{\underline{k}}) \frac{df_{\underline{k}}}{d\varepsilon_{\underline{k}}} d^3k\right] \text{ suppose } A \gg 4J\int v_{\underline{k}}^2 g(\varepsilon_{\underline{k}}) \frac{df_{\underline{k}}}{d\varepsilon} d^3k$$

To evaluate A:

$$\text{as } d^3k = 4\pi k^2 dk = 4\pi k^2 \frac{m}{\hbar^2 k} d\varepsilon = \frac{4\pi\sqrt{2m}\, m}{\hbar^3} \varepsilon^{\frac{1}{2}} d\varepsilon$$

$$A = \int_0^\infty v_{\underline{k}}^2 \frac{df_{\underline{k}}}{d\varepsilon_{\underline{k}}} d^3k = \frac{8\pi\sqrt{2m}}{\hbar^3} \int_0^\infty \varepsilon^{3/2} \frac{df}{d\varepsilon} d\varepsilon$$

We consider $\frac{df}{d\varepsilon}$ to behave as a δ function at ε_F, ie $\frac{df}{d\varepsilon} \sim -\delta(\varepsilon - \varepsilon_F)$

$$\therefore A \approx -\frac{8\pi\sqrt{2m}}{\hbar^3} \varepsilon_F^{3/2} = -\frac{12\pi^3 n}{m}$$

$$\text{then } \rho \simeq c\rho_M \left[1 - \frac{4Jm}{12\pi^3 n} v_{\varepsilon_F}^2 \int g(\varepsilon_{\underline{k}}) \frac{df_{\underline{k}}}{d\varepsilon_{\underline{k}}} d^3k\right] \text{ (as in the case for } \tau_{\underline{k}})$$

$$= c\rho_M \left[1 - \frac{4Jm}{12\pi^3} \frac{3\pi^2\hbar^3}{(2m)^{3/2}\varepsilon_F^{3/2}} \frac{2\varepsilon_F}{m} \int g(\varepsilon_{\underline{k}}) \frac{df_{\underline{k}}}{d\varepsilon_{\underline{k}}} d^3k\right]$$

$$= c\rho_M \left[1 - (\hbar^2 J/\pi m k_o) \int g(\varepsilon_{\underline{k}}) \frac{df_{\underline{k}}}{d\varepsilon_{\underline{k}}} d^3k\right] \quad (3\text{-}3\text{-}5\text{-}6)$$

Using equation (3-3-3-1"') for $g(\varepsilon_{\underline{k}})$, the integral in (3-3-5-6) becomes

$$\int \sum_{\underline{k}'} \frac{1}{N} \frac{f^\circ_{\underline{k}'}}{\varepsilon_{\underline{k}'} - \varepsilon_{\underline{k}}} \frac{df^\circ_{\underline{k}}}{d\varepsilon_{\underline{k}}} d^3k = \frac{V}{(2\pi)^3 N} \iint \frac{f^\circ_{\underline{k}'}}{\varepsilon_{\underline{k}'} - \varepsilon_{\underline{k}}} \frac{df^\circ_{\underline{k}}}{d\varepsilon_{\underline{k}}} d^3k\, d^3k'$$

$$= -\frac{4m^3 V}{\pi N\hbar^6} \iint \frac{(\varepsilon_{\underline{k}}\varepsilon_{\underline{k}'})^{\frac{1}{2}}}{\varepsilon_{\underline{k}'} - \varepsilon_{\underline{k}}} f^\circ_{\underline{k}} \frac{df^\circ_{\underline{k}'}}{d\varepsilon_{\underline{k}'}} d\varepsilon_{\underline{k}} d\varepsilon_{\underline{k}'}$$

$$= -\frac{8m^3 V \varepsilon_F}{\pi N\hbar^6} - \frac{4m^3 V\varepsilon_F}{\pi N\hbar^6} \iint \ln\left|\frac{\sqrt{\varepsilon_{\underline{k}}} - \sqrt{\varepsilon_{\underline{k}'}}}{\sqrt{\varepsilon_{\underline{k}}} + \sqrt{\varepsilon_{\underline{k}'}}}\right| \frac{df^\circ}{d\varepsilon_{\underline{k}}} \frac{df^\circ}{d\varepsilon_{\underline{k}'}} d\varepsilon_{\underline{k}} d\varepsilon_{\underline{k}'}$$

(3-3-5-7)

The integral in the last term is calculated as follows:

$$\iint \ln\left|\frac{\varepsilon_k - \varepsilon_{k'}}{\varepsilon_k + \varepsilon_{k'} + 2\sqrt{\varepsilon_k \varepsilon_{k'}}}\right| \frac{df^\circ}{d\varepsilon_k} \frac{df^\circ}{d\varepsilon_{k'}} d\varepsilon_k \, d\varepsilon_{k'} =$$

$$\iint \ln\left|\frac{\varepsilon_k - \varepsilon_{k'}}{4\varepsilon_F}\right| \frac{df^\circ}{d\varepsilon_k} \frac{df^\circ}{d\varepsilon_{k'}} d\varepsilon_k \, d\varepsilon_{k'}$$

$$= \iint \ln\left|\varepsilon_k - \varepsilon_{k'}\right| \frac{df^\circ}{d\varepsilon_k} \frac{df^\circ}{d\varepsilon_{k'}} d\varepsilon_k d\varepsilon_{k'} - \iint \ln 4\left|\varepsilon_F\right| \frac{df^\circ}{d\varepsilon_k} \frac{df^\circ}{d\varepsilon_{k'}} d\varepsilon_k \, d\varepsilon_{k'} = A - B$$

where $f = 1/\left(e^{\frac{\varepsilon-\varepsilon_F}{kT}} + 1\right)$, let $x = \frac{\varepsilon - \varepsilon_F}{kT}$, $kT\,dx = d\varepsilon$

then $\ln\left|\varepsilon_k - \varepsilon_{k'}\right| \frac{df}{d\varepsilon_k} \frac{df}{d\varepsilon_{k'}} d\varepsilon_k \, d\varepsilon_{k'} = \ln\left|(x-x')kT\right| \frac{dF(x)}{dx} \frac{dF(x')}{dx'} dx\, dx'$

$$= \ln\left|x-x'\right| \frac{dF(x)}{dx} \frac{dF(x')}{dx'} dx\, dx' + (\ln kT) \frac{dF(x)}{dx} \frac{dF(x')}{dx'} dx\, dx'$$

where $F(x) = \frac{1}{e^x + 1}$

$$A = \iint_{\varepsilon_F/kT}^{\infty} \ln\left|x-x'\right| \frac{dF(x)}{dx} \frac{dF(x')}{dx'} dx\, dx' + \ln kT \iint_{-\varepsilon_F/kT}^{\infty} \frac{dF(x)}{dx} \frac{dF(x')}{dx'} dx\, dx'$$

$$= A_1 + A_2$$

In metal $\varepsilon_F \gg kT$, so

$A_1 = \int_{-\infty}^{\infty}\int \ln\left|x-x'\right| \frac{dF(x)}{dx} \frac{dF(x')}{dx'} dx\, dx'$ is temperature independent

$$A_2 = \ln kT \int_{-\infty}^{\infty}\int \frac{dF(x)}{dx} \frac{dF(x')}{dx'} dx\, dx' = (\ln T + \ln K)\left[F(x)\, F(x')\right]_{-\infty}^{\infty} = \ln T + \ln K$$

$$B = \ln 4\left|\varepsilon_F\right| \int_{-\infty}^{\infty}\int \frac{dF(x)}{dx} \frac{dF(x')}{dx'} dx\, dx' = \ln 4\left|\varepsilon_F\right|$$

So the integral in (3-3-5-7) = A - B = const + ln T

and (3-3-5-6) becomes

$$\rho = c\rho_M \left\{1 - \hbar^2 J/\pi m k_o \left[-\frac{8m^3 v \varepsilon_F}{\pi N \hbar^6} - \left(\frac{4m^3 v \varepsilon_F}{\pi N \hbar^6}\right)(\text{const} + \ln T)\right]\right\}$$

$$= c\rho_M \left[1 + X + Y(\text{const} + \ln T)\right] \qquad (3\text{-}3\text{-}5\text{-}8)$$

where $X = \frac{\hbar^2 J}{\pi m k_o} \frac{8m^3 V \mathcal{E}_F}{\pi N \hbar^6} = \frac{8m^2 V \mathcal{E}_F J}{\pi^2 \hbar^4 N (2m)^{\frac{1}{2}} \mathcal{E}_F^{\frac{1}{2}} \hbar} = 6 \frac{J}{\mathcal{E}_F} \frac{n}{(N/V)} = 6 \frac{zJ}{\mathcal{E}_F}$

$$Y = \frac{\hbar^2 J}{\pi m k_o} \left(\frac{4m^3 V \mathcal{E}_F}{\pi N \hbar^6}\right) = \frac{(2m)^2 \mathcal{E}_F^2 J}{\pi^2 \hbar^4 N_o k_o \mathcal{E}_F} = \frac{k_o^3 J}{\pi^2 N_o \mathcal{E}_F} = 3 \frac{nJ}{N_o \mathcal{E}_F} = \frac{3zJ}{\mathcal{E}_F}$$

Neglect the 2 temperature independent terms in (3-3-5-8) which are of the order of $J/\mathcal{E}_F$ and we finally obtain the Kondo formula

$$\rho_{spin} = C\rho_M [1 + (3zJ/\mathcal{E}_F) \ln T] \qquad (3\text{-}3\text{-}5\text{-}9)$$

3.3.6 A Comment on the Physics of Resistivity Minimum

From Kondo's theory, we have

$$\rho = C \rho_M [1 + (3zJ/\mathcal{E}_F) \ln T]$$

If J is negative, ρ decreases as T increases for the temperature range where $C \rho_M > \left|(C \rho_M 3zJ/\mathcal{E}_F) \ln T\right|$

According to P.W. Anderson, this may be seen in the following way. In the general theory of ferromagnetism and antiferromagnetism, one may assume as part of the Hamiltonian a spin-spin interaction term between the i^{th} and j^{th} atoms to be

$$- J \underline{S}_i \cdot \underline{S}_j$$

Then it is known that a positive J value leads to a parallel alignment of the spins, hence ferromagnetism while a negative J value causes an antiparallel alignment of spins, hence antiferromagnetism.

Returning now to our spin-spin interaction in Kondo's theory. We can similarly imagine that a negative J value means antiferromagnetic

interaction between the impurities and the electrons. Hence electrons surrounding an impurity will have a spin opposite to that of the impurity. The electrons themselves however have parallel spin and hence they tend to spin-flip more. In the words of Anderson "the spin pulls electrons of opposite spin closer to itself so that they can then spin-flip scatter more easily". Recalling that processes with change of spin contribute to the major part of the transition probability, more spin-flip means more scattering which in turn implies higher resistance. Now as temperature increases, one expects that the anti-ferromagnetic effect decreases due to more thermal agitation. Therefore the spin-flip scattering decreases and hence a lowering of resistance. As T gets higher still, other scattering mechanisms, eg lattice scattering will become dominant and one expects ρ will increase again as T increases. So a resistivity minimum appears.

CHAPTER IV

Experimentation I - Thermometry

4.1 Introduction

To investigate the electrical, thermoelectric and thermomagnetic properties of PbS with temperature, we need first of all suitable thermometers for temperature measurements. The Au(0.03%Fe) - chromel thermocouple is found most adequate for the purpose. It has the advantage that the thermocouple junction has a small heat capacity, so it gives a fast response to temperature change and allows measurement of temperature at a local point. It is also sensitive enough in the required low temperature region.

We started our project with the calibration of the thermocouple. The Au (0.03% Fe)-chromel couple was calibrated against a platinum resistance thermometer, so the Pt resistance thermometer needs to be calibrated first.

The calibration of thermometers was carried out in collaboration with Dr. A.M. Forrest. The experiments and calculations were, however, done by the author. A paper "A platinum resistance thermometer calibration between 2°K and 273.15°K" was published jointly with A.M. Forrest in Journal of Scientific Instruments 1968 Series 2 Volume 1. This paper is presented in its original form below.

4.2 Calibration of Pt Resistance Thermometer

1 Introduction

In many laboratories it would be a great convenience to have a single basic temperature reference standard over the range 2–273·15°K which could be calibrated (and subsequently rechecked) without reference to a standards laboratory. In establishing such a standard the degree of accuracy obtainable is obviously of prime importance, but one must distinguish between the accuracy which would be required to set up an International Temperature Scale and an accuracy which would be sufficient for many laboratory purposes. It is our view that, for many experiments, a temperature accuracy to about ±0·05 degK is acceptable, particularly if that accuracy extends over a wide temperature range.

The present paper describes a simple procedure for calibrating a platinum resistance thermometer over the entire temperature range 2–273·15°K. The only pure cryogenic liquid required to effect the calibration is liquid helium, actual calibration measurements being made at the ice point, the boiling point of liquid helium, and in the temperature range 2–4·2°K. We have studied two platinum resistors.

2 Description of the platinum thermometers

Both platinum thermometers were obtained from the Rosemount Engineering Company and will be subsequently referred to as platinum I and platinum II. The wire in platinum I was sealed with glass within a ceramic former. The supporting ceramic tubes in platinum II, a more expensive thermometer, were hermetically sealed in a helium filled platinum sheath.

A calibration was purchased for platinum II; it consists of a temperature-resistance table for every degree between −183°C and 500°C, and a similar table for every tenth of a degree between 10°K and 90°K. The calibration is accurate to better than 0·01 degK in the region between 90°K and 273·15°K. In the region 10–90°K the calibration accuracy is to ±0·05°K. Values for R_0, the resistance at 0°C, and α, δ, β, the constants in the Callendar–Van Dusen equation, were provided with both thermometers. These are listed in table 1 together with the values of $W_{4\cdot2}$, the ratio of the resistance at 4·2°K to that at 273·15°K.

3 Calibration details

3.1 *90–273·15°K; the Callendar–Van Dusen equation*

If the resistance R_t at any temperature t in the region −182·97–0°C (90·18–273·15°K) is known, then that temperature may be calculated from the Callendar–Van Dusen equation

$$\frac{R_t}{R_0}=1+\alpha\left\{t-\delta\left(\frac{t}{100}-1\right)\left(\frac{t}{100}\right)-\beta\left(\frac{t}{100}-1\right)\left(\frac{t}{100}\right)^3\right\}.$$

The calibration data above 90°K supplied with platinum II was calculated by use of the Callendar–Van Dusen equation,

Table 1 The constants in the Callendar-Van Dusen equation and the reduced resistances, $W_{4\cdot2}$

	R_0 (Ω)	α	δ	β	$W_{4\cdot2}$
Platinum I	25·486	0·003923	$1\cdot49_3$	0·11	0·0008208
Platinum II	25·576642	0·0039267	$1\cdot491_4$	$0\cdot109_6$	0·0004421

and a similar calibration for platinum I was computed by using the values of α, δ and β supplied. Such a calibration is particularly important for the present studies because it provides a means for checking the calibration based on the Z function (§ 3.2), which extends below 90°K.

3.2 *12–170°K; the Z function*

Cragoe (1948) initially proposed that a universal 'Z function' of the form

$$Z=\frac{R_T-R_1}{R_2-R_1}$$

could be used to relate resistance to temperature for any platinum resistor. By measuring R_1 at a fixed temperature,

e.g. the boiling point of hydrogen, and R_2 at another fixed temperature, e.g. the boiling point of oxygen, for a platinum thermometer whose R_T variation with temperature is known, the variation of Z with temperature may be tabulated. For high purity material the Z function will be identical for different specimens and hence, once the form of the Z function is established, only measurements of R_1 and R_2 are necessary for the calibration of an uncalibrated thermometer. Suggested improvements on this technique, e.g. Corrucini (1960), Barber (1958), have concerned removal of inaccuracies in temperature of the order of 0·01 degK or less. These improvements usually involve measurement of resistance at more than two fixed points (e.g. at 20, 80 and 273·15°K (Corrucini), or at the boiling points of oxygen, hydrogen and neon (Barber)).

White (1959) has pointed out that in many laboratories helium is the only pure cryogenic liquid conveniently available and he has published a table of Z functions where R_1 is the resistance at 4·2°K and R_2 is the resistance at 273·15°K, i.e. Z is of the form

$$Z = \frac{(R_T - R_{4\cdot2})}{(R_{273\cdot15} - R_{4\cdot2})}.$$

In practice, White's table is not detailed enough and a computer interpolation programme based on an iterated linear interpolation method (Macon 1963) has been used to interpolate between his data points. Table 2 shows some of the results of this calculation. We have also included in table 2 values of the Z function above 170°K, the limit of White's table. These values have been calculated by use of the Callendar–Van Dusen equation to provide R_T. Details of the platinum thermometer calibration which White used to generate his Z function table are given later.

White claims that temperature measurements based on his Z function should be correct to within ±0·05 degK. The validity of this claim will depend on the purity of the platinum and an estimate of this is provided by the ratio $W_{4\cdot2}$. White suggests a maximum value of $W_{4\cdot2}$ of about 0·003 for the Z function calibration to be accurate to ±0·05 degK. This is almost certainly too high and C R Barber (private communication) has suggested that a limit of 0·0008 or 0·0009 would be more realistic. For values of $W_{4\cdot2}$ in excess of this errors would probably be greater than ±0·05 degK.

The use of White's Z-function tabulation above 90°K would be particularly convenient for a platinum resistor about which nothing was initially known, since only two resistance measurements, at 4·2°K and 273·15°K, are required to obtain a calibration. However, in this work, it has been decided to use Callendar–Van Dusen equation in the applicable range, since the constants α, β, δ and R_0 are known. The Z function has been used up to 170°K however, to enable a comparison to be made with the Callendar–Van Dusen equation in the range where they overlap.

3.3 *2–16°K; polynomial fitting*

Kos and Lamarche (1967) have shown that in the region 2–16°K the reduced resistance W_T of a platinum resistor is related to temperature T according to the equation

$$W_T = A + BT + CT^2 + DT^3 + ET^4 + FT^5$$

where A, B, C, D, E, and F are constants. They have used this as a basis for interpolation in the range 4·2–10°K, when calibration data in that range were initially unavailable. This interpolation is accurate to about 0·01 degK.

By use of a Tinsley type 5590 B vernier potentiometer in conjunction with a Keithley 149 millimicrovoltmeter as a null detector, the resistance of both platinum I and platinum II below 4·2°K has been measured as a function of temperature, which was obtained from helium vapour pressure measurements. For platinum I calibration data above 12°K were obtained as described above from Z functions, and for platinum II the calibration from 10°K was supplied. A computer curve fitting program, based on the principle of least squares, was used to fit the available resistance–temperature data from approximately 1·3–16°K. For both platinum I and platinum II the best fit was obtained for a polynomial of degree 4. Unlike the results of Kos and Lamarche, a worse fit was found for a 5 degree polynomial. In the case of platinum II the standard deviation for the 4th degree polynomial was $0{\cdot}313 \times 10^{-6}$ and for the 5th degree polynomial was $0{\cdot}605 \times 10^{-6}$. The difference was not so marked for platinum I ($0{\cdot}235 \times 10^{-6}$ and $0{\cdot}245 \times 10^{-6}$). Table 3 shows the computer calculated reduced resistances, the deviation of these from the experimental measurements and the corresponding temperature deviations for platinum I. Also shown in table 3 are the constants A, B, C, D and E occurring in the polynomial. Above 12°K the deviations of the 'experimental' resistance values from the calculated values represent deviations in temperature of less than 0·01 degK. A better fit was obtained for platinum II. In that case ten points were fitted below 4·2°K and twelve between 10·6°K and 15°K. The maximum resistance deviation at or below 4·2°K was $0{\cdot}52 \times 10^{-6}$ at 4·21°K corresponding to a temperature deviation of about 0·02 degK. Above 10·6°K the resistance deviations all corresponded to temperature deviations of less than 0·01 degK.

Table 2 Values of $Z = \dfrac{(R_T - R_{4\cdot2})}{(R_{273\cdot15} - R_{4\cdot2})}$ for T (°K) = 12·0 : 0·1 : 29·9

	·0	·1	·2	·3	·4	·5	·6	·7	·8	·9
12	0·000509	0·000525	0·000542	0·000559	0·000576	0·000595	0·000613	0·000632	0·000651	0·000671
13	0·000692	0·000712	0·000733	0·000755	0·000777	0·000800	0·000823	0·000847	0·000871	0·000896
14	0·000922	0·000947	0·000974	0·001001	0·001029	0·001057	0·001086	0·001115	0·001145	0·001176
15	0·001208	0·001240	0·001272	0·001305	0·001339	0·001374	0·001409	0·001445	0·001482	0·001519
16	0·001558	0·001596	0·001636	0·001676	0·001717	0·001759	0·001801	0·001844	0·001888	0·001933
17	0·001979	0·002025	0·002072	0·002120	0·002169	0·002218	0·002268	0·002320	0·002372	0·002425
18	0·002479	0·002533	0·002589	0·002645	0·002702	0·002761	0·002820	0·002880	0·002941	0·003003
19	0·003066	0·003129	0·003194	0·003259	0·003326	0·003393	0·003461	0·003531	0·003601	0·003672
20	0·003745	0·003818	0·003892	0·003967	0·004044	0·004121	0·004199	0·004279	0·004359	0·004441
21	0·004523	0·004607	0·004692	0·004778	0·004865	0·004952	0·005041	0·005132	0·005223	0·005315
22	0·005409	0·005503	0·005599	0·005695	0·005793	0·005892	0·005992	0·006093	0·006196	0·006299
23	0·006403	0·006509	0·006616	0·006724	0·006833	0·006943	0·007055	0·007167	0·007281	0·007396
24	0·007512	0·007629	0·007747	0·007866	0·007987	0·008109	0·008232	0·008356	0·008481	0·008608
25	0·008736	0·008864	0·008995	0·009126	0·009258	0·009392	0·009527	0·009663	0·009800	0·009939
26	0·010079	0·010219	0·010362	0·010505	0·010649	0·010795	0·010942	0·011091	0·011240	0·011391
27	0·011543	0·011696	0·011850	0·012005	0·012162	0·012320	0·012479	0·012640	0·012802	0·012964
28	0·013129	0·013294	0·013460	0·013628	0·013797	0·013967	0·014138	0·014311	0·014485	0·014660
29	0·014836	0·015013	0·015192	0·015372	0·015553	0·015735	0·015919	0·016104	0·016290	0·016477

Values of Z for T (°K) = 30·0 : 1·0 : 110·0

	0·0	1·0	2·0	3·0	4·0	5·0	6·0	7·0	8·0	9·0
30	0·016666	0·018616	0·020688	0·022877	0·025183	0·027602	0·030132	0·032768	0·035508	0·038346
40	0·041280	0·044303	0·047414	0·050607	0·053881	0·057230	0·060651	0·064140	0·067694	0·071309
50	0·074982	0·078708	0·082485	0·086309	0·090175	0·094083	0·098027	0·102008	0·106022	0·110069
60	0·114147	0·118253	0·122386	0·126545	0·130726	0·134928	0·139146	0·143379	0·147623	0·151877
70	0·156140	0·160416	0·164701	0·168993	0·173293	0·177599	0·181910	0·186228	0·190552	0·194880
80	0·199215	0·203553	0·207896	0·212244	0·216594	0·220947	0·225301	0·229656	0·234011	0·238366
90	0·242719	0·247069	0·251416	0·255761	0·260101	0·264437	0·268770	0·273098	0·277423	0·281744
100	0·286063	0·290379	0·294693	0·299003	0·303311	0·307615	0·311916	0·316214	0·320509	0·324801
110	0·329090	0·333375	0·337658	0·341938	0·346215	0·350490	0·354761	0·359030	0·363295	0·367558

T (°K)	180·0	200·0	220·0	240·0	260·0	273·15	295·0
Z	0·622939	0·704996	0·786393	0·867200	0·947486	1·00000	1·08681

4 Accuracy

A platinum thermometer with a value of α not less than 0·003920 may be used to realize the International Practical Temperature Scale, by use of the Callendar–Van Dusen equation from −182·97°C to 0°C. In that range, the error in such a temperature measurement, i.e. the deviation from the Thermodynamic Scale, will be less than 0·04 degC.

The International Temperature Scale does not extend below 90·18°K. In this region Rosemount Engineering Company effected the calibration of platinum II by using a 'three fixed point' method described by Corrucini (1960, 1962). Essentially this means the calibration of platinum II is relative to a scale set up in 1939 and maintained by platinum thermometers at the National Bureau of Standards. This 1939 NBS scale, ultimately based on gas thermometry, may deviate from the Thermodynamic Scale by ±0·02 degK. However, Corrucini has shown that calibrations on a group of high purity platinum resistance thermometers using the three fixed point method are internally consistent (and consistent with the 1939 NBS platinum scale) to better than 0·01 degK. Hence the error of ±0·05 degK quoted in the purchased calibration of platinum II in the range below 90°K represents the possible deviation from the Thermodynamic Scale.

White's Z function tabulation is based on the resistance–temperature relationship of a thermometer (T4) initially described by Los and Morrison (1951). T4 was calibrated with reference to an NBS calibrated thermometer. Reference is also made to T4 by Corrucini. On the basis of comparisons made by Corrucini it is clear that the T4 calibration probably deviates from the 1939 NBS scale by less than 0·01 degK. As indicated earlier, White's statement that temperatures may be assessed from his tabulation with an accuracy to ±0·05 degK (deviation presumably from the Thermodynamic Scale) is likely to be true only for a limited class of thermometers with $W_{4\cdot2} < 0\cdot0008$ or 0·0009. The value of $W_{4\cdot2}$ for the thermometer T4 was 0·000453. Barber (private communication) has checked three calibrated platinum thermometers with $W_{4\cdot2}$ ranging from 0·00037 to 0·00072 against White's Z function table and has obtained divergences of less than 0·05 degK in each case.

For a comparison of the Z function calibration with that based on the Callender–Van Dusen equation, a certain temperature T in the overlap region has been considered and the corresponding 'Callendar–Van Dusen resistance' has been noted. This resistance is used to calculate a Z function Z_{CD} which is compared with the value Z_W of the Z function from White's table at the temperature T. An example of this type of comparison at 110·15°K is shown for platinum I and platinum II in table 4, in which are also shown calculated values of $\Delta Z\ (= |Z_{CD} - Z_W|)$ and the corresponding temperature difference ΔT. Similarly, the supplied calibration for platinum II below 90°K has been compared with that based on White's Z function tabulation, and typical comparisons at 13·8°K and 60°K are also shown table 4.

In fact, the difference ΔZ and the corresponding ΔT have been calculated for platinum II at fifteen temperatures roughly 10 degK apart, ranging from 12°K to 170°K. Nowhere in that region does ΔT exceed 0·023 degK, which is consistent with the calibration accuracy claimed for platinum II by the manufacturers and also with the accuracy claimed by White for his Z function tabulation. The only available check on the Z function based calibration of platinum I was the Callendar–Van Dusen equation above 90°K. Z_{CD}, ΔZ and the corresponding ΔT were calculated at intervals of 10 degrees from 90°K to 170°K. At 90°K there was a deviation ΔT of 0·065 degK, which was reduced to 0·06 degK at 100°K, and to 0·05 degK at 110·25°K, thereafter falling steadily to 0·04 degK at 170°K.

It is evident from the work of Kos and Lamarche that the accuracy of their 'interpolated temperatures' in the range 4·2–10°K is about the same as the accuracy of their basic calibration data below 4·2°K and above 10°K. It is likely that the same criterion may be applied to platinum I and platinum II. Of course, there is no available check of the actual accuracy of the platinum I calibration in the region 12–15°K, but the smoothness of the fit of the data below 4·2°K to that above 12°K probably suggests that the accuracy above 12°K is not much worse than ±0·05 degK, certainly less than ±0·1 degK.

5 Conclusion

We have developed a rather simple procedure for calibrating a platinum resistance thermometer over the range 2–273·15°K. From 12–273·15°K the Z function tabulation of White may be used, which only involves actual calibration at the ice-point and at the boiling point of helium. Above 90·18°K the Callendar–Van Dusen equation may also be used to calibrate the platinum resistance thermometer if the constants α, β and δ occurring in that equation are known. Calibration data below 4·2°K can be used in conjunction with such data in the

range 12–15°K as the basis for polynomial fitting which may then provide a calibration in the 4·2–12°K gap.

It is clear from observations on platinum II that the above procedure can achieve an accuracy to ±0·05 degK from 2–273·15°K. However, at the moment there is clearly not enough evidence to indicate whether or not this accuracy will always be achieved for a platinum resistance thermometer with $W_{4\cdot2} < 0\cdot0008$ or 0·0009.

Acknowledgments

We gratefully acknowledge the assistance and advice we have had from Dr D M Finlayson. We are also indebted to Wan Kay-Kong for his help with the computer programming.

References

Barber C R 1958 *P. V. Com. Int. Poids et Mesures* 26A, T58

Corrucini R J 1960 *Rev. Sci. Instrum.* 31 637–40

Corrucini R J 1962 *Temperature, Its Measurement and Control in Science and Industry* (New York: Reinhold) Vol. 3, Part 1, Paper 36

Cragoe 1948 *P. V. Com. Int. Poids et Mesures* 21 T84

Kos J F and Lamarche J L G 1967 *Can. J. Phys.* 45 339–54

Los J M and Morrison J A 1951 *Can. J. Phys.* 29 142–50

Macon N 1963 *Numerical Analysis* (New York: Wiley) chap. 7

White G K 1959 *Experimental Techniques in Low Temperature Physics* (Oxford: University Press) pp. 113–5

Table 3 Polynomial curve fitting for platinum I

Temperature (°K)	Computer calc. reduced resistance	Dev. of exper. value	ΔT(degK)
1·80	$0\cdot79673 \times 10^{-3}$	$0\cdot18 \times 10^{-6}$	0·03
2·13	$0\cdot79902 \times 10^{-3}$	$-0\cdot15 \times 10^{-6}$	−0·01
2·46	$0\cdot80154 \times 10^{-3}$	$-0\cdot32 \times 10^{-6}$	−0·04
2·75	$0\cdot80406 \times 10^{-3}$	$-0\cdot94 \times 10^{-7}$	−0·005
2·98	$0\cdot80614 \times 10^{-3}$	$0\cdot58 \times 10^{-6}$	0·055
3·40	$0\cdot81054 \times 10^{-3}$	$0\cdot11 \times 10^{-6}$	0·01
3·61	$0\cdot81296 \times 10^{-3}$	$0\cdot35 \times 10^{-7}$	0·00
3·76	$0\cdot81483 \times 10^{-3}$	$-0\cdot66 \times 10^{-6}$	−0·055
3·88	$0\cdot81635 \times 10^{-3}$	$0\cdot18 \times 10^{-6}$	0·01
4·05	$0\cdot81861 \times 10^{-3}$	$-0\cdot12 \times 10^{-6}$	−0·01
4·21	$0\cdot82099 \times 10^{-3}$	$0\cdot25 \times 10^{-6}$	0·02
12·00	$0\cdot13324 \times 10^{-2}$	$0\cdot76 \times 10^{-7}$	0·00
12·20	$0\cdot13656 \times 10^{-2}$	$-0\cdot87 \times 10^{-7}$	
12·40	$0\cdot14004 \times 10^{-2}$	$0\cdot50 \times 10^{-8}$	
12·60	$0\cdot14369 \times 10^{-2}$	$-0\cdot71 \times 10^{-8}$	
12·80	$0\cdot14752 \times 10^{-2}$	$0\cdot12 \times 10^{-6}$	
13·00	$0\cdot15153 \times 10^{-2}$	$0\cdot17 \times 10^{-7}$	
13·20	$0\cdot15573 \times 10^{-2}$	$0\cdot31 \times 10^{-7}$	
13·40	$0\cdot16012 \times 10^{-2}$	$0\cdot96 \times 10^{-7}$	
13·60	$0\cdot16472 \times 10^{-2}$	$0\cdot49 \times 10^{-7}$	
13·80	$0\cdot16952 \times 10^{-2}$	$-0\cdot18 \times 10^{-6}$	
14·00	$0\cdot17453 \times 10^{-2}$	$-0\cdot46 \times 10^{-7}$	
14·20	$0\cdot17977 \times 10^{-2}$	$-0\cdot23 \times 10^{-6}$	
14·40	$0\cdot18524 \times 10^{-2}$	$0\cdot15 \times 10^{-7}$	
14·60	$0\cdot19094 \times 10^{-2}$	$-0\cdot93 \times 10^{-7}$	
14·80	$0\cdot19688 \times 10^{-2}$	$0\cdot79 \times 10^{-7}$	
15·00	$0\cdot20307 \times 10^{-2}$	$0\cdot16 \times 10^{-6}$	

Coefficients of the polynomial: $A = +0\cdot78936410 \times 10^{-3}$; $B = +0\cdot15113760 \times 10^{-5}$; $C = +0\cdot16521690 \times 10^{-5}$; $D = -0\cdot17333743 \times 10^{-6}$; $E = +0\cdot28286009 \times 10^{-7}$

Table 4

	Temperature (°K)	Z_{CD}	Z_W	$\Delta Z = \lvert Z_{CD} - Z_W \rvert$	ΔT (degK)
Platinum I	110·15	0·32998	0·32973	$2\cdot5 \times 10^{-4}$	0·05
Platinum II	110·15	0·32963	0·32973	1×10^{-4}	0·02

	Temperature (°K)	Z_C	Z_W	$\Delta Z = \lvert Z_C - Z_W \rvert$	ΔT (degK)
Platinum II	60	0·11410	0·11415	5×10^{-5}	0·01
Platinum II	13·8	0·000875	0·000871	4×10^{-6}	0·02

Z_{CD}, Z function based on Callendar–Van Dusen resistance; Z_W, Z function from White's table; Z_C, Z function based on supplied calibration; ΔT, temperature difference corresponding to ΔZ

4.3 Gold + 0.03% Iron - Chromel Thermocouple

4.3.1 Thermocouple Junction

The Au (0.03% Fe) and chromel wires were obtained from Johnson Matthey and Co. Ltd. The thermocouple made from the above materials was found to have high sensitivity over a wide temperature range from 4°K to room temperature, and was especially suitable for use at cryogenic temperatures. The wires are insulated with diamel, an epoxy based synthetic enamel. Before the thermocouple junctions were formed, the enamel was removed by applying "Strip X" for 1 to 2 minutes.

At first the junctions were made by soft soldering. Such junctions always gave poor reproducibility at helium temperatures from run to run. The output thermal e.m.f. values for two different thermocouples made from the same reels of wire differed by as much as 20 to 30 μV at 4.2°K. This could be due to an additional e.m.f. arising from the soft solder as an impurity.

It was found that the junction made by spot welding the wires together gave satisfactory results. The spark welding of the junction was performed by discharging a condenser with capacity of 18μF charged to about 150V. Two wires were arranged end-on with one of them fixed. When the condenser started to discharge, the other wire was pushed forward and a spark welding took place, a beautiful spherical junction was formed.

It was found that the voltage needed to charge the condenser in order to give a good joint depended on the length of wires of Au(Fe) and chromel. The wires of about 10 to 20 inches long required the

18μF condenser to be charged to 140 to 160 volts while for longer wires the voltage needed to be higher. If the voltage is too high, the spark is too severe. We usually needed thermocouples with rather long terminals. Great care must be taken to prevent any mechanical strain or prolonged heating of wires.

4.3.2 Calibration of the Thermocouple

The thermocouple was calibrated against an already calibrated platinum resistance thermometer. The Pt resistance thermometer, covered with a thin layer of thermal grease was inserted in a tightly fitting cavity drilled in a copper block of $1\frac{3}{8}$ inches in diameter and 2 inches in height. A hole with diameter 1mm and depth of about 1cm next to the Pt resistance thermometer was filled with Woodsmetal which melted when the Cu block was partially immersed in hot water. The thermocouple junction is thus easily soldered to the Cu block. Due to the big heat capacity of the large Cu block and the high thermal conductivity of Cu, the temperature of the thermocouple junction and the platinum was taken to be the same. The Cu block was suspended by a rod from the top of the cryostat through some insulating material, and was surrounded by a Cu radiation shield. Four leads from the Pt resistance thermometer and the thermocouple leads were brought out from the top of the cryostat through the glass-metal seal. A helium glass dewar was employed.

The temperature below 4.2°K was achieved by pumping the helium bath, and the thermal e.m.f. was calibrated directly against the helium vapor pressure. The temperature above 4.2°K was obtained by allowing the Cu block to warm up after the helium level had dropped below the Cu block,

and the thermal e.m.f. was read from a potentiometer.

By using Tinsley type 5590B vernier potentiometers in conjunction with a Keithley 149 millimicrovoltmeter as amplifier together with a Rikadenki 2-pen recorder, the thermocouple e.m.f. and the corresponding resistance of the platinum were obtained continuously as temperature rose from 4.2°K up to room temperature. The heating rate was very slow. It took nearly 36 hours for the temperature to rise from 4.2°K to 100°K. The average heating rate for the first ten degrees from helium temperature upward was about one hour per degree, and for the next ten degrees or so it was about 40 minutes per degree. The heating rate increased as the liquid helium disappeared from the dewar. This happened in our case when the temperature was about 30°K. Liquid nitrogen surrounding the helium was topped up all the time. The heating rate from 30°K to 70°K was about 12 minutes per degree, and was about 10 minutes per degree upward to 100°K.

The reference junction of the thermocouple was maintained at the triple point of water. This arrangement was simple, and accurate enough for our purposes.

4.3.3 Triple Point Cell

The triple point of water is the equilibrium temperature between water, ice and water vapour. It is equal to 273.16°K. The triple point cell may be obtained from Spembly Technical Products Ltd., England. The cell was prepared for use by first cooling it to 0°C by immersing it in a bath of ice for at least one hour and then chilling the re-entrant tube by filling it with liquid nitrogen. The tube must

be sufficiently dry before N_2 was added. Then a fairly uniform sheath of ice of about 1cm thick was formed round the tube. Water of about 20°C was then placed in the re-entrant tube so as to melt a thin layer of ice, leaving a very pure ice-water interface in contact with the re-entrant tube in which the thermocouple junction was to be placed. The water inside the re-entrant tube was replaced afterward by ice-cold sugar water, which would soon take up the temperature of the triple point and ensure good thermal contact between the thermocouple junction and the walls of the cell. The temperature of the triple point in the re-entrant tube was kept steady by surrounding the triple point cell with ice.

4.3.4 Thermoelectric E.M.F., Sensitivity and Reproducibility

Au (0.03% Fe)-chromel thermocouple is known to have high sensitivity over a wide range of temperature. The thermoelectric e.m.f. depends on the reference temperature. The Law of Successive temperatures states : "If two dissimilar homogeneous metals produce a thermal e.m.f. of E_1 when the junctions are at temperature T_1 and T_2 and a thermal e.m.f. of E_2 when the junctions are at T_2 and T_3, the e.m.f. generated when the junctions are at T_1 and T_3 will be $E_1 + E_2$." Thus the voltage readings obtained when the reference junction temperature is arbitrarily fixed can be shifted by a constant amount to a value which corresponds to the reference junction temperature being at a specified common value.

Our thermal e.m.f. value is 4584 μV at 4.2°K with the triple point temperature as reference temperature. It changes by $\pm$5μV from run to run.

This is about equivalent to $\frac{1}{3}$ of a degree. This uncertainty at 4.2°K is probably not mainly due to the intrinsic properties of the thermocouple itself, for example the inhomogeneity of the thermocouple wires or any defect in the thermocouple junction. It is most likely due to our experimental set-up, which among other things used the rather big temperature difference between the reference junction and the variable junction. For temperature below 30°K when there is liquid helium still in the dewar, the accuracy is estimated to be better than a quarter of a degree while above 30°K the error increases to $\frac{1}{2}$°K at nitrogen temperature. In graph 4.1 (p. 78) the thermal e.m.f. of one of the thermocouples is plotted against temperature (solid curve). The crossed points denote a separate calibration run for the same thermocouple.

It was found that for thermocouples made from wires of the same spool, the thermal e.m.f. at helium temperature varied within 5μV; while for those made from different spools, the variation may be as big as 25μV. The dotted curve in graph 4.1 (p. 78) shows the same kind of plot for another thermocouple made from a different spool. It can be seen that the curve is shifted by more or less the same amount for the whole temperature region. Therefore for a new thermocouple, we need only measure the thermal e.m.f. at 4.2°K, then the calibration is obtained by making a constant shift from the chosen standard calibration. For accurate work each thermocouple must be calibrated in service.

Part of our later work required the measurement of the temperature dependence of resistivity and thermoelectric power of PbS. As the variation of resistivity and thermoelectric power are not too sensitive

with temperature within a small temperature region, an error of about half a degree in our calibration is tolerable. Another part of our work involved measurement of small temperature gradients along the sample. This was done by using a differential thermocouple.

The sensitivity of the thermocouple at any temperature is given by the slope of the e.m.f. vis temperature curve at that temperature. A least square fitting method was used with the help of an IBM 1620 computer to give a reasonably good fitting polynomial of order seven. Sensitivity is computed by differentiating this polynomial. In graph 4.2 (p.79) the sensitivity is plotted against temperature. The minimum sensitivity is at 48°K and then it increases monotonically to room temperature. The sensitivity of the thermocouple was also calculated by another method used by Berman who defined an average sensitivity $f(T) = E(T)/(T - T_{ref})$ where E(T) is the thermocouple e.m.f. appropriate to temperature T, when the other junction is at a reference temperature T_{ref}, and the sensitivity S(T) is given by the following relation

$$S(T) = f(T) + (T - T_{ref}) \frac{df(T)}{dT}$$

This was also evaluated by the computer. The sensitivity calculated by the two methods is consistent to 0.4%.

4.3.5 Possible improvement

The error introduced in our calibration may be due to the following sources:

1. Intrinsic properties of the thermocouple itself, this includes inhomogeneity of the thermocouple wires, and the imperfection of the junctions.

This inhomogeneity may be caused by composition of the wire, or by strain in the wires etc. A suggestion was given by R. Powell of N.B.S. when he was in St. Andrews for LT 11. The inhomogeneity of a thermocouple wire may be examined by the so-called short-range, medium range and long range tests.

For short range tests, the given wire is wrapped on a plastic rod and dipped into liquid helium or nitrogen. The ends of the wire are connected to a potentiometer, the fluctuations in readings will show the effects of inhomogeneities. The e.m.f. should be less than $\pm 5\mu V$ for accuracy in temperature to be better than half a degree. After the short range test, the wires are then prepared for medium range test. A symmetrical differential thermocouple is fabricated from the two materials under test. The two terminals are connected to the potentiometer, and the junctions are dipped into separate baths of liquid helium or liquid nitrogen with the same temperature. The thermoelectric voltage is then measured. Then interchanging the junctions in the two baths and also reversing the leads to the potentiometer; the new thermoelectric voltage is measured. The average of the two readings, as well as the difference between them gives an indication of how good the homogeneity of the wires and the junctions are. The long range test is essentially the same as the short range test. One cuts out short portions from the two ends of a long wire and performs the short range test on them. If they satisfy the required limit, then one may safely use the middle piece.

The method of welding the thermocouple joint we used is quite

good, one needs only to pay attention to avoid straining the junction after it is made.

2. Improvement in experimental set up: Our variable temperature junction of the thermocouple was soldered to the Cu block and the wire was brought directly out of the helium dewar through the top of the cryostat which was at room temperature. A large temperature gradient along the wires may cause unwanted e.m.f.'s especially if the wire is not homogeneous enough. It was suggested by Powell that at least one foot of wire immediately above the junction should be wound round the Cu block so as to temper the temperature gradient along the wires.

Another suggestion to improve our set-up is to fix several circular aluminium plates equidistantly placed above the Cu block right to the top. Fill glass wool in the space between the plates. Some holes are drilled in the plates for escaping gas. This arrangement will help to reduce radiation and prevent convection currents.

To obtain higher accuracy, the reference temperature should be near to the variable temperature junction. So for measurement from 4°K to 30°K the reference junction would be better at 4.2°K.

3. Some errors were introduced by the measuring circuit. The main trouble we had was from earthing problems. Improper earthing of the instruments could introduce an error of more than 10μV as well as very high noise level.

The terminals of the potentiometer should be shielded to prevent spurious e.m.f.'s caused by draught.

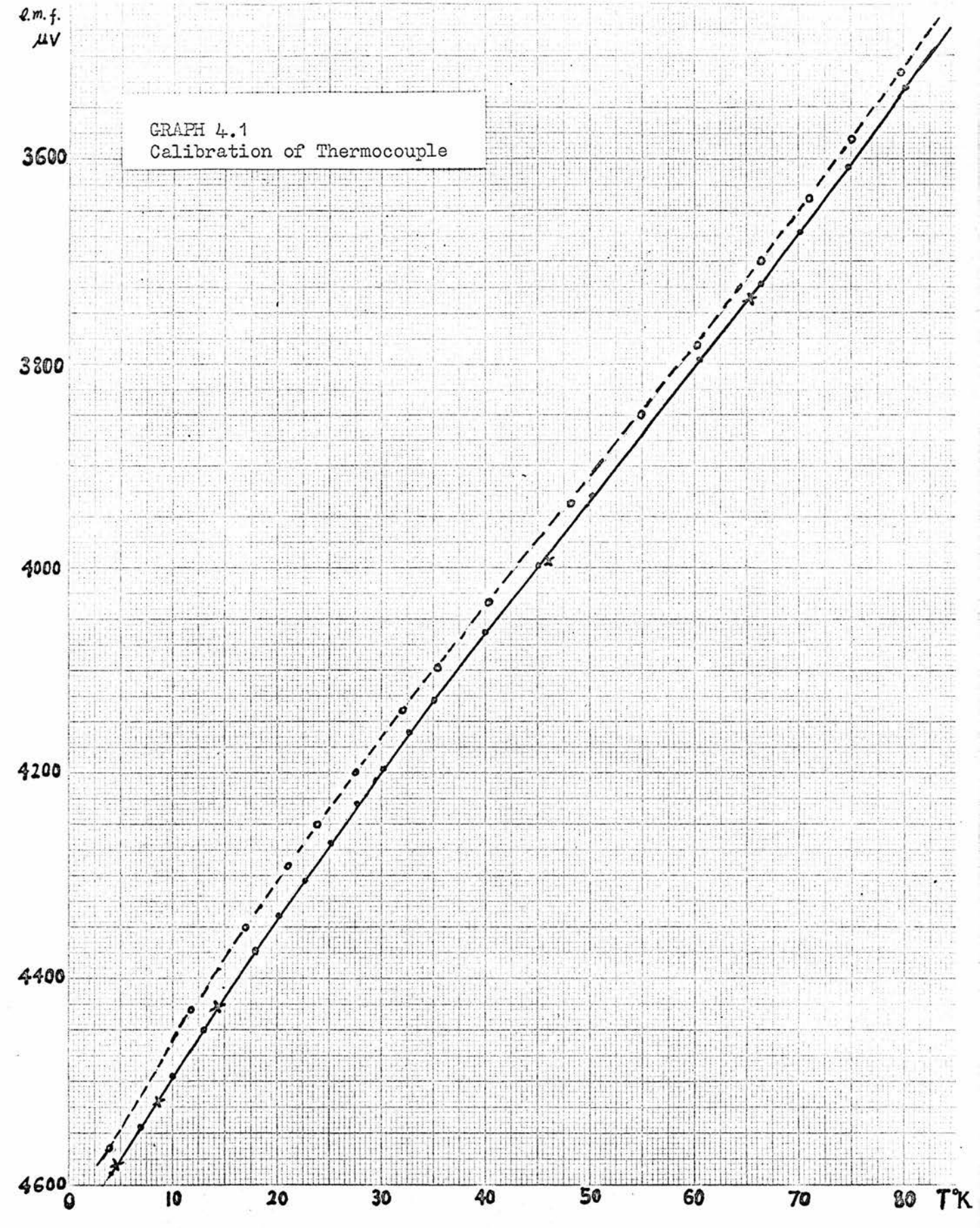
e.m.f.
μV
GRAPH 4.1
Calibration of Thermocouple
3600
3800
4000
4200
4400
4600
0
10
20
30
40
50
60
70
80
T°K

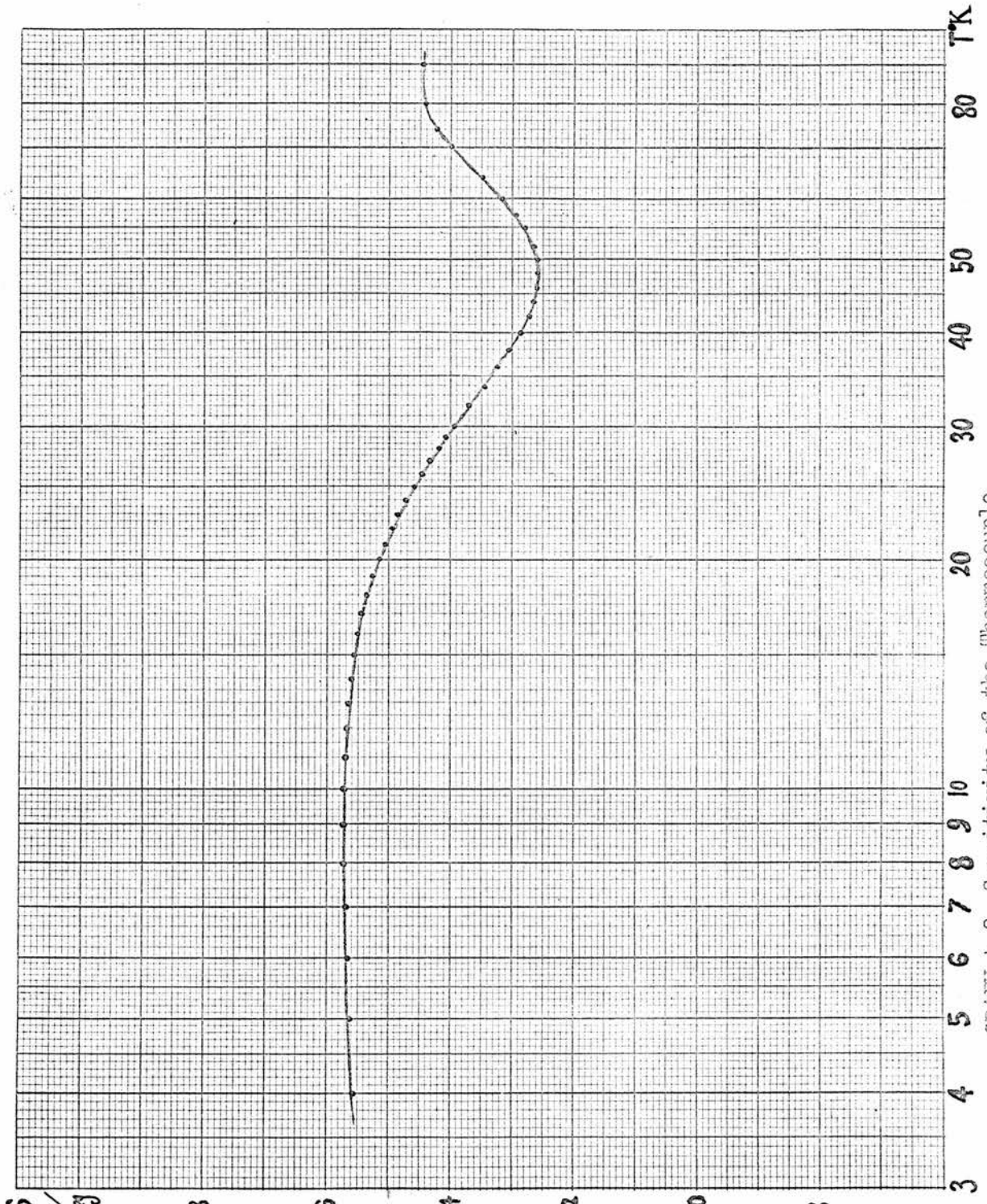

GRAPH 4.2 Sensitivity of the Thermocouple

CHAPTER V

Experimentation II - Measurements on Resistivity, Thermoelectric and Thermomagnetic Effects.

5.1 Introduction

Although there has been a good deal of works on the electrical and thermal properties of lead sulphide with carrier concentration higher than 10^{17}/c.c, there is still much to be discovered especially for purer samples in the low temperature region. In particular, the thermomagnetic effects of PbS in the low temperature region have hardly been investigated. Our work mainly involves the study of the temperature dependence of resistivity and thermoelectric power as well as the thermomagnetic effects at low temperatures for n-type PbS samples with carrier concentration of the order of 10^{16}/c.c.

PbS exists in nature as the mineral galena. The crystal structure is face-centred cubic and the edges of the unit cell are equal to 5.9×10^{-8} cm.

In this chapter we present our experimental procedure, including the selection of samples, and the description of the apparatus.

5.2 Selection of Samples

The samples were obtained by cleaving from a block of galena along (100) planes using a sharp razor blade. Rectangular samples were easily obtained in this way. The average crystal dimensions were 8mm in length, and 1 by 1.5mm in crossection. The surfaces were bright and gave a very good reflection after cleavage. It became oxidised

after some time and required cleaning by thioureaic acid. Two ends of the sample were copper plated in order to obtain good contact with current probes.

The homogeneity of the sample was checked by measuring the resistivity of the sample at $\frac{1}{2}$mm intervals or so along its length, and the measurements of Hall effect with the voltage probes in different positions over the middle regions were also made. The samples used may be regarded as fairly homogeneous as the variation of these measurements was less than 10%.

The carrier concentration and the carrier sign were determined by Hall effect measurements. The Hall constant R defined by $E_H = R\ j\ B$ is equal to $\frac{3\pi}{8}\ \frac{1}{ne}$ for non degenerate semiconductors and 1/ne for degenerate semiconductors, where j is the current density passing through the sample in magnetic field B and n is the number of electrons per cm^3. A number of samples with electron concentration from 9.5×10^{15} to 10^{19} per cm^3 were found. The Hall effect measurements were carried out at room temperature, and some had been checked at helium temperature. Within the accuracy required the Hall constant may be considered temperature independent.

5.3 Resistivity Measurements

The resistivity of a number of samples was measured from 1.4°K to 100°K by the usual potentio-metric method. The temperature of the crystal from 4.2°K downward was obtained directly from helium vapor pressure while from 4.2°K upward, the thermocouple e.m.f. was used.

To ensure that the thermocouple measured the sample temperature accurately, the rate of change of temperature had to be kept to a minimum.

5.3.1 Crystal Holder and Cryostat

The sample holder is shown in Fig 5-1 (p. 91). Two movable small rectangular copper blocks served as the current probes which were soldered to the current leads. The current probes were pressed to the ends of the sample by springy BeCu straps, and the potential probes also of BeCu were pressed on to the sample. The copper leads made good mechanical contact with the potential probes. This avoided the thermal e.m.f. produced in solder connections. The sample holder was in good thermal contact with a large copper block (Fig. 5-2 (p. 91)). The thermal capacity of this large copper block ensured a slow rise of the sample temperature and the temperature of the holder. Meanwhile we also inserted in the copper block a Pt resistance thermometer and one junction of a differential thermocouple which had the other junction attached to the sample. This enabled us to carry out a further check on the sample temperature.

Two junctions of two thermocouples were fixed on the surface of the sample using nail varnish or G varnish which was an electrical insulator but proved to be quite a fair thermal conductor. One of the thermocouples with its other junction at the triple point of water gave us the temperature reading. The other was the differential thermocouple, having one junction soldered in the copper block giving us a means of

checking the temperature difference between the sample itself and the block. We also checked the calibration of the thermocouple against the Pt resistance thermometer from time to time during measurement.

The sample holder was surrounded by a copper radiation shield. A pair of glass dewars was employed.

5.3.2 Electrical Measuring Apparatus

Two potentiometers of Tinsley Type 5590 B coupled with a Keithley 149 millimicrovoltmeter were used to measure the thermocouple e.m.f. and the potential across the sample. The outputs of the Keithleys were fed into a Rikadenki 2-pen recorder which recorded the 2 voltages simultaneously and continuously. The readings were accurate to $\pm$ 1 μV with a noise level less than 1 μV.

The electrical circuit and the schematic diagram is shown in Fig. 5-3 (p. 92). A current of 10 ma was maintained by adjusting variable heli-pot resistors. Current was measured by measuring the potential difference across the standard 10 Ω resistor, and the current was supplied by two 2-volt accummulators in series. The terminals of the differential thermocouple and the potential leads of the Pt resistance thermometer were connected to the other inputs of the two potentiometers. Therefore a switch over in the potentiometer set enabled us to check the temperature difference between the sample and the Cu block as well as the thermocouple calibration against Pt. A similar set up for the current supply to the Pt was required. The current could be reversed by a reversing switch from time to time

and one obtained an average value of potential readings. The accuracy in current measurement is better than 0.1%, and the error in potential is less than 0.15%.

The reading of the differential thermocouple varied from 0 to $\pm$1.2 μV, which was equivalent to a temperature difference less than 0.1°K. The temperature of the sample may therefore be regarded as the same as that of the Cu block. The Pt resistance thermometer inserted in the Cu block gave a direct reading of the temperature of the Cu block. The reading differed from the thermocouple reading by $\pm\frac{1}{2}$ degree. This is within the error of the thermocouple calibration.

5.3.3 Thermal E.M.F. in Resistivity Measurements

When no current passes through the circuit, there should be no potential difference between the two potential leads of the sample. It was found that a potential reading which varied with temperature was detected when the current was completely cut off. This was due to thermal e.m.f.'s occurring at the two junctions where the potential probes were connected to the potential leads. As seen from Fig. 5-1(p. 91) the two junctions were situated at different heights in the holder, and so a small temperature difference existed between them. It was found that this thermal e.m.f. reached as much as 200 μV when the junctions were first connected by solder, but was greatly reduced when the Cu wires were screwed firmly to the junctions instead of using solder. A thermal e.m.f. varying from zero to 6 μV still existed, and it has been taken into account when calculating the resistivity.

To reduce still further this spurious e.m.f. the positions of two junctions should be arranged to be at the same level in the sample holder.

5.4 Crystal Holder and Cryostat for Thermoelectric and Thermomagnetic Effect Measurements

The most crucial point in the measurements of thermal effects is to maintain a constant temperature gradient along the sample. Four potential probes which were used to measure the transverse and longitudinal effects were needed in addition to the thermocouples. A crystal holder which can be used for measuring practically all thermal and electrical effects from 1.4°K upward was designed and made by the author.

A drawing of the holder is seen in Fig. 5-4 a (p. 93), and on page 95 a photograph of the actual crystal holder is shown. The crystal holder is made of glass fibre, and was contained in a copper can of $2\frac{1}{2}$ cm diameter and 10 cm in length. The copper can was immersed in the helium bath when doing experiments. Two eureka heaters of a 100 Ω resistance were wound on copper block which were pressed against the two ends of the sample. The shape of the heater is shown in Fig. 5-4 e (p. 94). The positions of two heaters could be adjusted by sliding the copper blocks along its flat bottom. Two slots were cut in the bottom of the holder Fig. 5-4 b (p. 93) in order that the screw sticking out from the copper block could move freely along the slot. The screw served as the current connection. It also helped to fix the position of the heaters when a nut was screwed on from the back

of the holder. The upper heater was soldered to the top of the copper can by 3 copper straps, therefore it served as a heat sink because when no current was passed through it, its temperature was the same as the copper can which was at helium temperature. The temperature of the other heater was controlled by passing a constant current through it. A steady uniform temperature gradient was essential in the measurement, and so not too big a temperature difference should be applied between the two copper blocks. For measurement at temperatures well above 4.2°K, the temperature of the upper copper block was raised and maintained constant by passing a constant current through it.

Four potential probes made contact with the side faces of the crystal from the two sides of the sample holder through the holes shown in Fig 5-4 c (p.94). Probes 1 and 2 (Fig. 5-4 a (p.93)) are for measuring transverse effects while 3 and 4 are for longitudinal effects. The probes were made of BeCu wire and were soldered at right angles to BeCu strap with thermal free solder as shown in Fig. 5-4 d (p.94). The junctions for connecting the straps to the potential leads were arranged at the same level for probes 1 and 2 as well as for probes 3 and 4.

Nine copper wire leads together with 4 thermocouple leads were brought out from the top of the cryostat through the stainless tube which also served as the suspension of the sample holder.

The copper can was soldered to its cap with Woods metal after the crystal was mounted and ready for a run. A thin sheet of mica was

glued to the wall of the copper can to avoid short circuiting any wire touching the can. The copper can was pumped hard through the stainless tube to provide thermal insulation. A helium glass dewar with a tail of inner diameter 28 mm and 16 cm long was employed.

5.5 Calibration of Magnetic Field and Crystal Orientation in the Field

For the thermomagnetic and Hall effect measurements, a Newport 4 inch electromagnet type A was used. Current to the magnet was supplied by a 10 amp d.c. power source. The magnetic field was measured at different current values from 0 to 10 amps. A water cooling supply was needed for currents higher than 6 amps. The magnet was calibrated by a Rawson rotating coil flux meter with an accuracy of about 1%. With a pole gap equal to 46 mm, the calibration of magnetic field against current is shown in Fig. 5-5 (p.96).

In our experiments, we wanted the magnetic field to be perpendicular to current flow. An optical method was used to achieve this. The magnet was so arranged that the sample sat midway between the poles. A small rectangular piece of steel with a mirror attached to one face was pivoted to rotate freely, so that it would set itself parallel to the magnetic field when put in between the pole pieces. The sample holder was rotated until the optical reflections from both the mirror and the crystal showed that they were parallel. A mark was made for the orientation of the holder with respect to the top of the crystal, then the sample holder was rotated by 90° again to give the required position of the sample in the magnetic field.

5.6 Measurements of Thermoelectric and Thermomagnetic Effects

Fig. 5-6 (p.97) shows the schematic diagram including temperature control circuit. Maintenance of a constant temperature gradient along the sample was an important requirement of the experiment. The large copper heater blocks with big heat capacity helped to give a steady temperature gradient. An electrical circuit by Woodhams et al was also employed to stabilize the temperature. Among other things the circuit included a Mullard OC 35 transistor and a Mullard ORP 11 photoconductive cell whose resistance varied from 650 Ω to 7 KΩ when the intensity of illumination falling on the cell from the galvanometer lamp changed. Minimum resistance occurred when the cell was fully illuminated. The photo cell was connected to the base of the OC 35 transistor, with the heater coil forming the emitter load. The photo cell was inside the Tinsley type M.R.4 galvanometer which was used as the null detector for potential measurements of the thermocouple. The position of the cell was such that it was half illuminated by the light spot of the galvanometer when the temperature of the sample was at the desired value. Minimum heater current was obtained when the cell was fully covered by the light spot while in the absence of illumination maximum current was obtained. If the temperature of the sample increased due to excess heating, the light spot moved away from its zero position and the photo-conductive cell received more illumination. Therefore this gave rise to a decrease in heater current, and the temperature of the sample was thus adjusted automatically. It was found that this temperature control

stabilized temperature to within 0.2°K over the temperature range measured for a period of two hours provided the temperature gradient was not too big. In fact for a whole set of measurements of longitudinal or transverse Nernst effect against different values of magnetic field below 20°K, the stabilization in temperature was better than 0.06°K during the measuring time of about 20 to 30 minutes. The stability decreased for higher temperatures when bigger heater currents were required then.

A differential thermocouple was employed to measure the temperature gradient, it had its two junctions attached by nail varnish to the sample in positions close to the measuring probes. A temperature difference from 0.5 to 2 degrees was maintained between the two junctions. A fluctuation of thermal e.m.f. reading from zero to 0.5 μV was recorded for measurements below 20°K. This is equivalent to a temperature of less than 0.05°K. A constant temperature gradient was verified by the good stability of the temperature reading from the differential thermocouple.

Manual control of the heater currents for both heaters was required for measurements well above helium temperature and below nitrogen temperature. The average temperature of the sample varied by 0.4°K in these measurements while the error in measuring the temperature gradient was estimated to be about 1%. The boiling rate of helium was rather fast when current was passed through the upper heater coil. Therefore measurements above 50°K were not easy as the liquid helium level dropped too fast and a steady temperature gradient along the sample was difficult to maintain. For measurements above nitrogen temperature, the copper

can was either surrounded by N_2 or, when the copper can had reached N_2 temperature, the helium dewar was evacuated while the N_2 dewar was topped up all the time to keep a steady temperature.

A change in sample temperature of about one degree gave a deflection of the light spot on the galvanometer scale of about 2 cm while the heater current varied by 8 to 10%. During the measurement, the current was constant to 0.5%.

Potential probes 1, 2 and 3,4 were connected to two different sets of Tinsley Type 5590 B vernier potentiometer, which read to an accuracy of 0.1 μV. The error in potential readings varied from 0.05% to 2%. This included the uncertainty due to the slight instability in temperature control.

The transverse Nernst voltage was measured by probes 1 and 2 for different values of magnetic field in both directions. It was found that the transverse Nernst voltage changed sign with magnetic field. Thermoelectric power was measured through probes 3 and 4. As the thermoelectric power of Cu is known to be much smaller than the thermoelectric power of PbS by 2 to 3 orders of magnitude, we thus regarded our measurements as the absolute thermoelectric power of the sample. The longitudinal Nernst voltage was obtained by measuring the change of thermoelectric power in various magnetic fields. It was found that the longitudinal Nernst voltage did not change sign with magnetic field.

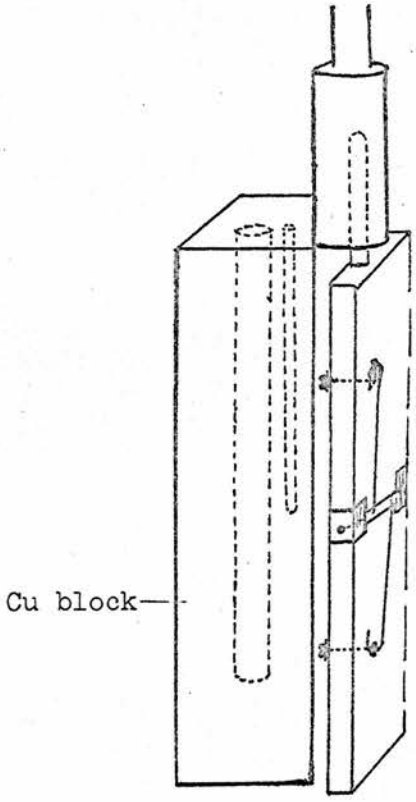

Fig.5.2

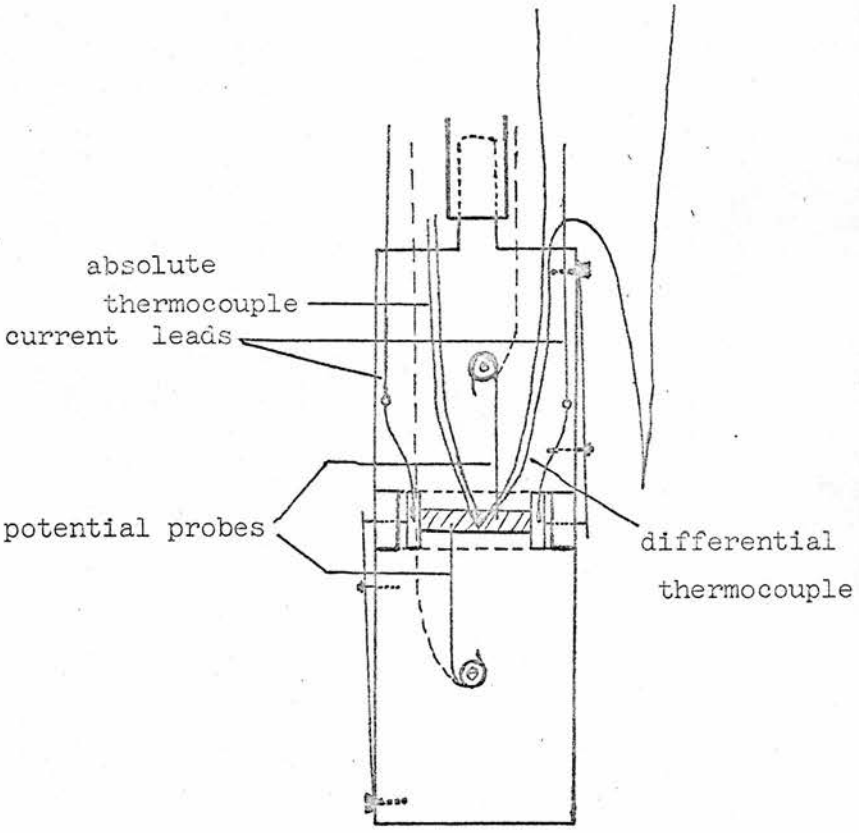

Fig.5.1

Sample Holder for Resistivity Measurements

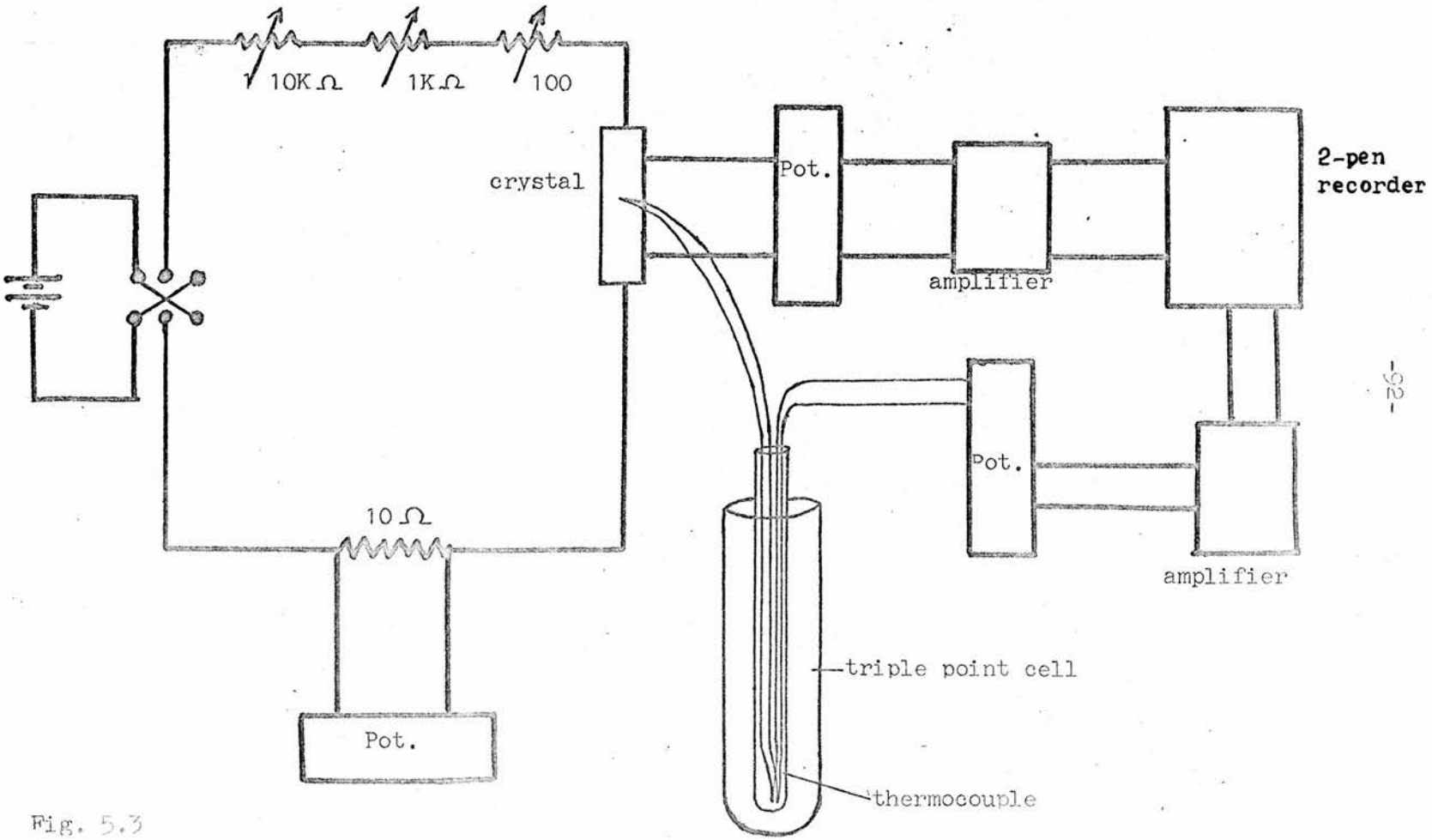

Fig. 5.3

Circuit and Schematic Diagram for Resistivity Measurements

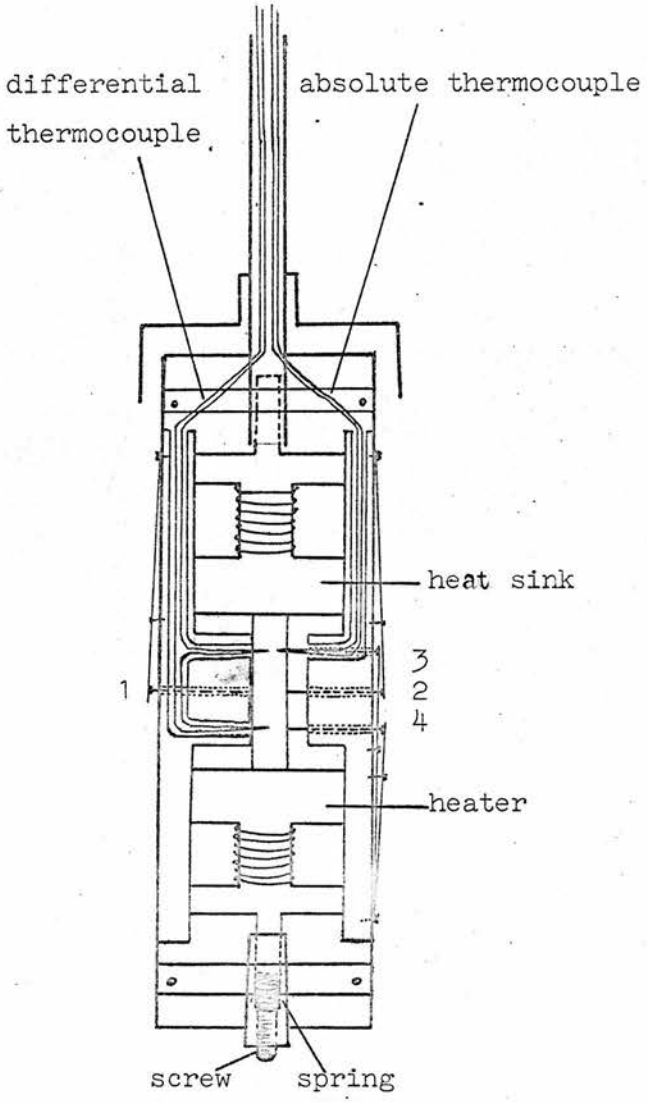

Fig. 5.4 a
Front View of Sample Holder

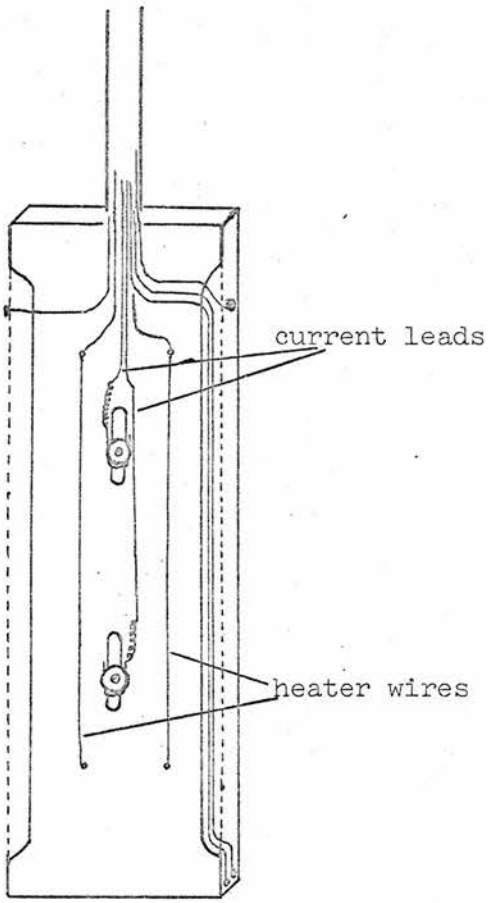

Fig. 5.4 b
Back View of Sample Holder

Sample Holder for Thermo-electric and Thermomagnetic Measurements

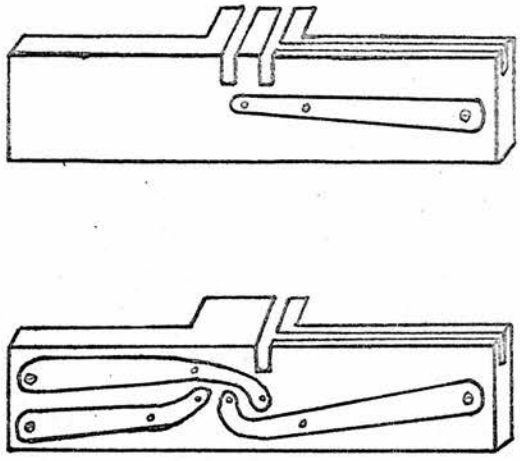

Fig. 5.4 c
Sample Holder Side View

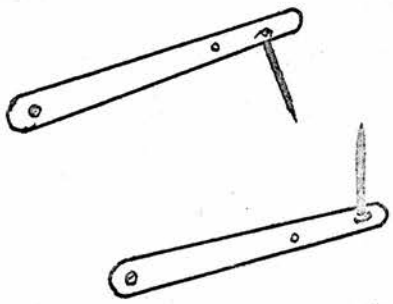

Fig. 5.4 d
Potential Probes

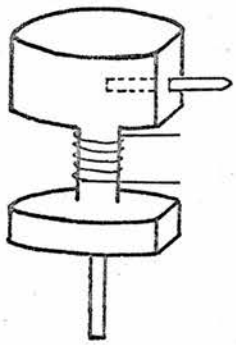

Fig. 5.4 e
Heater

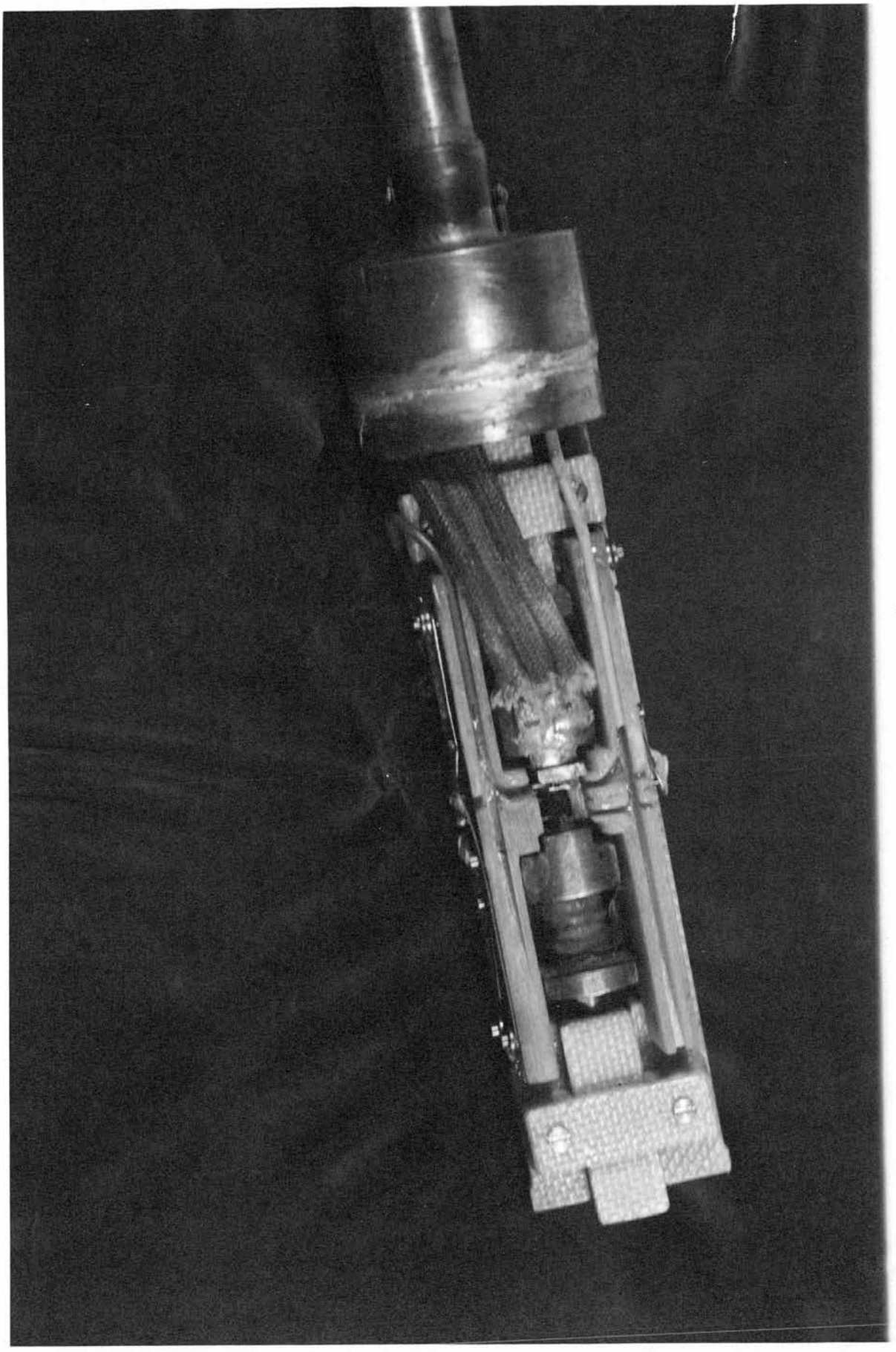

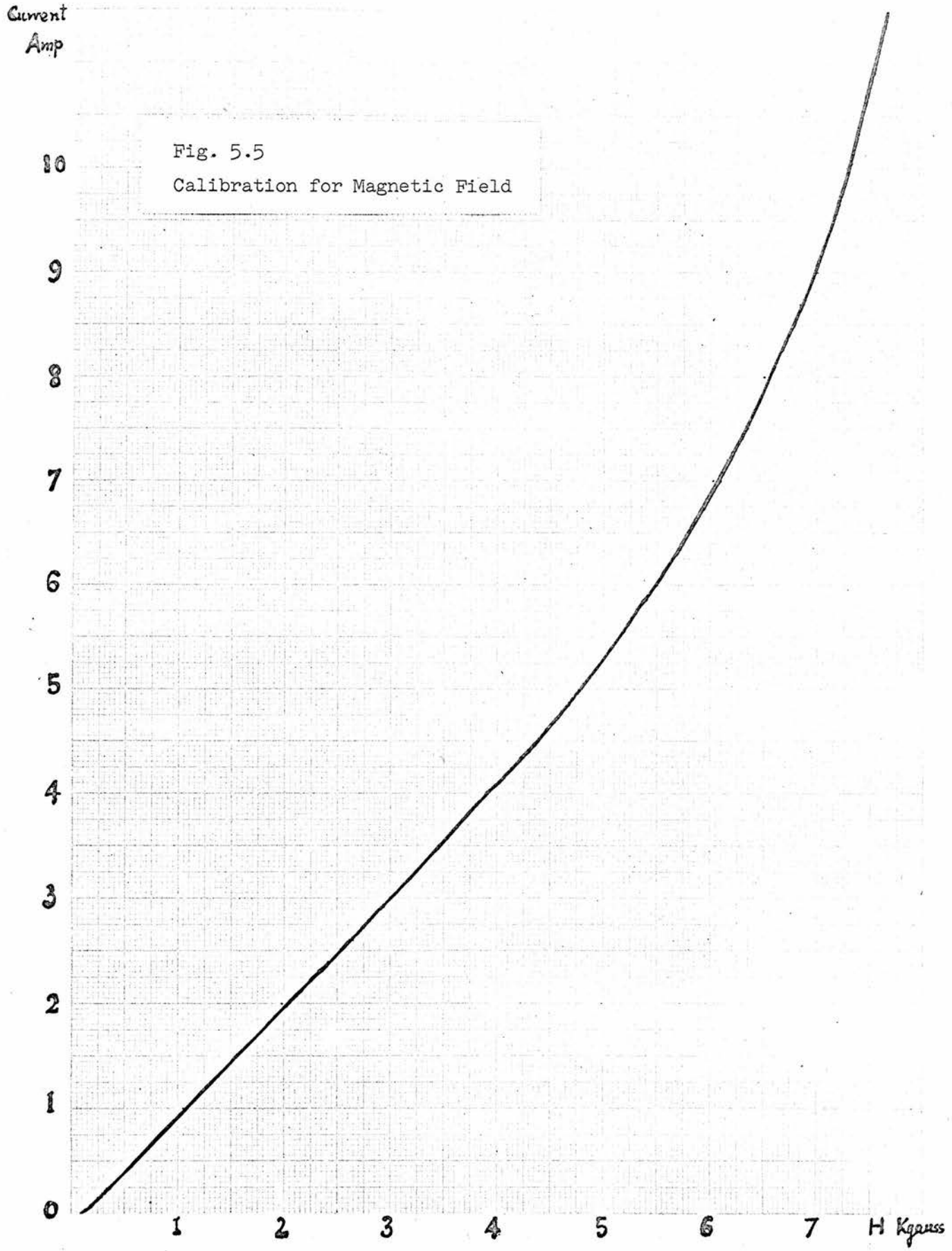

Fig. 5.5
Calibration for Magnetic Field

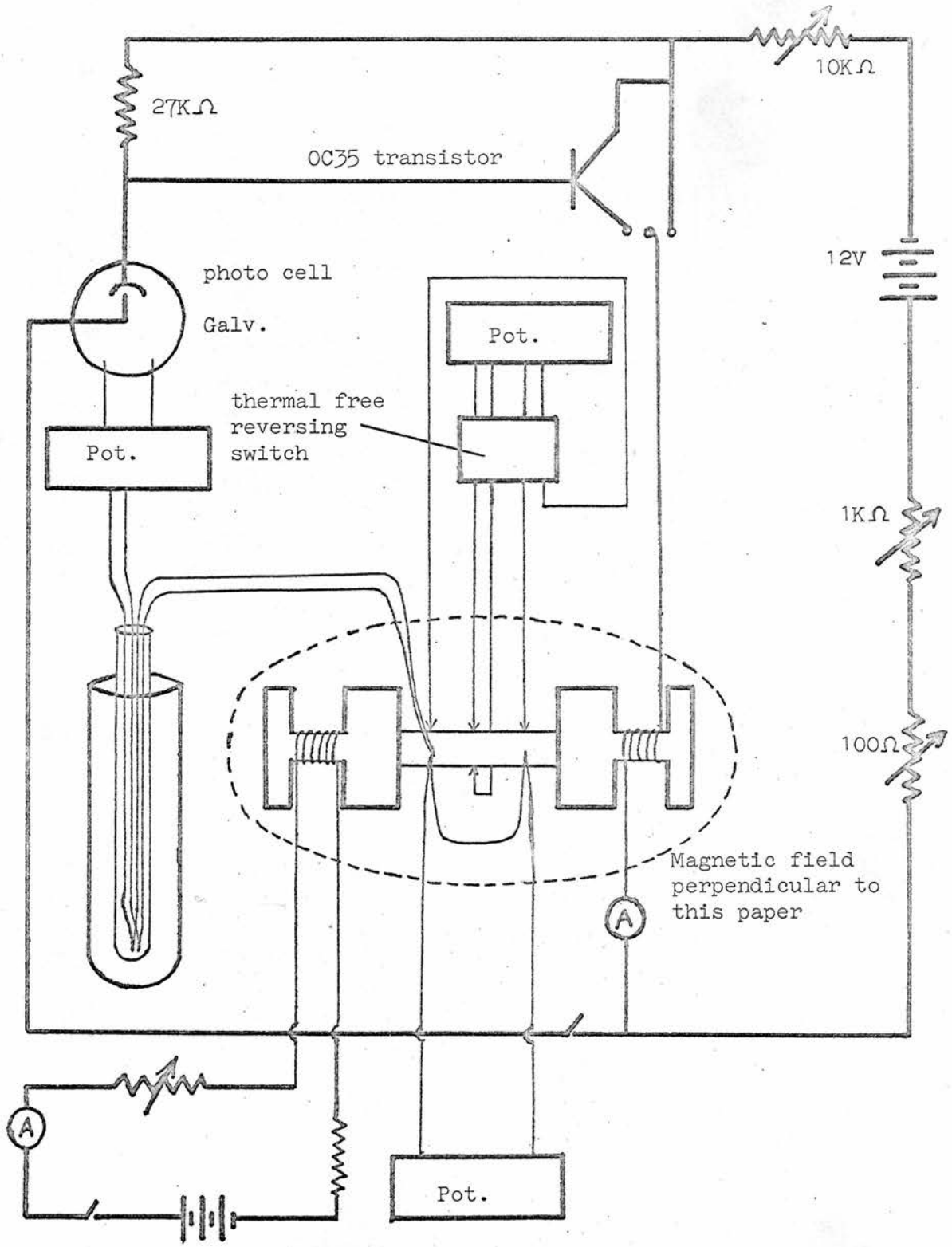

Fig. 5.6

Schematic Diagram and Circuit for Thermo-electric and Thermomagnetic Measurements

CHAPTER VI

Discussion of Resistivity Measurements

6.1 Resistivity Results

Measurements of the resistivity of a number of n-type PbS crystals with electron concentrations ranging from 9.5×10^{15}/c.c. to 2.4×10^{17}/c.c. were carried out in the temperature range between 1.4°K and 80°K. Some measurements were also obtained for samples No. 1 to No. 4 down to 0.5°K. The characteristics of the sample are shown in Table 6-1 (p.101). The results for samples No. 1 to No. 6 are shown in Fig.6.1(p.105), and for samples No. 7 to No. 14 are shown in Fig. 6.2 (p.106).

It can be seen that a resistivity minimum occurs for the majority of the samples under investigation. The temperature corresponding to the resisitivity minimum T_{min} is higher for lower electron concentrations, and decreases as concentration increases. Also the depth of the minimum, which is defined as the resistivity measured at the lowest temperature obtainable or extrapolated to absolute zero ρ_o minus that at T_{min} (ρ_{min}) decreases as concentration increases as seen in Fig. 6.1 (p.105), Fig. 6.2 (p.106) or Table 6-3 (p.103). For samples No. 7 to No. 12, the temperature dependence of the resistivity at low temperatures becomes rather weak but a shallow minimum which decreases rather rapidly with concentration can still be seen. For samples No. 13 and No. 14, the T_{min} vanishes and resistivity increases very slowly with increasing temperature even at the lowest temperature obtainable.

The dependence of T_{min} and the depth of resistivity minimum $\Delta\rho$ on carrier concentration n can be approximately represented by

$$T_{min} \propto n^{-0.37} \quad ; \qquad \Delta\rho \propto n^{-3.0}$$

In Fig. 6.3, (P. 107) T_{min} is plotted against carrier concentration n. From the extrapolation of the curve, we expect that T_{min} will occur below 1°K for low 10^{17}/c.c. crystals. Hence for our samples No. 13 and No. 14, if the measurements were continued below our temperature range, we might observe a very shallow minimum as the depth decreases very rapidly with increasing n as shown in Fig. 6.4 (p.108). For high carrier concentration crystals, say above 5×10^{17}/c.c., the minimum may disappear all together as is the case with the disappearance of negative magnetoresistance observed by Finlayson and Mathewson which I shall mention later.

Quantitative investigation of the temperature dependence of resistivity revealed a logarithmic dependence of resistivity on temperature in the low temperature region for samples showing a minimum, and the curves tail off from a straight line as the temperature gets lower as shown in Fig. 6.5 (p.109) for samples No. 1 to No. 6, and Fig. 6.6 (p.110) for samples No. 7 to No. 10. An expression was obtained to fit the data in the straight line portion of these curves. The expression is given by

$$\rho = a - b \ln T \qquad (6\text{-}1\text{-}1)$$

Where a, b are positive parameters as shown in Table 6-2 (P.102) with value $a > b \ln T$. The dependence of a, b on the carrier concentration n for lower

concentration samples may be approximated by

$$a \propto n^{-2.4} \quad ; \quad b \propto n^{-3.0}$$

A power law $\rho \propto T^{-c}$ was also tried to fit the experimental points for the resistivity temperature relation for a number of samples. In Fig. 6.7 (p.111), the experimental points are compared with (a) the logarithmic fit equation (6-1-1) and (b) a $(-\frac{3}{2})$-power law which represents ionized impurity scattering. It is obvious that the logarithmic dependence on temperature fits the experimental values very well while the power fitting does not. This conclusion is reinforced by Fig. 6.8 (p.112) where experimental points of $\ln\rho$ are plotted against $\ln T$. A straight line is not obtained and thus any simple power law is not appropriate. We then may say that ionized impurity scattering is not the predominant mechanism. Thermomagnetic effects measurements (see chapter 7) also leads to the same conclusion.

For temperatures well above T_{min} the resistivity can be approximated by the formula

$$\rho = g + d\,T^{p} \qquad (6\text{-}1\text{-}2)$$

where p is a constant varying between 1.8 to 2.5 for different samples. The temperature dependence of the resistivity in this temperature range is similar to that obtained previously by Finlayson and Greig and other workers. The quantities g, d and p are positive parameters and their values for six samples are shown in Table 6-2 (p. 102).

Sample	n/c.c.	$\mathcal{E}_F$ (eV)	T_d	$\rho_{4.2}$ Ωcm	$\mu_{4.2}$ $\frac{cm^2}{V\ Sec}$	$\rho_{\Omega cm}$ room temp
1	9.5×10^{15}	1.367×10^{-3}	15.8	15.071×10^{-2}	4361	1.925
2	1.1×10^{16}	1.504×10^{-3}	17.4	10.82×10^{-2}	5204	1.525
3	1.38×10^{16}	1.750×10^{-3}	20.3	8.028×10^{-2}	5642	1.300
4	1.52×10^{16}	1.867×10^{-3}	21.6	6.043×10^{-2}	6805	1.051
5	1.76×10^{16}	2.057×10^{-3}	23.8	4.689×10^{-2}	7582	8.954×10^{-1}
6	2.15×10^{16}	2.352×10^{-3}	27.3	3.920×10^{-2}	7416	7.60×10^{-1}
7	2.76×10^{16}	2.778×10^{-3}	32.2	2.30×10^{-2}	9845	5.685×10^{-1}
8	3.84×10^{16}	3.465×10^{-3}	40.2	1.830×10^{-2}	8894	5.06×10^{-1}
9	5.13×10^{16}	4.197×10^{-3}	48.7	1.757×10^{-2}	6935	3.82×10^{-1}
10	5.33×10^{16}	4.307×10^{-3}	49.9	1.348×10^{-2}	8698	3.52×10^{-1}
11	7.01×10^{16}	5.168×10^{-3}	59.9	0.927×10^{-2}	9626	2.3×10^{-1}
12	8.68×10^{16}	5.962×10^{-3}	69.1	0.694×10^{-2}	10375	1.97×10^{-1}
13	1.43×10^{17}	8.319×10^{-3}	96.5	0.44×10^{-2}	9933	8.69×10^{-2}
14	2.44×10^{17}	11.875×10^{-3}	138	0.26×10^{-2}	9852	7.89×10^{-2}

Table 6-1

Sample	n/c.c.	a	b	g	d	p
1	9.5×10^{15}	0.2135	0.439×10^{-1}	0.260×10^{-1}	0.537×10^{-4}	1.8
2	1.1×10^{16}	0.1474	0.281×10^{-1}	0.255×10^{-1}	0.172×10^{-4}	2.0
3	1.38×10^{16}	0.998×10^{-1}	0.138×10^{-1}	0.423×10^{-1}	0.476×10^{-5}	2.2
4	1.52×10^{16}	0.715×10^{-1}	0.811×10^{-2}	0.433×10^{-1}	0.371×10^{-5}	2.2
5	1.76×10^{16}	0.544×10^{-1}	0.532×10^{-2}	0.301×10^{-1}	0.181×10^{-5}	2.3
6	2.15×10^{16}	0.454×10^{-1}	0.482×10^{-2}			
7	2.76×10^{16}	0.236×10^{-1}	0.451×10^{-3}			
8	3.84×10^{16}	0.187×10^{-1}	0.225×10^{-3}	0.195×10^{-1}	0.326×10^{-6}	2.5
9	5.13×10^{16}	0.179×10^{-1}	0.283×10^{-3}			
10	5.33×10^{16}	0.135×10^{-1}	0.444×10^{-4}			
11	7.01×10^{16}	0.939×10^{-2}	0.285×10^{-4}			

Table 6-2

Sample	C	C No/cm^3	T_{min} exp	T_{min} Cal	$\Delta\rho_{exp}$	$\Delta\rho_{cal}$
1	5.34×10^{-6}	2.6×10^{16}	28.4	30.2	11.27×10^{-2}	1.253×10^{-1}
2	5.66×10^{-6}	2.76×10^{16}	27.1	28.5	5.99×10^{-2}	7.85×10^{-2}
3	9.81×10^{-6}	4.78×10^{16}	25.1	26.2	3.07×10^{-2}	3.81×10^{-2}
4	1.19×10^{-5}	5.79×10^{16}	24.7	23.4	1.74×10^{-2}	1.93×10^{-2}
5	1.48×10^{-5}	7.19×10^{16}	23.8	22.5	1.212×10^{-2}	1.46×10^{-2}
6	1.38×10^{-5}	6.72×10^{16}	20.9		1.026×10^{-2}	
7	3.06×10^{-4}	1.49×10^{18}	10.5		0.81×10^{-3}	
8	9.47×10^{-4}	4.61×10^{18}	9.85	9.5	0.48×10^{-3}	0.43×10^{-3}
9	7.83×10^{-4}	3.81×10^{18}	15.5		0.76×10^{-3}	
10	15.1×10^{-3}	7.35×10^{19}	6.9		0.90×10^{-4}	
11	15.34×10^{-3}	7.47×10^{19}	3.9			

Table 6-3

Table 6-4

Sample	a_o	C	C No/cm^3	C' No/cm^3	$(\frac{J'}{N'})_v$ eVcm^3	J' eV
1	0.1477	1.91×10^{-6}	9.3×10^{15}	6.16×10^{14}	0.16×10^{-18}	8.36×10^{-5}
2	0.906×10^{-1}	1.31×10^{-6}	6.4×10^{15}	11.06×10^{13}	0.25×10^{-18}	1.31×10^{-4}
3	0.545×10^{-1}	1.6×10^{-6}	7.8×10^{15}	12.17×10^{14}	0.091×10^{-18}	4.7×10^{-5}
4	0.304×10^{-1}	9.14×10^{-7}	4.4×10^{15}	2.60×10^{14}	0.129×10^{-18}	6.74×10^{-5}
5	0.189×10^{-1}	6.21×10^{-7}	3.0×10^{15}	4.17×10^{13}	0.207×10^{-18}	1.10×10^{-4}
6	0.163×10^{-1}	6.34×10^{-7}	3.1×10^{15}	0.94×10^{10}	0.341×10^{-17}	1.78×10^{-3}

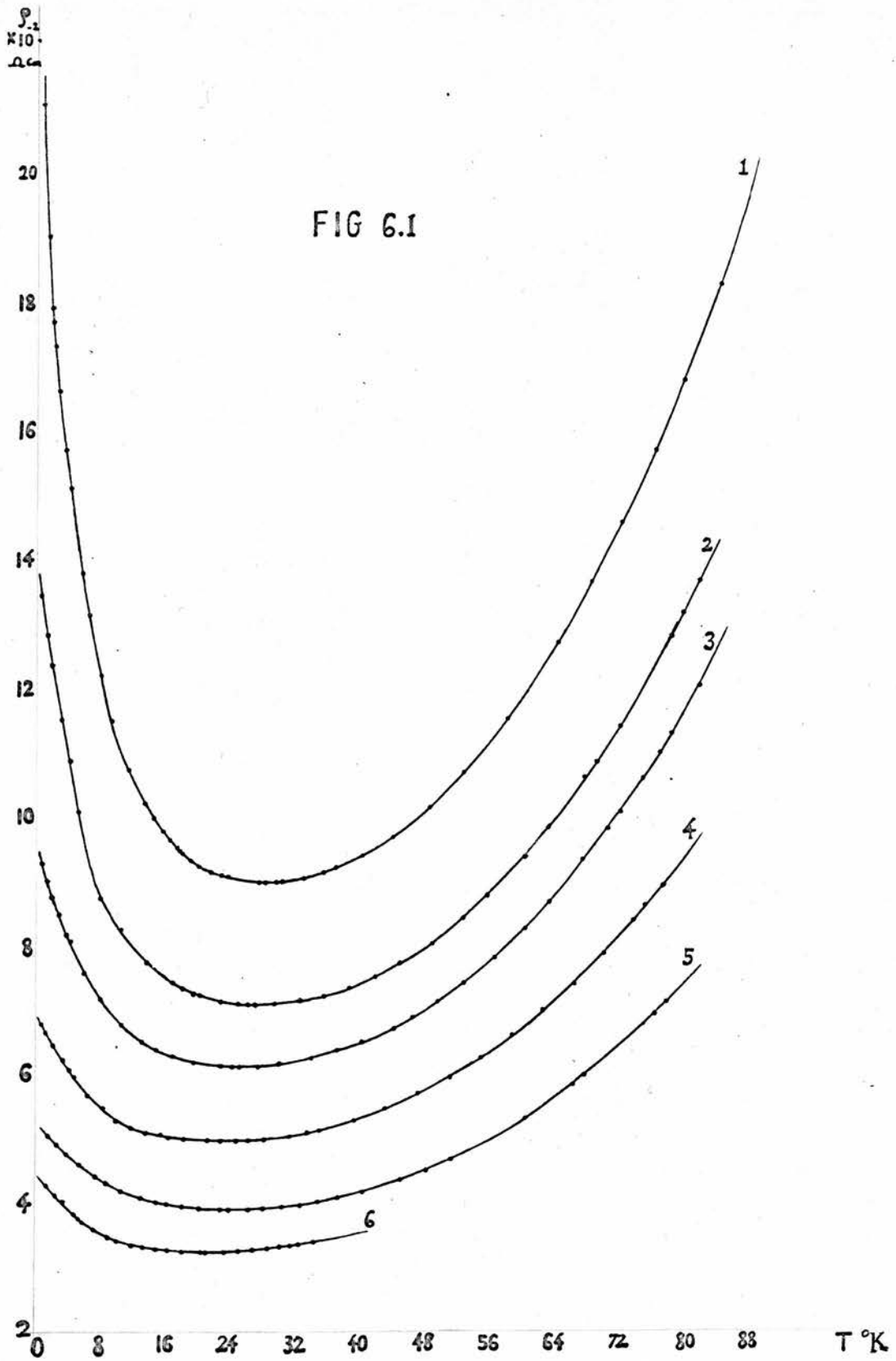
ρ
×10
Ω cm
20
18
16
14
12
10
8
6
4
2
0
8
16
24
32
40
48
56
64
72
80
88
T °K
1
2
3
4
5
6

FIG 6.1

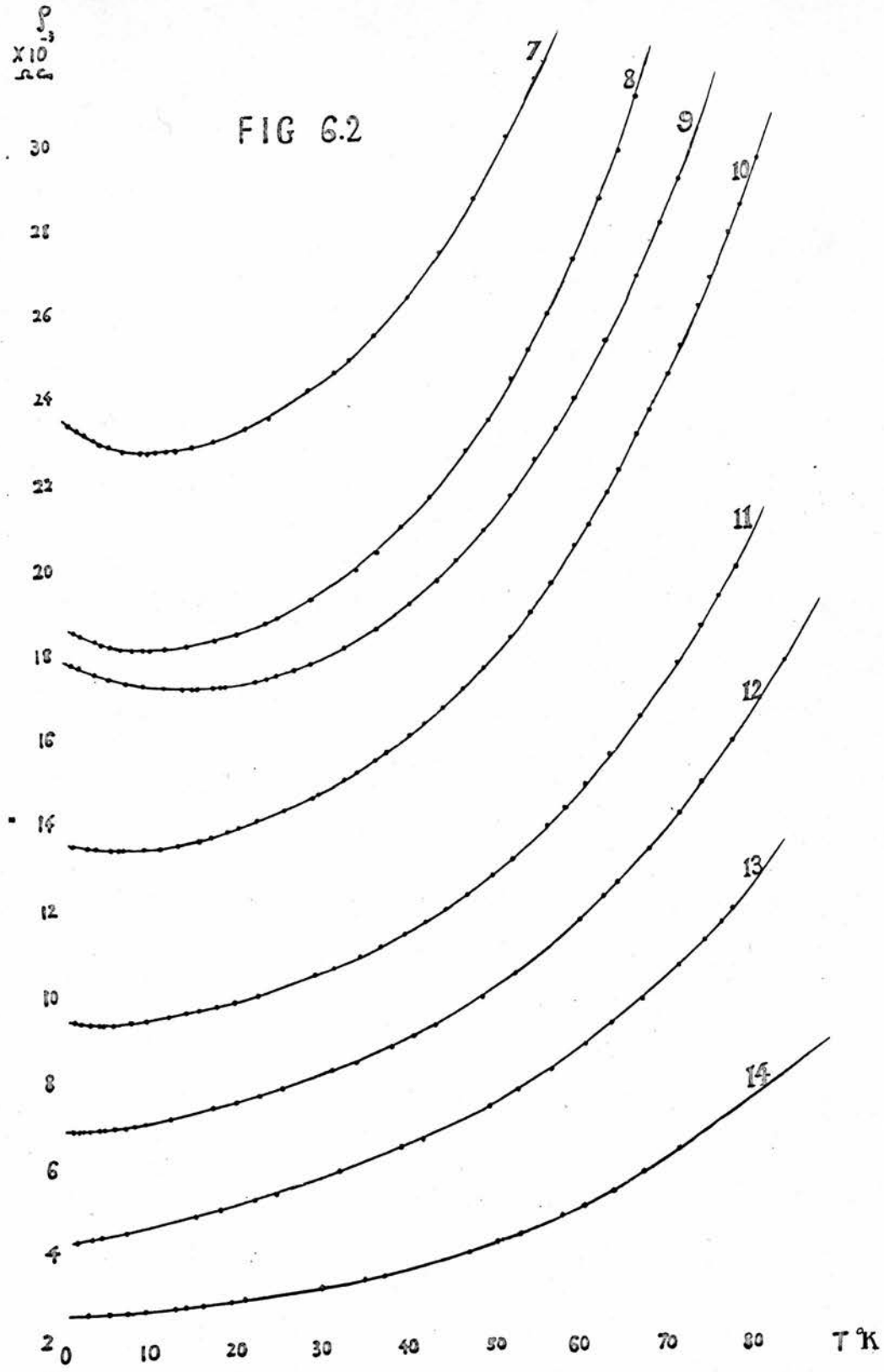
FIG 6.2
$\rho_{\square}$
X10
Ω cm
30
28
26
24
22
20
18
16
14
12
10
8
6
4
2
0
10
20
30
40
50
60
70
80
T °K
7
8
9
10
11
12
13
14

Fig. 6.3

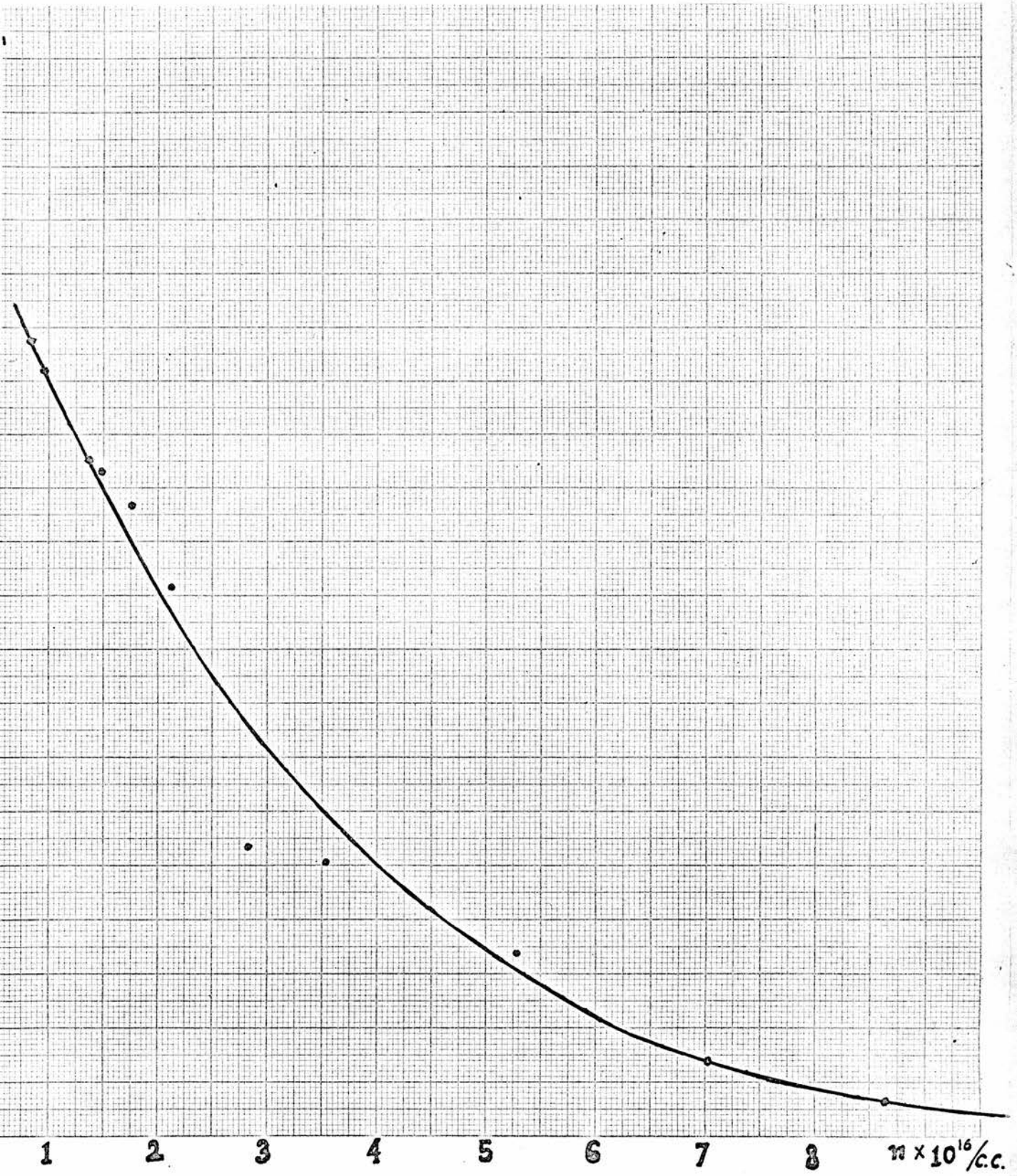

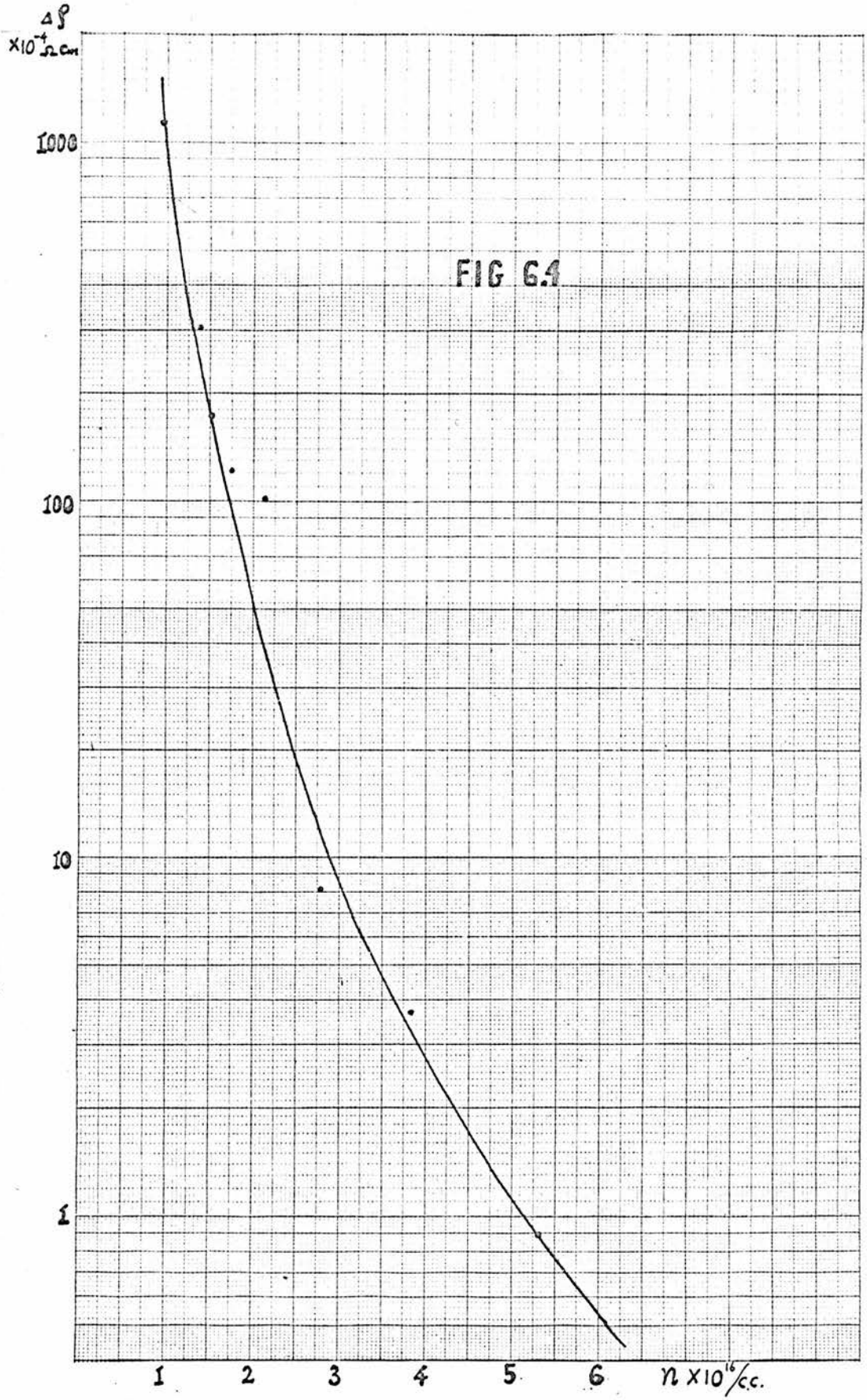

FIG 6.4

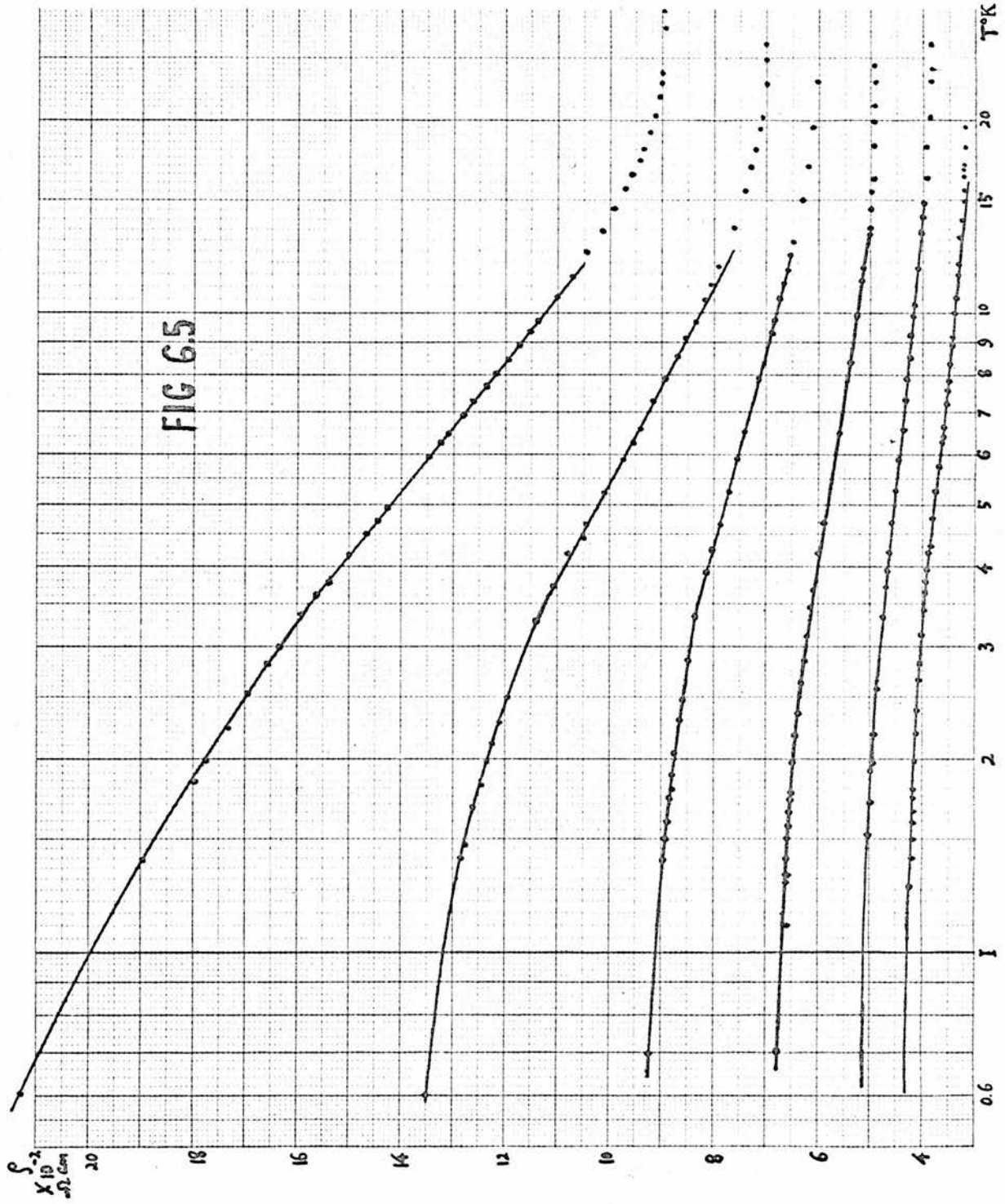
FIG 6.5
ρ
X 10
Ω cm
20
18
16
14
12
10
8
6
4
0.6
1
2
3
4
5
6
7
8
9
10
15
20
T°K

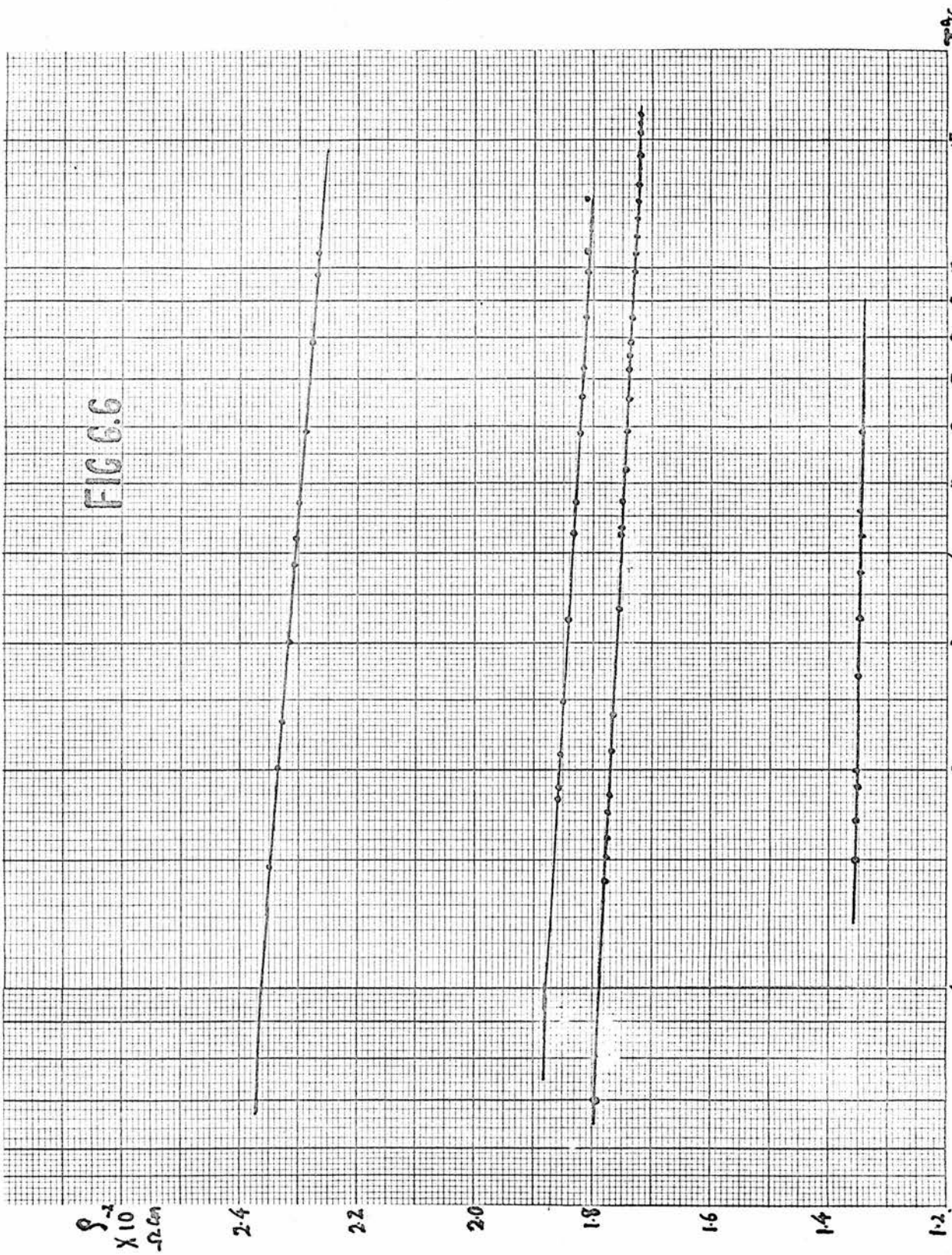

FIG 6.6

Fig. 6.7

• experimental point

× point calculated from $\rho = a - b \ln T$

⊙ point calculated from $\rho \propto T^{-3/2}$

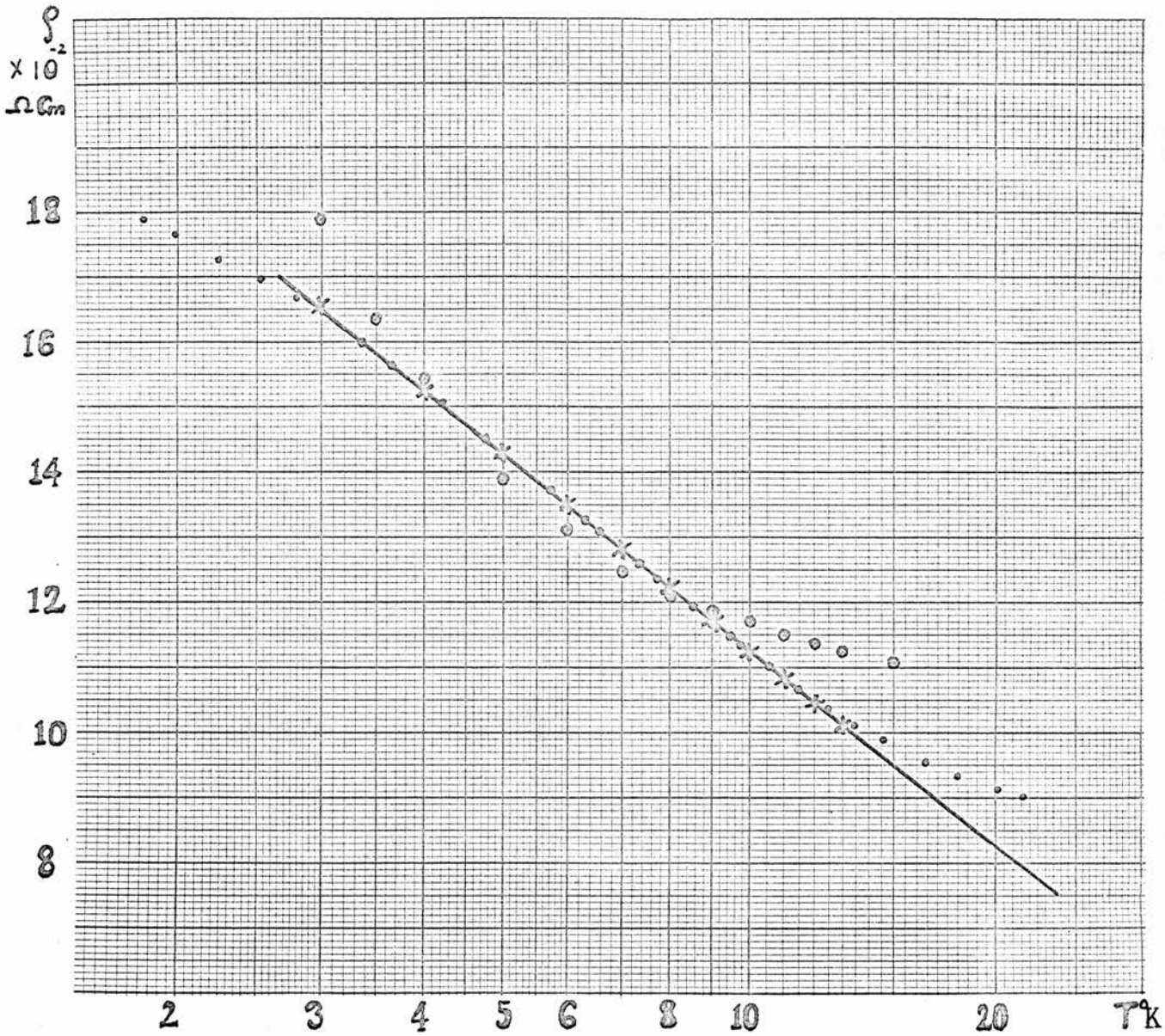

Fig. 6.8

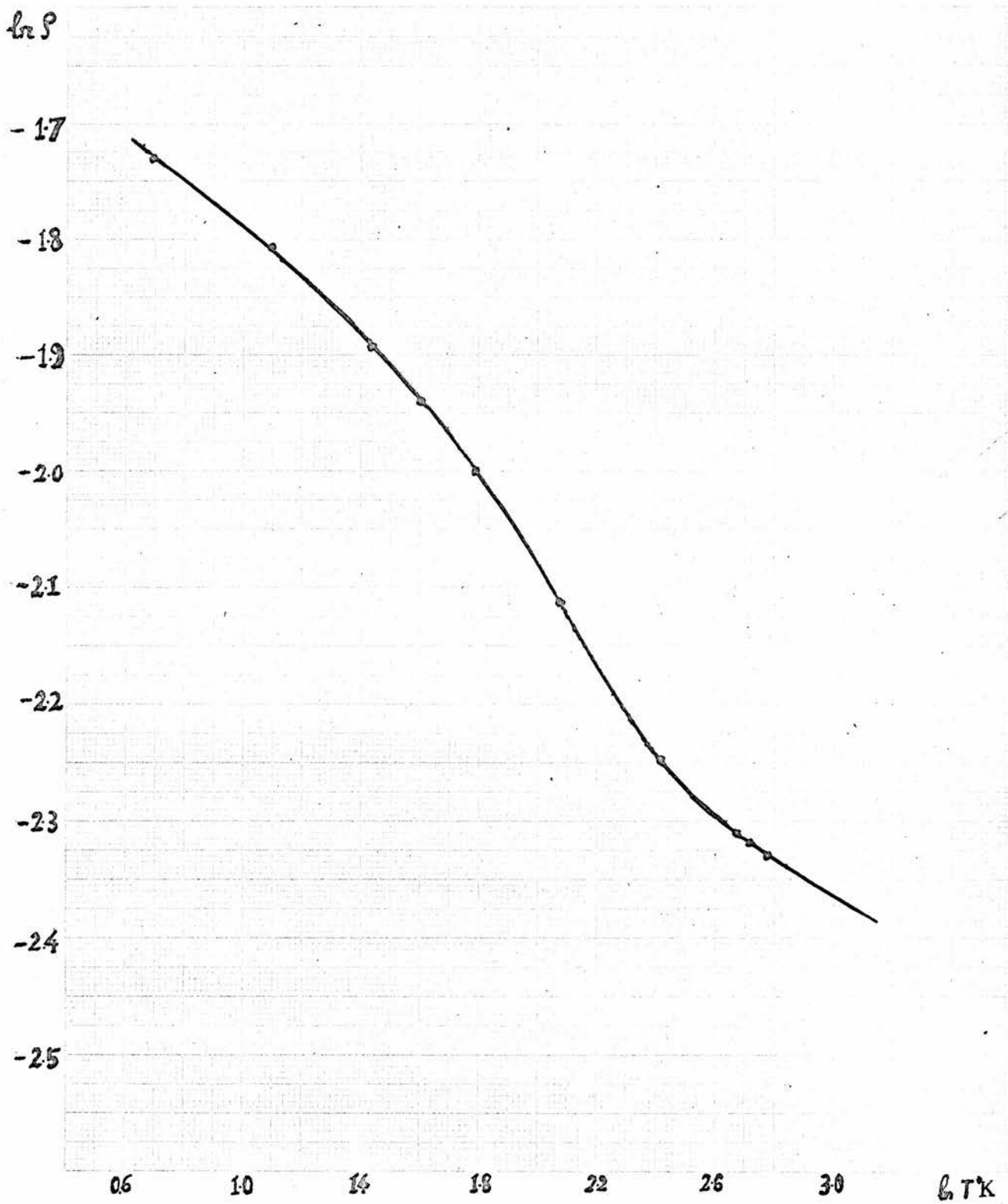

Fig. 6.9

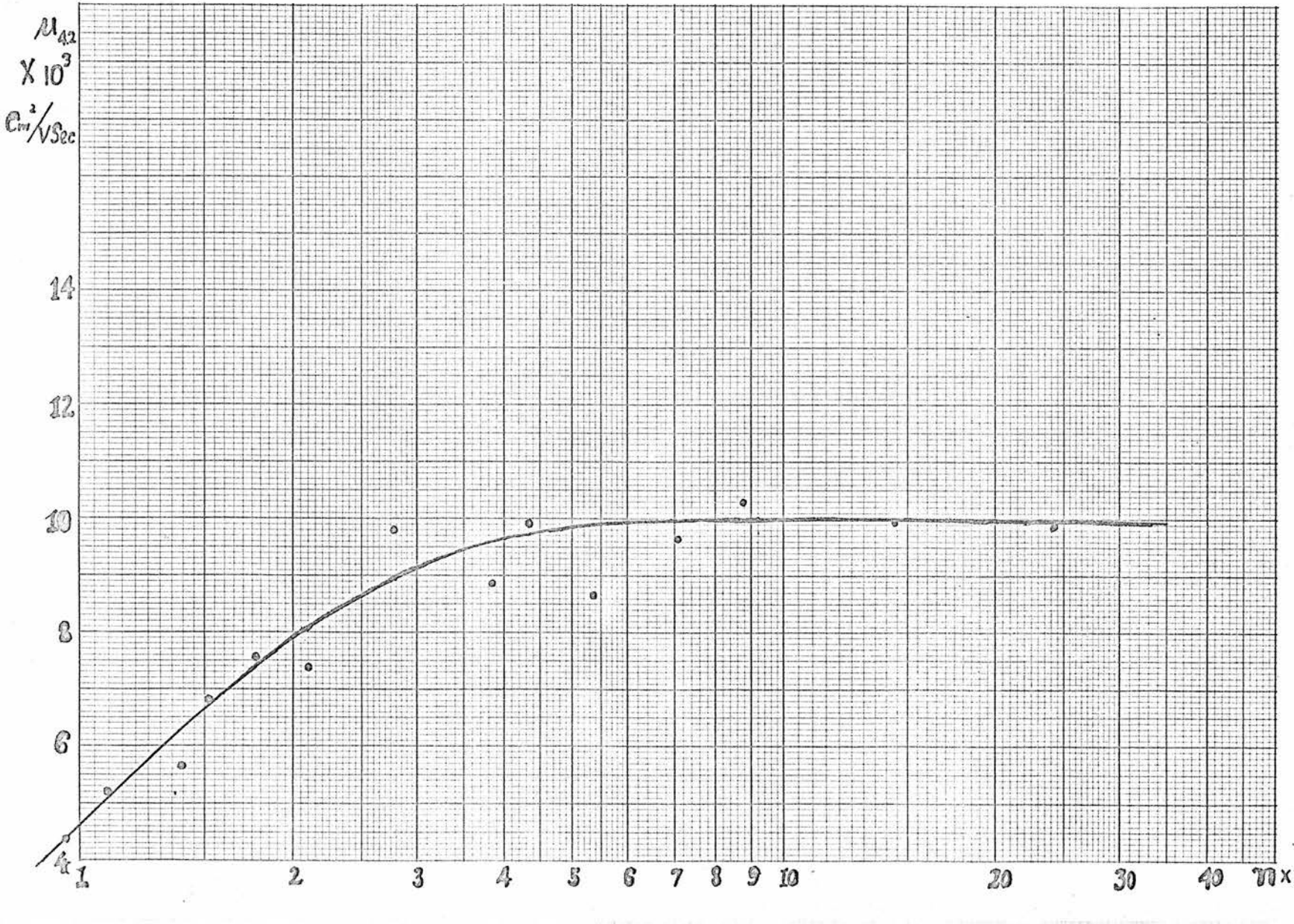

6.2 Discussion of Results

6.2.1 Localized magnetic moments

The observed logarithmic dependence of resistivity on temperature in PbS is similar to that observed in the dilute solutions of Mn in Cu. Magnetic susceptibility measurements on those alloys show the existence of localized magnetic moments. It is quite well known that the occurrence of a resistivity minimum always happens in those materials which have localized magnetic moments. Sarachik et al (1964) observed a resistivity minimum in a dilute alloy of Fe in Mo-Nb having localized magnetic moments which were detected by susceptibility measurements; while those alloys with different compositions which had no localized magnetic moments showed no resistivity minimum. Although there are no direct measurements of susceptibility on PbS, magneto-resistance measurements have been carried out by Finlayson, Mathewson and I. Johnson, and a negative magneto-resistance was observed for crystals with carrier concentrations lower than 5×10^{17}/cc. These results support the existence of localized spins in PbS.

The dependence of the negative magneto-resistance effects on carrier concentration n is somewhat similar to the dependence of the resistivity minimum on n. At the same temperature, say 4.2°K, the negative magneto-resistance effect was strongest for the lowest carrier concentration under investigation. The effect decreased as the carrier concentration increased, and for carrier concentrations greater than about 5×10^{17}/c.c., the negative magnetoresistance effect was not

observed. It was also shown experimentally that the negative magnetoresistance effect was temperature dependent. The effect tended to be weaker as temperature increased, and became rather weak at about 26°K for low 10^{16} carriers/c.c. samples. The magnetoresistance between 26°K and 77°K was not measured, while at 77°K, normal magnetoresistance was found. So we may estimate that the negative magnetoresistance disappears at a temperature between 30°K and 40°K for purer samples, and this temperature at which the negative magnetoresistance disappears decreases as carrier concentration increases and it may be associated with the T_{min} in resistivity measurements. For carrier concentrations of 5×10^{17}/cc a resistivity minimum was not observed and negative magnetoresistance was also not detected. The close correlation of these two effects suggests that they are due to the same kind of scattering mechanism. Toyozawa explained the negative magnetoresistance effect by considering the interaction between localized spins and the conduction electrons. According to Kondo's theory, the resistivity minimum may be regarded as due to the interaction between the localized spins and the spin of conduction electrons. Hence we may claim that these two experimental measurements strongly suggest the existence of localized spins in PbS crystals.

6.2.2 Origin of Localized Spins

In the original Kondo theory, the localized spins are simply due to the existence of magnetic impurities like Mn. However, localized spins may still appear under certain circumstances even if there are no

magnetic impurities according to Toyozawa.

Consider a semiconductor with random distribution of impurities with conduction in the impurity band. Let us label the impurity sites by subscript m. We assume that electrons can transfer between different sites and that a pair of electrons with opposite spins feel repulsive energy U if, and only if, they occupy the same site. Then the Hamiltonian for this system under magnetic field can be written as

$$H = \sum_{m} \sum_{n} \sum_{\pm} V_{mn} a^{*}_{m\pm} a_{n\pm} + U \sum_{m} n_{m+} n_{m-} - \mu B \sum_{m} (n_{m+} - n_{m-})$$

where $a^{*}_{m\pm}$ and $a_{m\pm}$ denote the creation and annihilation operators for an electron with spin + or spin - respectively at the m^{th} site.

The meaning of each term is readily seen to be:

(1) The first term represents our first assumption that electrons may transfer from site to site. The transition probability is determined by $\langle m\pm | H | n\pm \rangle = V_{mn}$

(2) The second term represents interaction between two electrons at the same site since $\langle m+, m- | U \sum_{m} n_{m+} n_{m-} | m+, m- \rangle = U$ where $| m+, m- \rangle$ represents a site with a spin up electron and a spin down electron at the m^{th} site. This means that interaction exists only for a pair of electrons with opposite spins at the same site.

(3) The third term is just the energy due to interaction with the external magnetic field.

Having got this Hamiltonian, Toyozawa then proceeded to solve for the energy eigenvalues and eigenfunctions for such a system, using the Hartree-Fock method. He then evaluated the expectation value of the

occupation number operators $n_{m\pm} = a^*_{m\pm} a_{m\pm}$ for spin-up and spin-down respectively at the m^{th} site. Note that the quantum expectation value of an operator representing a physical quantity is equal to the average measured value for that physical quantity. Therefore the expectation value of, say n_{m+} which is usually denoted by $\langle n_{m+} \rangle$, will be equal to the average number of electrons with spin-up at the m^{th} site. $\langle n_{m+} \rangle = \frac{1}{2}$ and $\langle n_{m-} \rangle = \frac{1}{2}$ will mean that there are as many electrons with spin up as there are electrons with spin down. The m^{th} site will exhibit no net localized spin. However if $\langle n_{m+} \rangle = 1$; $\langle n_{m-} \rangle = 0$ we would have a localized spin pointing in the up direction appearing at the site. Toyozawa found that for such a semiconductor with random distribution of impurity sites, then for a particular site m we have

$$\langle n_{m+} \rangle \sim 1 \quad \text{and} \quad \langle n_{m-} \rangle \sim 0$$

$$\text{or} \quad \langle n_{m-} \rangle \sim 1 \quad \text{and} \quad \langle n_{m+} \rangle \sim 0$$

if the site is sufficiently isolated from neighbouring sites. We therefore obtain the important result that even for a material without magnetic impurities, localized spin may indeed appear as a consequence of the random array of impurity sites and electron correlation. Localized spins appear in those sites which are sufficiently isolated from their neighbours. Note that as there is only one electron at a particular site, the localized spin value is $\pm\frac{1}{2}$ only.

6.2.3 Calculation of Concentration of Localized Spins and Interaction Strength Due to Spin-Spin Interaction

By assuming s-d interaction between magnetic impurity atoms and electrons, Kondo obtained formula (3-3-5-9) for a logarithmic temperature

dependence of resistivity

$$\rho_{spin} = C\rho_M \left(1 + \frac{3zJ}{\varepsilon_F} \ln T\right) \qquad (3\text{-}3\text{-}5\text{-}9)$$

where $$\rho_M = 3\pi m J^2 S(S+1)/2e^2 \hbar \varepsilon_f \qquad (3\text{-}3\text{-}5\text{-}5)$$

The notation is the same as in chapter III.

We used the above formula to calculate the concentration of localized magnetic moments. Curve fitting of experimental data for the appropriate temperature region gave

$$\rho = a - b \ln T \qquad (6\text{-}1\text{-}1)$$

Comparing equation (3-3-5-9) and (6-1-1) we have

$$a = C\rho_M \quad \text{and} \quad -\frac{b}{a} = \frac{3zJ}{\varepsilon_F} \qquad (6\text{-}2\text{-}3\text{-}1)$$

From (3-3-5-5)

$$C = \frac{a}{\rho_M} = \frac{2a e^2 \hbar \varepsilon_F}{3\pi m^* J^2 S(S+1) V/N} \qquad (6\text{-}2\text{-}3\text{-}2)$$

As PbS is of F.C.C. crystal structure the volume of the primitive cell is equal to $l^3/4$, where l is the edge of the unit cube which is known to be 5.9×10^{-8} cm. So N= the total no. of atoms in the crystal = total no. of unit cell = V/volume of primitive cell = $4V/l^3$.

z = number of conduction electrons per atom = $nV/N = n\, l^3/4$

where n is the carrier concentration given in Table 6-1 (p.101) for samples under investigation.

ε_F is calculated from n by formula $\varepsilon_F = \frac{\hbar^2}{2m^*} (3\pi^2 n)^{2/3}$

The quantity S in equation (6-2-3-2) is the maximum spin value for localized spin. We assume S = 5/2 following P.W. Anderson;

A. Nakamma and N. Kinoshita as in the case of Mn in Cu; then equation (6-2-3-2) becomes

$$C = \frac{12\, e^2\, I^3\, a^3\, n^{4/3}}{35\,(3)^{2/3}\,\pi^{7/3}\,\hbar\, b^2} = 5.688 \times 10^{-34}\ \frac{a^3\, n^{4/3}}{b^2}$$

with the values of a, b and n given in Table 6-2 (p.103), the values of C for samples No. 1 to No. 11 were calculated and shown in Table 6-3 (p.103), together with the number of localized spins per unit volume CNo.

Notice that the number of localized spins per unit volume is greater than the carrier concentration of the sample, and also the number of localized spins increases with increasing carrier concentration n, this appears to be very unsatisfactory. Firstly it means Toyozawa's theory on the origin of localized spins cannot be applied to our case. Secondly, we expect from Kondo's theory that as CNo increases, the depth of resistivity, which may be regarded as a measure of the Kondo effect, should also increase. This is, however, not the case according to our results.

Fortunately this difficulty may be resolved by the following consideration. In our calculations, we tacitly assumed that the resistivity was entirely due to the Kondo type spin-spin interaction. However, this may not be the case. For a metal, it is known that impurity scattering contributes a temperature independent term to the resistivity in the low temperature region. When applying Kondo's formula

to such a case, the constant term must be subtracted from the experimental "a" value in order to obtain the true "a" value for use in Kondo's formula. It is reasonable therefore to assume that for our PbS at low temperature, a scattering mechanism other than the Kondo spin-spin interaction exists. This idea gains support also from an examination of ρ-T curve for high concentration crystals. We see that for such samples, the low temperature tails of the ρ-T curves tend to flatten out and resistivity minima are not observed as the concentration gets higher. One can say that for such crystals, the spin-spin interaction is not dominant and that the flat tail of the ρ-T curves are due to some other kind of scattering mechanism.

A plot of mobility versus carrier concentration is shown in Fig. 6.9 (p.113). Notice that the curve tends to a constant value as concentration increases, we therefore assume that the scattering mechanism contributes a more or less constant mobility to all our samples, and we take the value to be that of the saturated value in the mobility curve which is 10^4 cm^2/V sec. These assumptions enable us to make quantitative estimate of those constant resistivity terms to be subtracted from the experimental "a". It is calculated by $\rho_o = 1/ne\mu$ with $\mu = 10^4$ cm^2/V sec. When this is subtracted from the experimental "a" value a new set of values "a_o" are obtained. These represent the constant part of the resistivity due to spin-spin interaction, and is shown in Table 6-4 (p.104). The values of a_o were calculated only for sample No.1 to No. 6 because the error involved in

the calculation with the estimated constant mobility will be too big for high concentration samples. Now the a value in equation (6-1-1) was replaced by a_o and equated to equation (3-3-5-9). The value C and the number of localized spins per unit volume were calculated and shown in Table 6-4 (p.104) third and fourth column. We see that the results are reasonable, namely the concentration of localized spins is smaller than the conduction electron concentration. Toyozawa's theory on the origin of localized magnetic moments may then be applicable in our case. Also the number of localized spin decreases as the effect gets less pronounced, which is similar to that in dilute magnetic alloys. We therefore conclude that for the temperature region below T_{min}, there is a scattering mechanism other than the spin-spin interaction which contributes to the temperature independent term in resistivity. We cannot for the time being determine the origin of this. It might be similar to the residual resistance in metals mostly caused by static lattice defects such as impurity atoms, vacancies and dislocations etc. However the spin-spin interaction between conduction electrons and localized spins is the main scattering mechanism for low carrier concentration samples since the localized spin concentration is bigger. As the localized spin decreases, the scattering due to spin-spin interaction becomes weaker and other contributions become important.

The next thing now is to compute the spin-spin interaction coupling strength. Using equation (6-2-3-1) with a replaced by a_o'', the J

values which represent coupling strength were calculated for samples No. 1 to No. 6 and found to be of order of 10^2 eV. This value is certainly too big. The appearance of this big J value could be due to two things: the first being the fact that Kondo's formula which was derived for metals might not be correct for semiconductors as the Fermi energy $\mathcal{E}_F$ in a semiconductor is about three orders of magnitude smaller than in a metal, (we will discuss this problem later); the second being the nature of localized spins. The localized spins in dilute magnetic alloys are due to the actual magnetic moments which are well localized in unit cells and that all the magnetic moments take part in the interaction.

S. Tanaka and Y. Katayama using Toyozawa's idea on the origin of localized spins suggested that in InSb the localized spins spread over a wide region of volume Ω' containing many unit cells, in contrast to that in dilute magnetic alloys whose localized spin is well localized within a unit cell of volume Ω. Let

N = total no. of unit cells in the crystal = $N_0 V$

V = volume of the crystal; N_0 = no. of unit cells per unit volume

N' defined by $N'\Omega' = N\Omega$ gives the number of localized spins in the crystal.

Then replacing the J/N in the Kondo interaction Hamiltonian by J'/N', they arrived at a formula similar to Kondo's

$$\rho_{spin} = C' \rho_M \left\{1 + 4n(\mathcal{E}_F)\left(\frac{N}{N'}\right) J \ln\left(\frac{kT}{\mathcal{E}_F}\right)\right\} \qquad (6\text{-}2\text{-}3.3)$$

where $$\rho_M = \frac{N}{N'} \frac{3\pi\, m^* J'^2 S(S+1)}{2 e^2 \varepsilon_F \hbar} \frac{V}{N} \qquad (6\text{-}2\text{-}3\text{-}4)$$

with $n(\varepsilon_F)$ = density of states at the Fermi energy per atom =

$$\frac{n_o(\varepsilon_F)}{4N_o} = \frac{1}{4N_o} \frac{(2m)^{3/2}}{2\pi^2 \hbar^3} \varepsilon_F^{\frac{1}{2}}$$

Taking the effective Bohr radius as the spreading of the wave function of the localized spin, they were able to calculate the localized spin concentration and estimate the magnitude of the coupling strength J'.

These ideas and their formulae were used to repeat our calculations. With "a" replaced by "a_o" in equation (6-1-1), we have

$$\rho = a_o - b \ln T = a' - b \ln \left(\frac{kT}{\varepsilon_F}\right) \qquad (6\text{-}2\text{-}3\text{-}5)$$

where $$a' = a_o - b \ln \left(\frac{\varepsilon_F}{k}\right)$$

Combining it with equation (6-2-3-3) we have

$$\frac{J'}{N'} = -\frac{b}{a'} \frac{1}{4n(\varepsilon_F)N} = -\frac{b}{a'} \frac{1}{n_o(\varepsilon_F)V}$$

$$\left(\frac{J'}{N'}\right)_v = \frac{J'}{N'} V = -\frac{b}{a'} \frac{1}{n_o(\varepsilon_F)} \qquad (6\text{-}2\text{-}3\text{-}6)$$

From equation (6-2-3-4)

$$\rho_M = N\left(\frac{J'}{N'}\right)^2 V \frac{3\pi\, m^* S(S+1)}{2 e^2 \varepsilon_F \hbar} = N_o \left(\frac{J'}{N'}\right)_v^2 \frac{3\pi m^* S(S+1)}{2 e^2 \varepsilon_F \hbar}$$

From equation (6-2-3-3) and (6-2-3-5) we have

$$a' = C' \rho_M$$

Then $$C' N_o = \frac{a'}{\left(\frac{J'}{N'}\right)_v^2 3\pi\, m^* S(S+1)/2 e^2 \varepsilon_F \hbar}$$

with the $S = \frac{1}{2}$, the localized spin concentration and the ratio J'/N' were calculated for sample No. 1 to No. 6 and shown in 5th and 6th columns of Table 6.4 (p.104). N' was calculated from $N' = N\Omega/\Omega'$ where Ω = volume of unit cell = $(5.9 \times 10^{-8})^3_{cc}$ in PbS; $\Omega' = \frac{4}{3}\pi \gamma_o^3 = 1.915 \times 10^{-15}$ cm^3, where γ_o = Bohr ratius = $(\frac{\varepsilon}{\varepsilon_o})\frac{m}{m^*}\, 0.53\text{Å} = 7.703 \times 10^{-6}$ cm (dielectric constant $\frac{\varepsilon}{\varepsilon_o} = 174.4$ and $\frac{m^*}{m} = 0.12$ for PbS) J' values were calculated and also shown in Table 6-4 (p.104). A negative J' represents antiferromagnetic interaction between the localized spin and the conduction electrons according to Anderson. The values varied from 10^{-5} to 10^{-3} eV which are reasonable. The J' value was higher for high carrier concentration crystals while $C'N_o$ was smaller. As the carrier concentration n decreased, $C'N_o$ increased and J' decreased. This can be seen from the values given in Table 6-4 (p.104) for sample No. 6 to No. 3. As the carrier concentration n further decreased, we had the opposite result, $C'N_o$ became smaller while J' became bigger. There appeared a maximum of localized spin concentration and minimum J' value as n changed from high to low value. We will come back to this point in the next section. The $C'N_o$ and J' values for No. 1 and No. 2 had the wrong order to what we expected. This could be due to experimental error which was magnified in the calculation.

6.2.4 The Origin of Localized Spin in PbS

The localized magnetic moments are due to either the actual magnetic impurities in PbS crystals or the result of electron correlation and random array of impurity sites. The first possibility is not very

plausible because of the fact that the majority of impurities in n type PbS come from a stoichiometric excess of Pb atoms in the lattice, although a minority of Mn atoms was found in some PbS samples from the same source as those under investigation, by neutron activation experiment done in the Reactor Centre in East Kilbride. The existence of Mn does not necessarily give magnetic moments. Furthermore the calculation of coupling constant J using Kondo's formula based on the assumption that magnetic moments are due to actual magnetic impurities did not give satisfactory results; whereas the calculation using Tanaka's formula based on the idea of Toyozawa led to reasonable results. We therefore have to attribute our localized spins to the same origin as those in Toyozawa's theory.

We have mentioned the conditions for Toyozawa's theory to be applicable before. The localized spins are associated with semi-isolated sites. As the carrier concentration increases such isolated sites must decrease and so the number of localized spins must decrease and finally, with sufficiently high carrier densities, disappear altogether. In our case this appears to happen for $n > 5 \times 10^{17}$ electrons/c.c. On the other hand one might expect the reverse to be the case for actual magnetic impurities. Toyozawa also predicted a decrease in the number of spins at very low impurity densities. A plot of spin concentration $C'N_o$ versus carrier concentration n is given below.

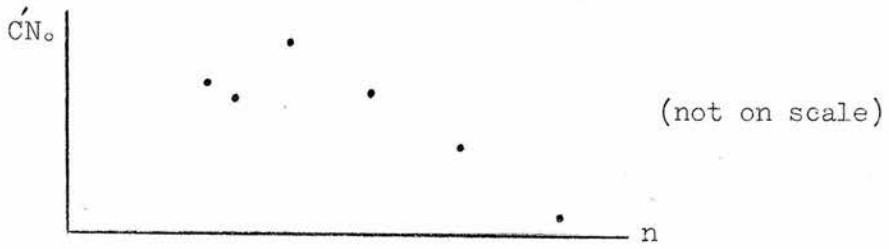

One sees that indeed $C'N_0$ decreases at both high and low n. It appears that the origin of localized spin for PbS is indeed the same as that described by Toyozawa's theory.

6.2.5 T_{min} $\Delta\rho$ and an Empirical Expression for ρ near Minimum

The resistivity below T_{min} can be represented by the expression $\rho = a - b \ln T$ where resistivity decreases with increasing temperature while above T_{min} it increases with temperature and may be expressed by the formula $\rho = g + dT^p$. Therefore a resistivity minimum ρ_{min} corresponding to T_{min} is expected. We assume that near T_{min}, the resistivity is mainly due to both the Kondo type scattering and the usual lattice scattering. Then the total resistivity may be expressed as the sum of both contributions.

$$\rho = a - b \ln T + g + d T^p$$

Now we want to see how far this can represent the experimental results. Differentiating it with respect to T and equating it to zero we obtain the temperature at which the minimum occurs

$$T_{min} = \left(\frac{b}{p.d}\right)^{\frac{1}{p}}$$

With the values of b, p, d for samples No. 1 to No. 5 and No. 8, the calculated T_{min} values are shown in Table 6-3 (p.103). Comparing the

calculated T_{min} with T_{min} values obtained experimentally, we can see that they agree with each other quite well. So we may say that in the temperature region around minimum, both scattering mechanisms mentioned above contributed to resistivity with more or less equal weight.

Now we consider the depth of the minimum defined as the resistivity measured at the lowest temperature or extrapolated to absolute zero ρ_o minus that at T_{min} (ρ_{min}). The resistivity ρ_{min} at T_{min} is represented by $\rho_{min} = a - b \ln T_{min} + g + dT^p$. Suppose we use the same expression for resistivity at T_o, then $\rho_o = a - b \ln T_o + g + dT_o^p$ and $\Delta\rho = \rho_o - \rho_{min} = b[\ln(\frac{T_{min}}{T_o}) - \frac{1}{p}] + d T_o^p$. For simplicity we let $T_o \simeq 1°K$, d is so much less than the first term that we can neglect it. $\Delta\rho$ so calculated for samples No. 1 to No. 5 and No. 8 are shown in Table 6-3 (p.103). The discrepancy between the calculated values and the experimental values is seen to be appreciable. This means that we really should not use the above phenomenological expression for the resistivity in a region not near T_{min}. However in what follows we shall only make rough calculations, we may therefore still try to use the expression. We are not particularly interested in the actual value of $\Delta\rho$ for each sample. We are more concerned with the relationship between $\Delta\rho$ and concentration. Direct experimental data fitting gives $\Delta\rho_{exp} \propto n^{-3.0}$. A similar result is obtained from the above empirical formula $\Delta\rho_{cal} = b[\ln \frac{T_{min}}{T_o} - \frac{1}{p}]$. Notice that the factor $[\ln \frac{T_{min}}{T_o} - \frac{1}{p}]$ is not a sensitive function of n. It varies from about 1.8 to 2.4 for all our samples under investigation. So we may take $\Delta\rho_{cal} \propto b$, while

b is also found to be: $b \propto n^{-3.0}$, so we have a first order agreement of dependence of $\Delta\rho$ on n between these two results.

One noticed that for lower carrier concentration samples the number of localized spins $C'N_0$ decreased. This appeared to contradict the above result, namely $\Delta\rho_{exp}$ being a measure of the magnitude of the Kondo effect should be expected to decrease as $C'N_0$ decreased and vice versa. This apparent contradiction is resolved by noting the "magnitude of the Kondo effect" depends on the interaction coupling strength J' as well. As seen in Table 6-4 (p.104), J' for those samples increased to compensate for the decrease in $C'N_0$ resulting in a bigger depth of resistivity $\Delta\rho_{exp}$.

6.2.6 An Attempt to Adapt the Kondo Formula for Semiconductors

Kondo's resistivity formula was derived for a metal. It was seen from our explicit calculation in Chapter III that the approximation $\frac{\varepsilon_F}{kT} \sim \infty$ was made. This is legitimate for a metal where $\varepsilon_F \gg kT$ for the low temperature range concerned. However this is not so for semiconductors in general, especially those with low concentration. For example, at T = 10°K for PbS of $n = 10^{16}$/c.c., $\varepsilon_F \approx kT$. Therefore it appears that we should not use Kondo's formula as it stands. It does not seem easy to obtain a completely satisfactory and simple formula for such cases. We try to reevaluate integrals A_1, A_2 and B in the resistivity expression in Chapter III (p. 61), for integration limit from $-\frac{\varepsilon_F}{kT}$ to ∞ instead of from $-\infty$ to $-\infty$. The resulting formula for ρ will then be expected to be a complicated function of T in view of the fact that all

integrals are now temperature dependent. An explicit formula is not obtained because the integral A_1 can be evaluated only numerically. We contented ourselves with an order of magnitude calculation to see by how much the J value would be modified as a result. We take $\mathcal{E}_F/kT = 1$

$$A_1 = \iint_{-1}^{\infty} \ln|x-x'| \frac{dF(x)}{dx} \frac{dF(x')}{dx'} dx\,dx'$$

$$A_2 = \ln kT \iint_{-1}^{\infty} \frac{dF(x)}{dx} \frac{dF(x')}{dx'} dx\,dx' = \ln kT[F(x)F(x')]_{-1}^{\infty}$$

$$= \ln kT\left(\frac{1}{e^{-1}+1}\right)^2 \approx 0.5 \ln kT$$

$$B = \ln 4|\mathcal{E}_F| \iint_{-1}^{\infty} \frac{dF(x)}{dx} \frac{dF(x')}{dx'} dx\,dx' = \ln 4\,|\mathcal{E}_F| \left(\frac{1}{e^{-1}+1}\right)^2 \approx 0.5 \ln 4|\mathcal{E}_F|$$

A_1 was computed using the Simpson's rule for numerical integration. As the integrand decreases rapidly as x increases to the order of 10, it is sufficient to evaluate the integral from -1 to 10. The value was found to be 0.02725. Extending the upper limit to 15 will only give an additive term of order 10^{-5}, then $A - B = A_1 + A_2 - B = 0.02725 + 0.5 \ln kT - 0.5 \ln 4\,\mathcal{E}_F$

$$= 0.02725 + 0.5 \ln \frac{k}{4\mathcal{E}_F} + 0.5 \ln T$$

so the expression for ρ becomes

$$\rho = C\rho_M [1+X+Y\ (0.02725 + 0.5 \ln \frac{k}{4\,\mathcal{E}_F} + 0.5 \ln T)]$$

$$= C\rho_M [1+X+Y\ (0.02725 + 0.5 \ln \frac{k}{4\,\mathcal{E}_F}) + Y\ 0.5 \ln T]$$

where $X = 6zJ/\mathcal{E}_F$; $Y = 3zJ/\mathcal{E}_F$.

However this expression turns out to be essentially the same as the original Kondo one and it does not lead to much change of J value.

It might be worth making a remark about the integral A_1. The integrand contains a factor $\ln|x - x'|$ which diverges as x approaches x'.

Therefore it is not easy to handle and there is a slight possibility that the integrand might behave so strangely near singularities as to invalidate the numerical integration used.

CHAPTER VII

Experimental Results on Thermomagnetic and Thermoelectric Measurements

7.1 Nernst Effect Measurements

The transverse and longitudinal Nernst effect measurements were carried out in the temperature range from 4°K to 80°K with different values of magnetic field for five n-type PbS samples of carrier concentration ranging from 1.03×10^{16}/c.c. to 1.2×10^{17}/c.c. The dependence of the transverse Nernst coefficient Q^{1} and the longitudinal Nernst coefficient Q^{11} on temperature with magnetic field 3.9 Kgauss for the five samples are shown in Fig. 7-1 (p.143) and Fig. 7-2 (p.144). It is seen from Fig. 7-1(p.143) that the transverse Nernst coefficient Q^{1} is negative below about 45°K and tends towards zero at absolute zero for all samples. As the temperature increases Q^{1} becomes more negative and also the difference between Q^{1} for different concentrations increases. These reach a minimum value between 15 and 30°K, the temperature dependence of the minimum increasing as the carrier concentration decreases. Above the minimum, the value increases and changes to positive between 40 and 50°K, and it remains positive at higher temperatures. It is seen that the temperature dependence of Q^{1} is stronger for low carrier concentration samples.

The dependence of longitudinal Nernst coefficient Q^{11} on temperature in a fixed magnetic field of 3.9 Kgauss for the five samples is shown in Fig. 7-2 (p.144). The measurements on the

longitudinal effect were mainly performed at temperatures below 20°K, and the values were found to be of negative sign for all the samples under investigation. The sign of the effect for all five samples at nitrogen temperature was checked and found to be positive. Some measurements were also made at temperatures round about 40°K. We found that the sign of the effect changed from negative at low temperatures to positive at higher temperatures. In fact for the high concentration sample No. 5, the sign changed at about 20°K. It is expected that the temperature at which Q^{11} changes sign will be more or less related to that in the transverse measurement, but according to the data available for sample No. 5, the temperature at which Q^{11} changes sign may be lower than that in the transverse case. The carrier concentration dependence of the Q^{11} can be seen from Fig. 7-2 (p.144). With the exception of sample No. 4, the dependence is seen to be stronger for lower carrier concentrations.

Fig. 7-3 (p.143) and Fig. 7-4 (p.144) show the dependence of $Q^{\perp}$ and Q^{11} on temperature with different values of magnetic field for sample No. 1. It is seen from the curves that the dependence is stronger for low magnetic field with the transverse measurements whereas the opposite was obtained for longitudinal measurements.

The dependence of the transverse voltage per degree on magnetic field from zero up to 8 Kgauss was measured at different temperatures and shown in Fig. 7-5 (p.147), Fig. 7-6 (p.148) and Fig. 7-7 (p.149) for samples No. 1, 2 and 3. Fig. 7-8 (p.150) and Fig. 7-9 (p.151) were

plotted the longitudinal Nernst coefficients against H^2 for sample No. 1 and No. 3

7.2 Discussion of the Results

From the results given in section 7.1, we know that both transverse and longitudinal Nernst effects have a negative sign at low temperatures and the effect changes sign at about 40°K. According to the theory given in Chapter II, a negative sign indicates that impurity scattering is predominant and a positive sign indicates acoustic scattering. We may therefore say that our results indicate that for temperatures above 40 to 50°K, the main scattering mechanism is due to acoustic vibrations. This is consistent with the resistivity measurements. We are dealing with the problem under the condition that $(\frac{\mu H}{c})^2 \ll 1$, so weak field formulae may be applied in our case. Now with r = 0 which represents acoustic scattering, the formula (2-2-2) becomes

$$E_y = \tfrac{1}{2}\,(1.1781)\,\frac{k}{e}\,\frac{\mu H}{c}\,\frac{\partial T}{\partial x}$$

and

$$\mathcal{E}_y = \frac{E_y}{\frac{k}{e}\,\frac{\partial T}{\partial x}} = 0.589\,\frac{\mu H}{c} \qquad (7\text{-}2\text{-}1)$$

With the measured value of the Nernst field, the mobility μ for sample No. 1 at T = 84°K was calculated and found to be equal to 2282 cm^2/v sec which is smaller by a factor 2 than the value 4650 cm^2/v sec calculated from the resistivity and the Hall effect measurements. This discrepancy could be due to some other kind of scattering such as phonon drag in addition to the predominant acoustic lattice scattering. In this

case the above formula for $\mathcal{E}_y$ needs to be amended. We shall discuss phonon drag in a separate section, but it appears that whatever is responsible for this discrepancy, it has a characteristic feature that does not show up in purely electrical measurements while on the other hand it is quite sensitive to thermal measurements.

When the temperature decreases, the influence of the lattice vibration on carriers reduces and some other kind of scattering becomes important. In general the most favourable scattering mechanism at low temperatures is due to ionized impurity scattering which gives rise to a Nernst effect of negative sign. As mentioned in Chapter II, if the scattering mechanism can be characterized by a relaxation time which has an energy dependence of form $\tau = \tau_0(\frac{\mathcal{E}}{kT})^{r-\frac{1}{2}}$. The r value can be determined directly from the Nernst effect measurements. The ratio $\mathcal{E}_y^2 / \mathcal{E}_x$ calculated from $\mathcal{E}_y^2/\mathcal{E}_x = (\frac{1}{2}-r)\, A_r^2/(2b_r-A_r^2)$ for different values of r are listed in the following table.

Table 7-1

r	0	0.5	0.75	1	2
$\mathcal{E}_y^2/\mathcal{E}_x$	+0.323	0	-0.2381	-0.4263	-0.702

To compare these values with our experimental data for various samples we plotted $\mathcal{E}_x$ and $\mathcal{E}_y$ against temperature for our five samples in different values of magnetic field and the curves are shown in Fig. 7-10 to Fig. 7-14 (from p.152 to p.156). The ratios $\mathcal{E}_y^2 / \mathcal{E}_x$ from experimental data for five samples are calculated for every two degrees from 20°K

and found to vary from -0.011 to -0.18. Comparing these with the theoretical ratios in Table 7-1, although we cannot positively identify the form of scattering we can be certain that ionized impurity scattering is not the major scattering mechanism in this temperature region. Recalling our discussion of the resistivity results, the scattering mechanism at temperatures below say 30°K is attributed to the spin-spin interaction. However, the theory and hence the formulae we discussed for our thermomagnetic effects in Chapter II, are based on the assumption that the scattering mechanism can be characterised by a power dependence of relaxation time on energy. The relaxation time due to spin-spin interaction is more complicated and completely different from the simple power law. If spin-spin interaction did contribute to our thermomagnetic effect it would not be surprising to find that the present formulae for the Nernst effect are not strictly applicable and this may account for our failure to find an identifiable r value. By examining the dependence of carrier concentration with both the transverse and longitudinal effects from Fig. 7-1 (p.143) and Fig. 7-2 (p.144) we found that the temperature dependence of both transverse and longitudinal effects decreases as the carrier concentration n increases except for the longitudinal effect measurement for sample No. 4. This dependence is similar to the resistivity result where low carrier concentration had deep resistivity minimum indicating stronger spin-spin interaction. Hence it is reasonable to assume that spin-spin interaction might indeed appear.

Now we examine the magnetic field dependence of the Nernst effect. From Fig. 7-5 (p.147) to Fig. 7-7 (p.149) we see that the transverse Nernst field has its absolute value increased monotonically with magnetic field at all temperatures measured. The dependence is linear at the lowest temperatures. It becomes non-linear when the temperature approaches the point at which the minimum occurs in the Q^1-T plot. At higher temperatures say about 40°K, the Nernst field is positive and it again depende on H linearly. All this shows that only at very low temperatures and at high temperatures say 40°K upward, the weak field approximation formula has a chance to be applicable to our case. We do not mean to say the weak field theory discussed in Chapter II is necessarily applicable, but it appears that any new theory applicable to our case should again have such a linear dependence on magnetic field H in the two temperature regions mentioned above. In Fig. 7-3 (p.145), the curves change over from positive for higher temperatures to negative at low temperatures. The appearance of a sharp minimum indicates changes of scattering mechanisms. Above the minimum the transverse Nernst coefficient Q^1 is approximately independent of magnetic field, this is consistent with the weak field formula for acoustic lattice scattering. On the other hand below the minimum there is a marked field dependence. Consider the negative magneto-resistance effect which is attributed to spin-spin interaction, for which resistance decreases and hence mobility increases as the magnetic field increases and so scattering must decrease with increase of field.

If the scattering mechanism at low temperatures gives rise to a relation of the form $Q^1 \propto \mu$ as in the weak field case, we expect an increase in μ as H increases and hence an increase of transverse Nernst coefficient Q^1. This is what is observed and so we have further evidence for spin-spin interaction in our low temperature region.

The dependence of the longitudinal Nernst coefficient Q^{11} on magnetic field is seen in Fig. 7-8 (p.150) and Fig. 7-9 (p.151). At temperatures where Q^{11} has a positive value, a Q^{11}-H^2 plot gives a straight line which is consistent with our weak field formula. At lower temperatures a straight line is not obtained. The reason may be the same as that used to explain the behaviour of Q^1.

We end this section with the following conclusion. From the variation of the transverse and longitudinal Nernst effects with temperature, we found that the effects are positive above say 40°K, and scattering in this region is mainly due to acoustic vibrations. The effects become negative at low temperature and a sharp minimum indicates a change of scattering mechanism. In this low temperature region, ionized impurity scattering is not important. In Chapter VI we found that the resistivity measurements could be explained in terms of a spin-spin interaction which increases as the electron concentration n decreases. Similarly we find here that the negative component of the transverse Nernst coefficient Q^1 increases as n decreases. We therefore suggest the existence of spin-spin interaction. This suggestion gains further support from the magnetic field dependence of the Nernst effect

in this temperature region. The increase of magnetic field leads to an increase of the transverse Nernst coefficient Q^1 and hence an increase of mobility, implying a decrease of resistivity. This is consistent with the results obtained from the negative magneto-resistance effects. On the other hand there is negligible magnetic field dependence at higher temperatures so the results above 40°K are consistent with acoustic scattering.

7.3 Measurements of Thermoelectric Power

7.3.1 Results

Measurements of thermoelectric power have been carried out for the five samples mainly in the temperature range from 5°K to 30°K. For samples No. 1 and No. 3 some measurements were also done at nitrogen temperature and upwards. The results are shown in Fig. 7-15 (p.157) where thermoelectric power Θ is plotted against ln T. As mentioned in Chapter II, in the non-degenerate temperature region, a Θ-ln T plot will give a straight line if the scattering mechanism can be represented by a simple power law of the form $\tau \alpha \varepsilon^{r-\frac{1}{2}}$. It is seen that the Θ - ln T dependence is non-linear in most cases. For sample No. 3, the curve appeared to be linear above about 30°K where the carriers satisfied the non-degenerate condition. The linearity in this region could mean that the scattering mechanism might be due to a single known type. The curve of sample No. 1 showed that it is non-linear even at the non-degenerate region. The explanation of this non-linearity could be due either to the change of effective mass

with temperature or to phonon drag. For samples No. 4 and No. 5, the degeneracy temperatures are above 40°K, and so the carriers are degenerate for the temperature range measured. Hence even an appearance of a straight line for sample No. 5 does not necessarily mean that a simple known type of scattering mechanism can be used to describe its behaviour. The dependence of the carrier concentration does not appear to have regular dependence on the thermoelectric power value. However, we try to treat the thermoelectric data from two different angles. Firstly we attempt to find the effective mass of the carriers and hence investigate whether the effective mass of PbS is temperature dependent. Secondly, we study whether phonon drag exists.

7.3.2 Analysis

From the analysis of the Nernst effect, we concluded that the main scattering mechanism above, say, 40°K is due to acoustic lattice scattering. Therefore in such a temperature range we are able to calculate directly the contribution to the thermoelectric power Ⓗ due to electrons. From equation (2-3-1) in Chapter II, i.e.

$$Ⓗ = \pm \frac{k}{e} \left[\frac{r+2}{r+1} \frac{F_{r+1}(\mu^*)}{F_r(\mu^*)} - \mu^*\right] \qquad (2\text{-}3\text{-}1)$$

the theoretical dependences of the thermoelectric power Ⓗ on μ^* are calculated for r=0, $\frac{1}{2}$ and 1 and shown in Fig. 7-16 (p.158). If the r value is known, then the experimental thermoelectric power will tell us the corresponding μ^*, and the effective mass can be calculated from equation (2-3-4). The dependence of $F_{\frac{1}{2}}(\mu^*)$ on μ^* is given in Fig. 7-17 (p.159). We now try to find the effective mass ratio from

the thermoelectric power value for sample No. 3. From expression (2-3-4) for m^*/m_o with $n=1.53 \times 10^{16}$/c.c., the effective mass ratio m^*/m_o at 70°K is calculated to be equal to 0.12 which agrees well with the accepted value. The change of m^*/m_o with T from 40°K to 80°K was found to be small ie from 0.1 to 0.126, a change of effective mass of this magnitude is possible. The calculations were repeated for sample No. 1, the effective mass ratio was found to be 0.31 at 70°K and the change of the value from 40°K to 80°K is from 0.17 to 0.35. The change of m^*/m_o is much bigger than that for sample No. 3 and is indeed unreasonably large. This discrepancy may be resolved by considering the effect of phonon drag in the next section.

Now as expected, the data for the low temperature region does not fit the theory given in Chapter II very well. A proper r value could not be found from the Nernst effect. In order to make a rough estimate of m^*/m_o using the existing formula, we took $r=\frac{1}{2}$ and repeated the calculation for sample No. 4 and No. 5. The ratio was found to vary from 0.27 to 2.02 from 5°K to 20°K. This means that even a rough estimation does not lead us anywhere.

7.4 Phonon Drag

Considering the high temperature region, we assume that the measured thermoelectric power Ⓗ and the Nernst field $\mathcal{E}_y$ to be the sum of the electron contribution and a phonon drag contribution. We take as our effective mass ratio the value 0.12, then from equation (2-3-4) and (2-3-1) the thermoelectric power at 84°K for sample No. 1 was

calculated and found to be 410 μV/deg. We regard this part of thermoelectric power as due to the contribution from electrons. Then the difference between this and the measured value 560 μV/deg is the phonon drag contribution Θ_{ph} which is equal to 150 μV/deg. Now the carrier mobility of sample No. 1 is equal to 4650 cm^2/V sec at 84°K according to resistivity and Hall effect measurements, then from equation (7-2-1) we obtained the electron contribution to the transverse Nernst field $\mathcal{E}_y$ with a magnetic field of 3.9 Kgauss which is equal to 10.68×10^{-2}. The experimental value $\mathcal{E}_y$ was found to be 5.069×10^{-2}. The phonon drag contribution to $\mathcal{E}_y$ is therefore equal to -5.612×10^{-2}. Using the phonon drag formula given in Chapter II, we can calculate the phonon drag contribution $(\mathcal{E}_y)_{ph}$. From equation (2-4-2) we have for the absolute value

$$(\mathcal{E}_y)_{ph} = \frac{(E_y)_{ph}}{(k/e)(\partial T/\partial x)} = \frac{((3\pi/8)-1)|\Theta_{ph}|}{k/e} \frac{\mu H}{c}$$

$(\mathcal{E}_y)_{ph}$ was calculated and found to be 5.617×10^{-2} which is in excellent agreement with the above value. Such good agreement may be due to a bit of luck. Nevertheless we can say that the scattering is very probably due to both acoustic scattering and phonon drag in this temperature region.

In the lower temperature region, we cannot easily estimate the phonon drag contribution.

From the measurements of thermoelectric power at temperature, we obtain the following conclusions. Above say 40°K where acoustic

scattering is predominant, the effective mass ratio m^*/m_o is found to change only slightly from 0.1 to 0.126 for temperatures ranging from 40°K to 80°K for samples which show a straight line for a Θ - ln T plot. It is suggested for those samples which do not give a straight line for a Θ - ln T plot phonon drag plays a part in addition to acoustic scattering. Calculation of the phonon drag contribution to the transverse Nernst field $\mathcal{E}_y$ confirms the above suggestion.

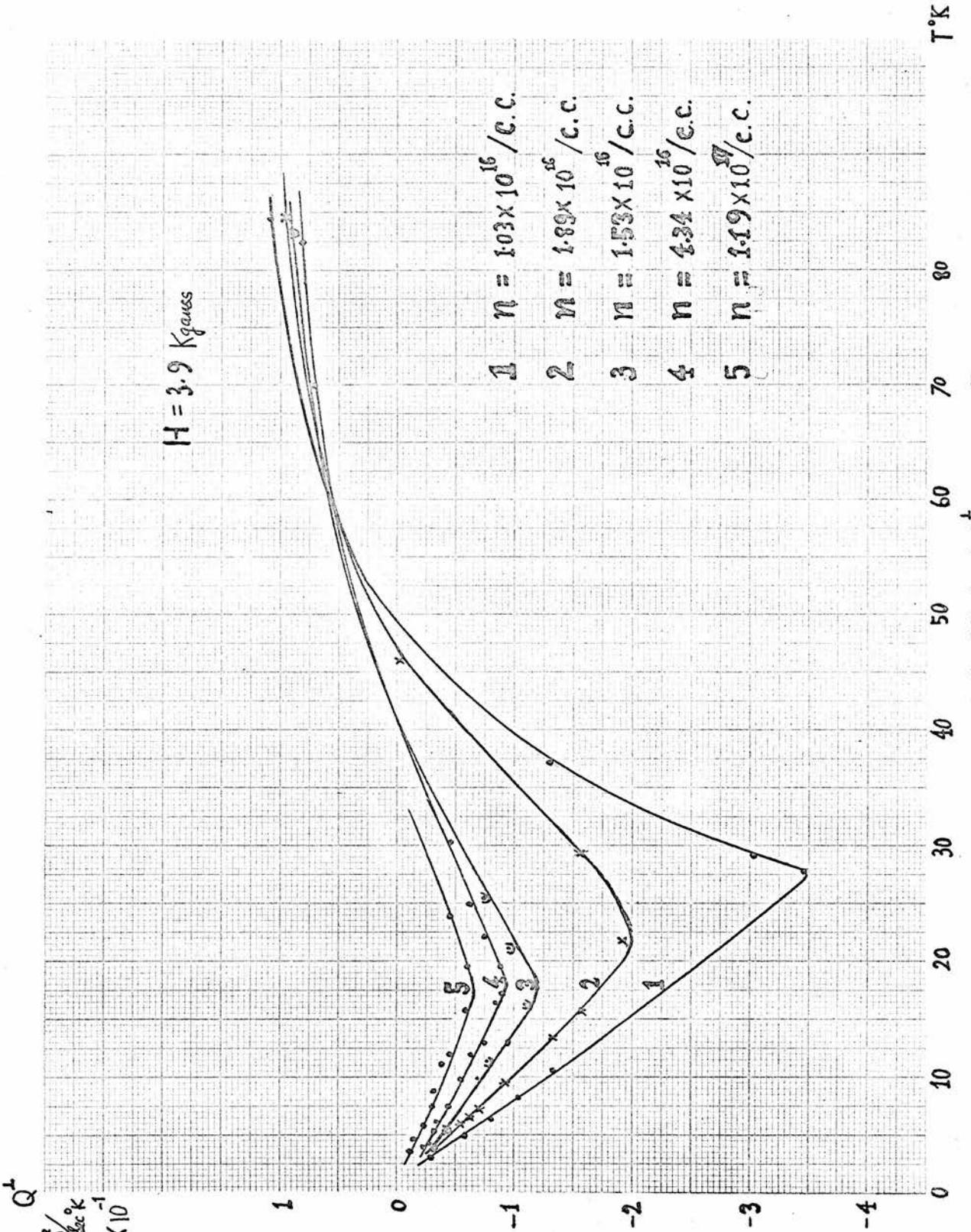

Fig. 7.1 Transverse Nernst Coefficient $Q^{\perp}$ versus T

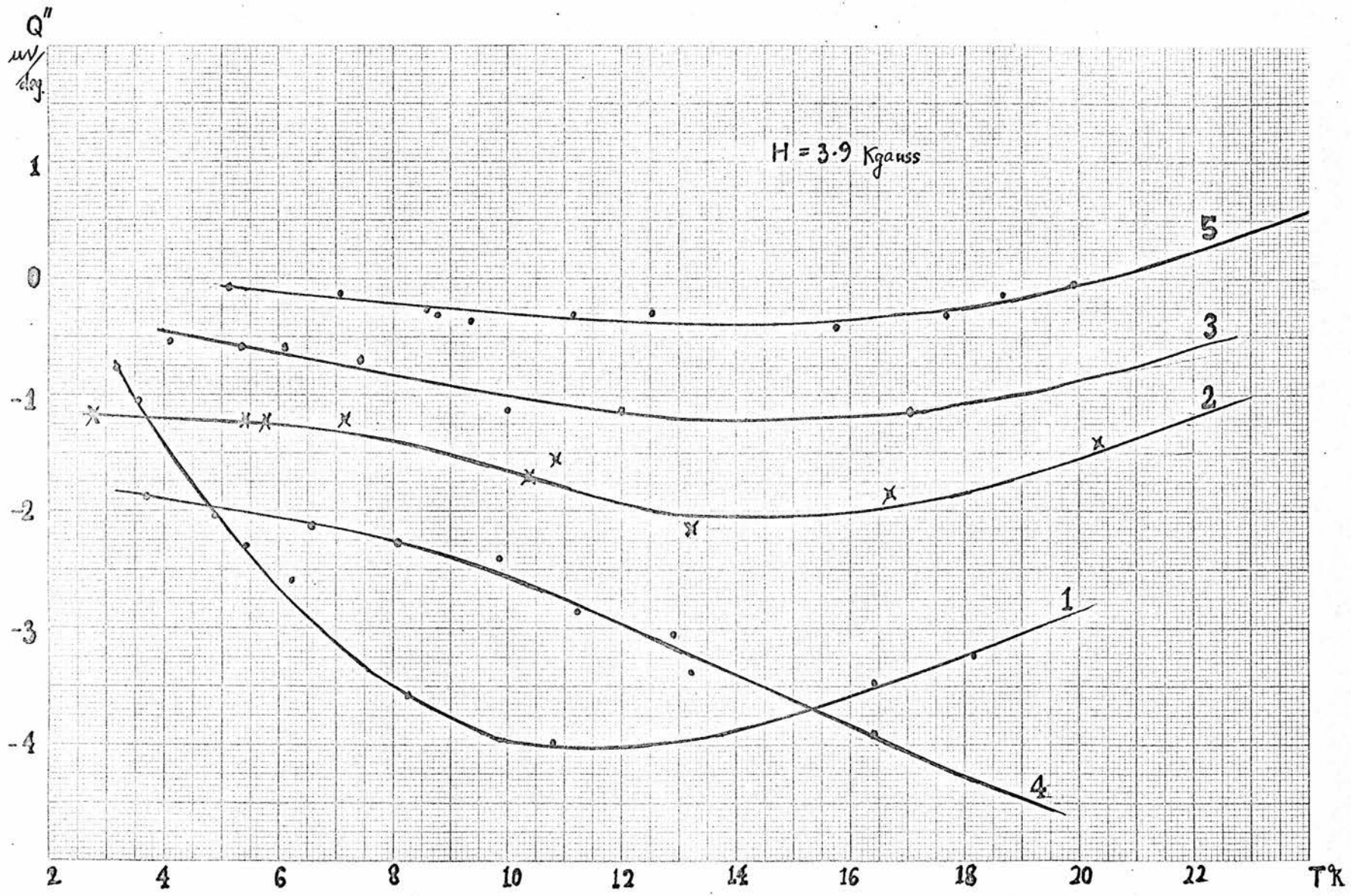

Fig. 7.2 Longitudinal Nernst Coefficient Q'' versus T

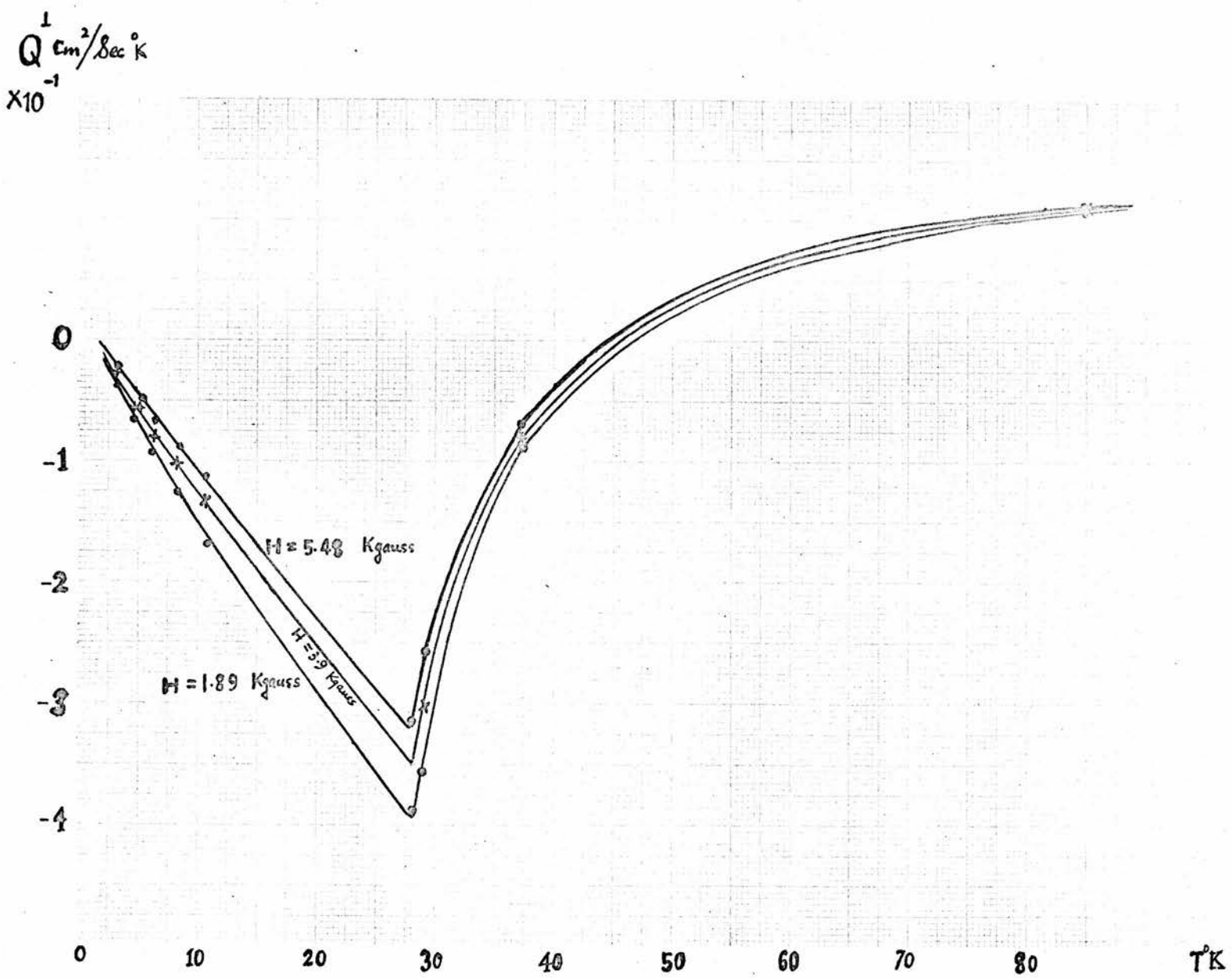

Fig. 7.3 Transverse Nernst Coefficient $Q^{\perp}$ versus T for Sample Number 1

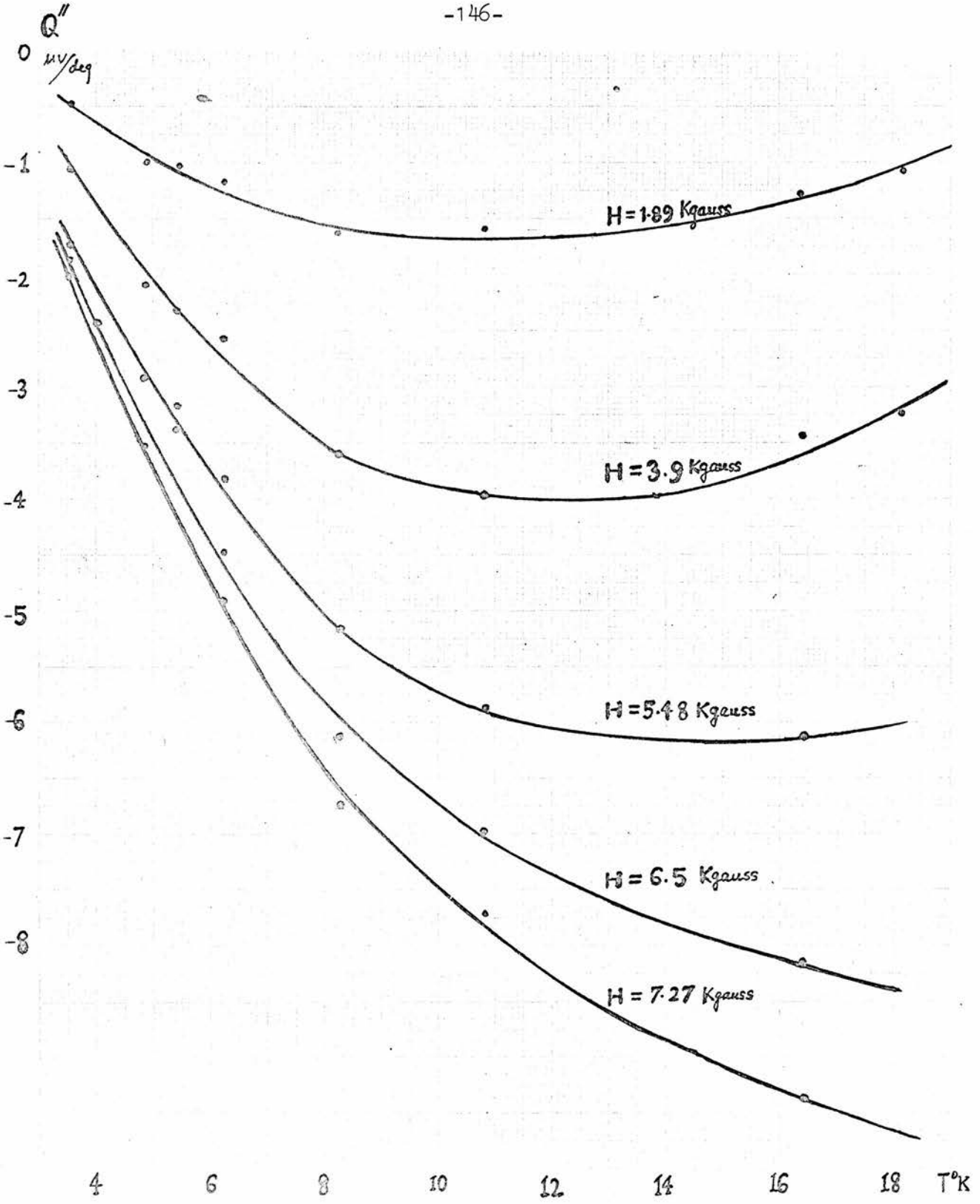

Fig. 7.4 Longitudinal Nernst Coefficient Q'' versus T for Sample Number 1

Fig. 7.5 Transverse Nernst Field versus Magnetic Field for Sample No. 1

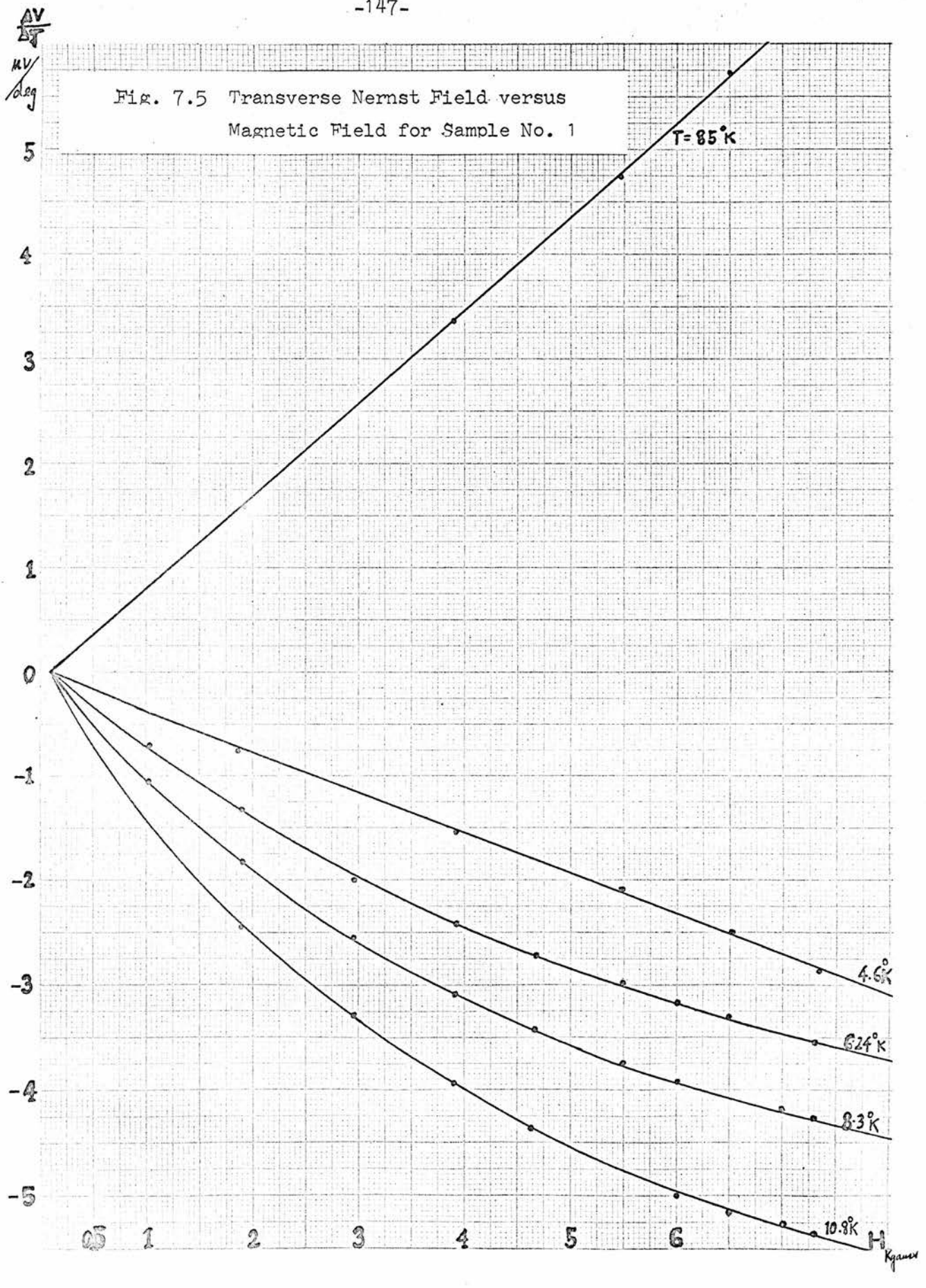

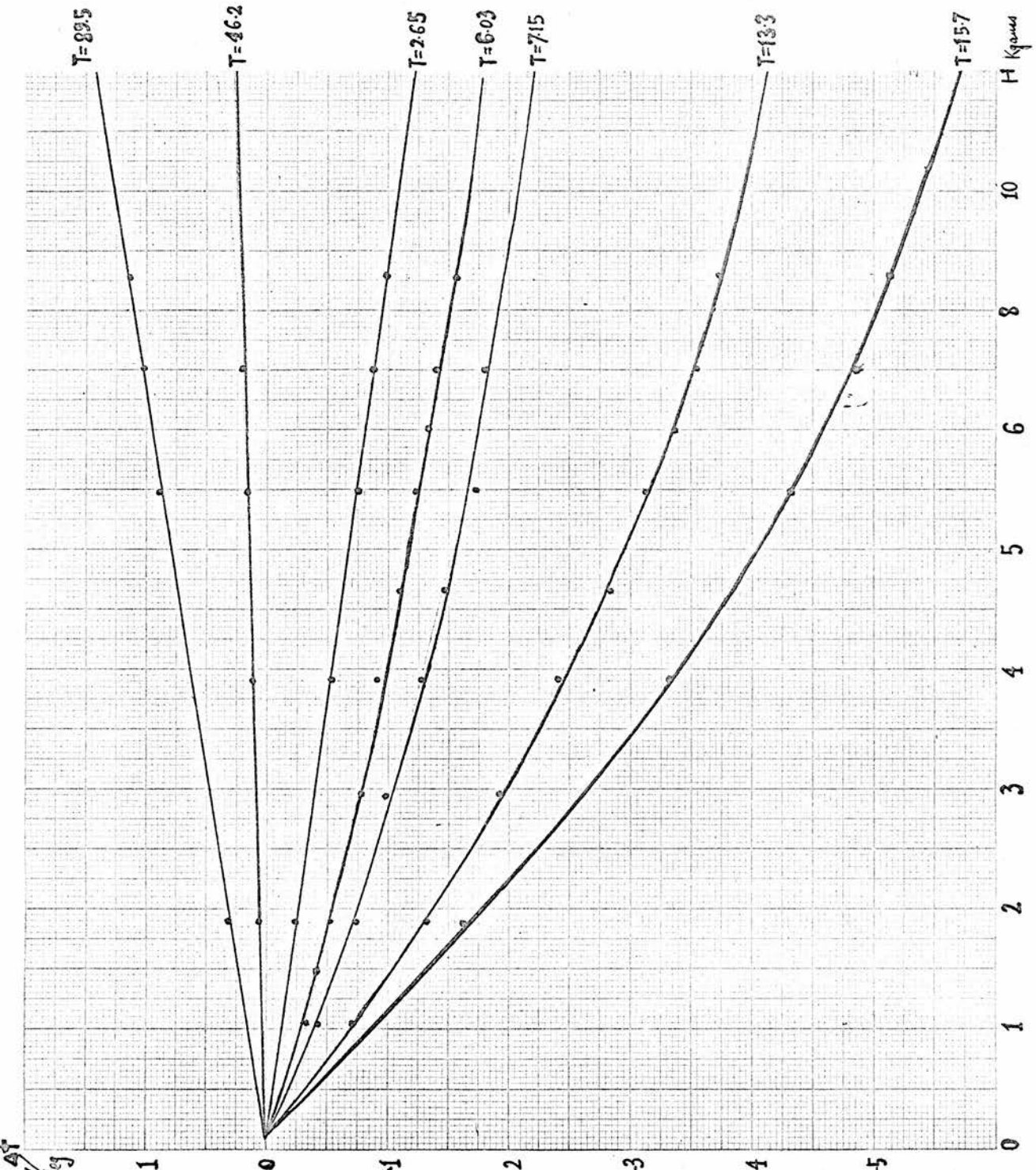

Fig. 7.6 Transverse Nernst Field versus Magnetic Field for Sample Number 2

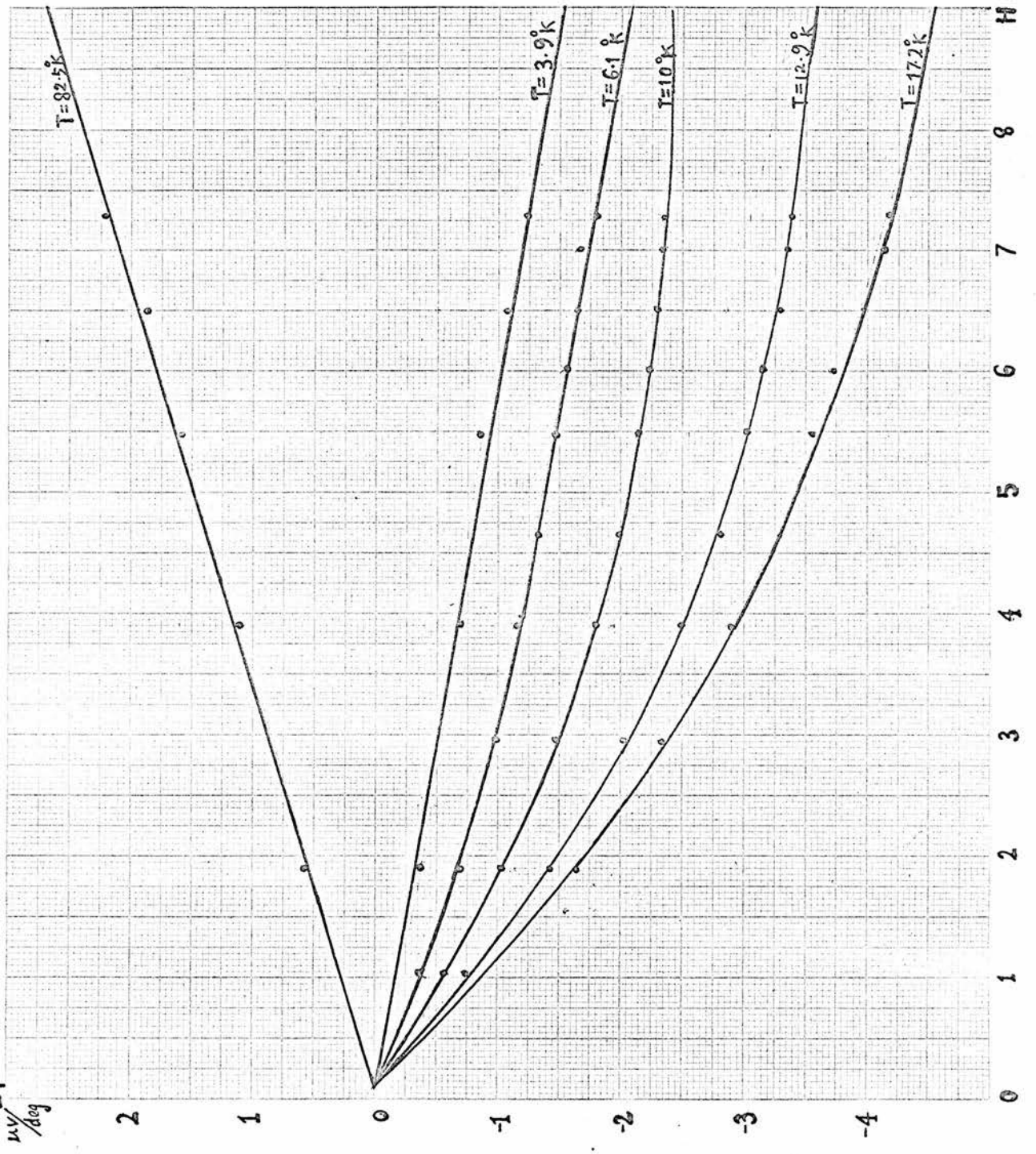

Fig. 7.7 Transverse Nernst Field versus Magnetic Field for Sample Number 3

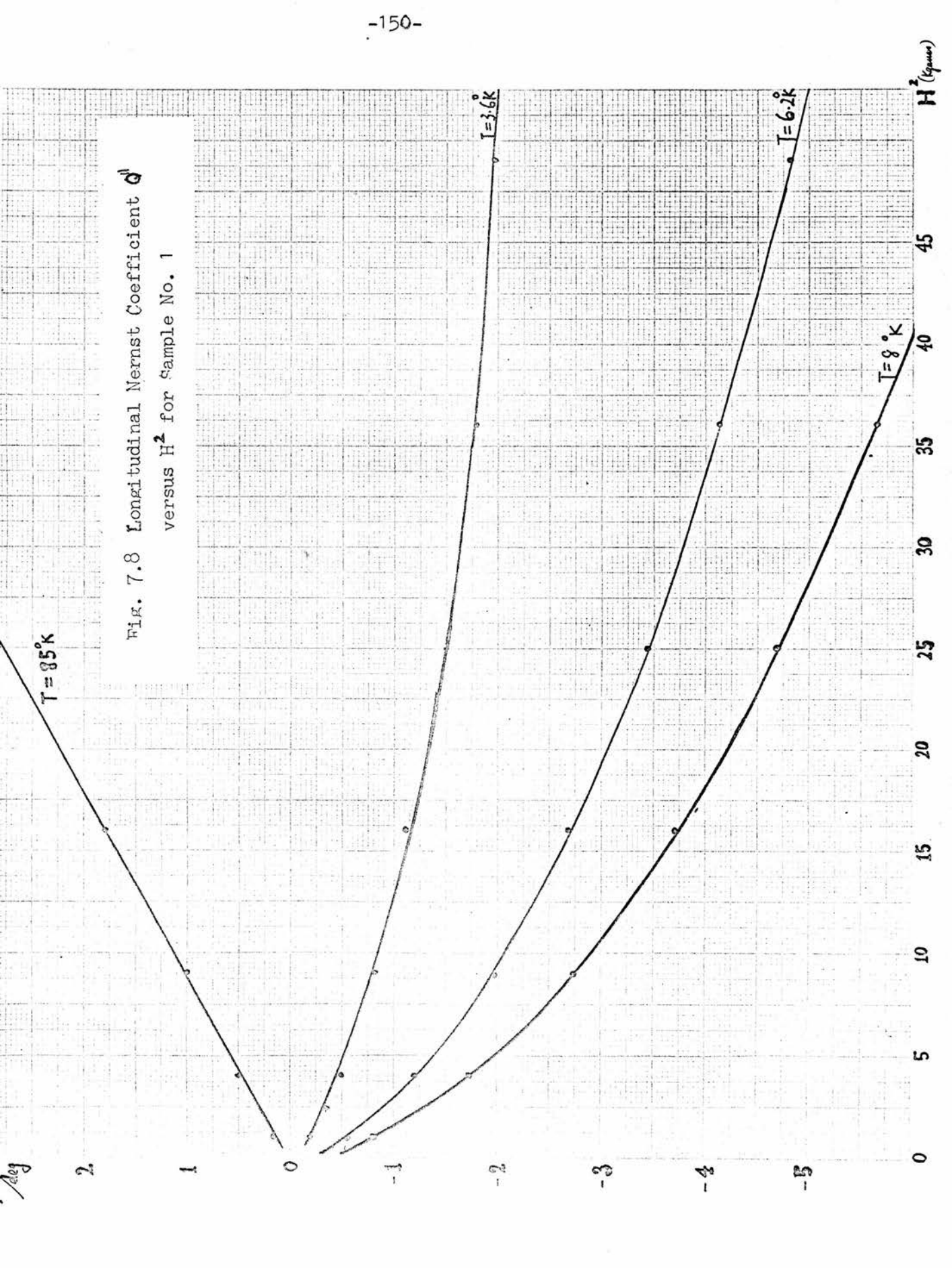

Fig. 7.8 Longitudinal Nernst Coefficient Q' versus H^2 for Sample No. 1

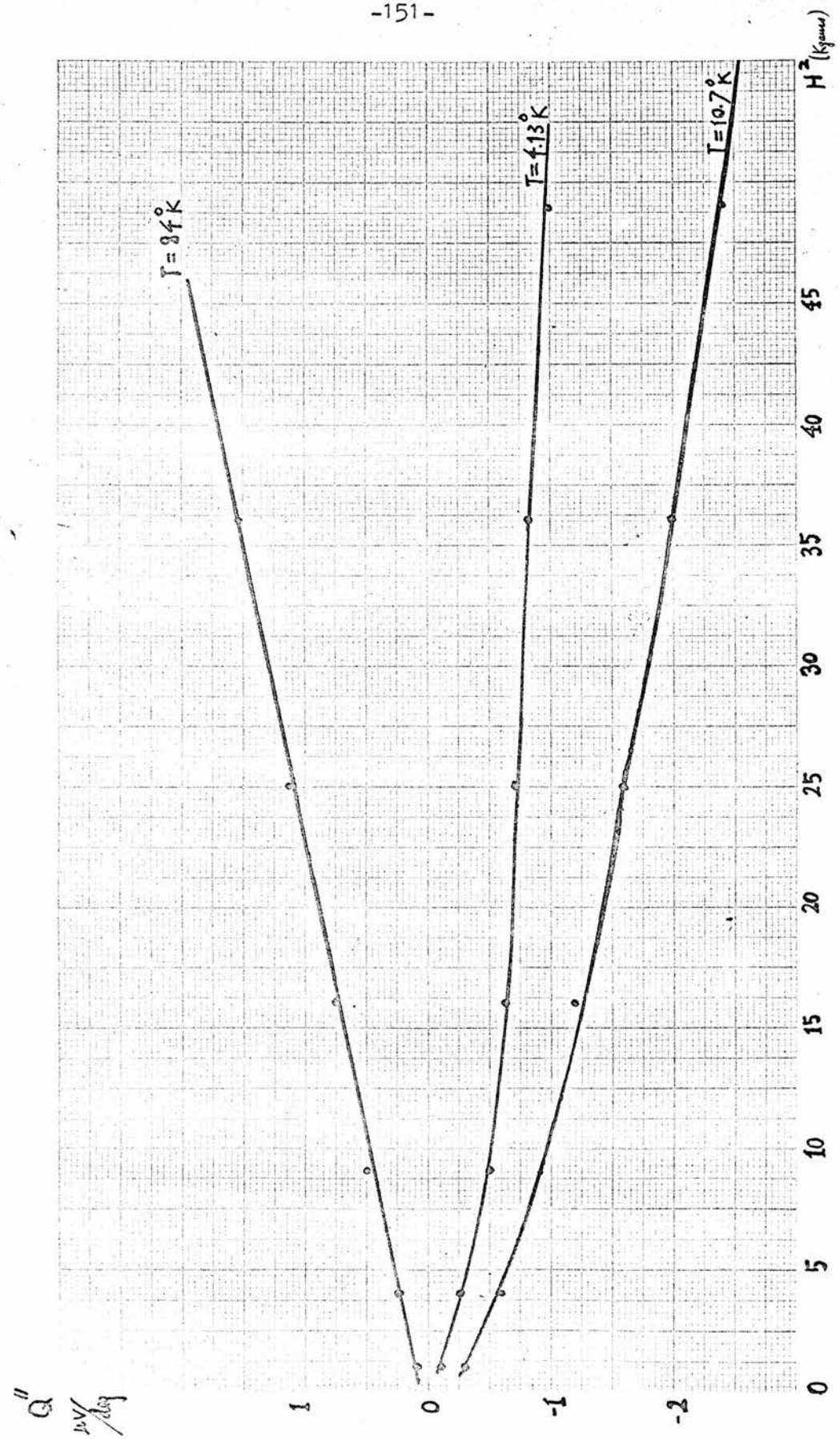

Fig. 7.9 Longitunidal Nernst Coefficient Q'' versus H^2 for Sample No. 3

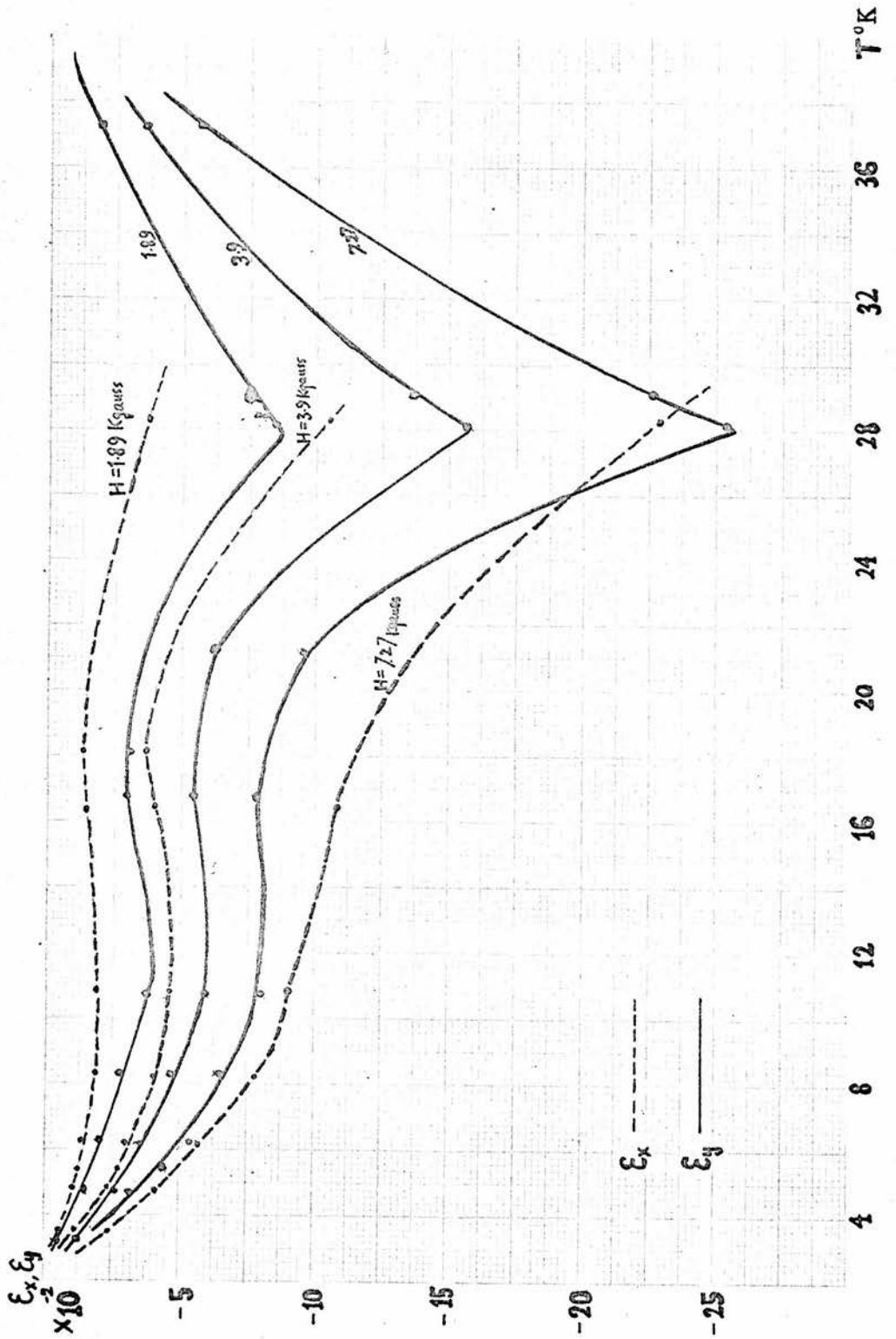

Fig. 7-10 Non-dimensional Nernst Field versus T for Sample No.1

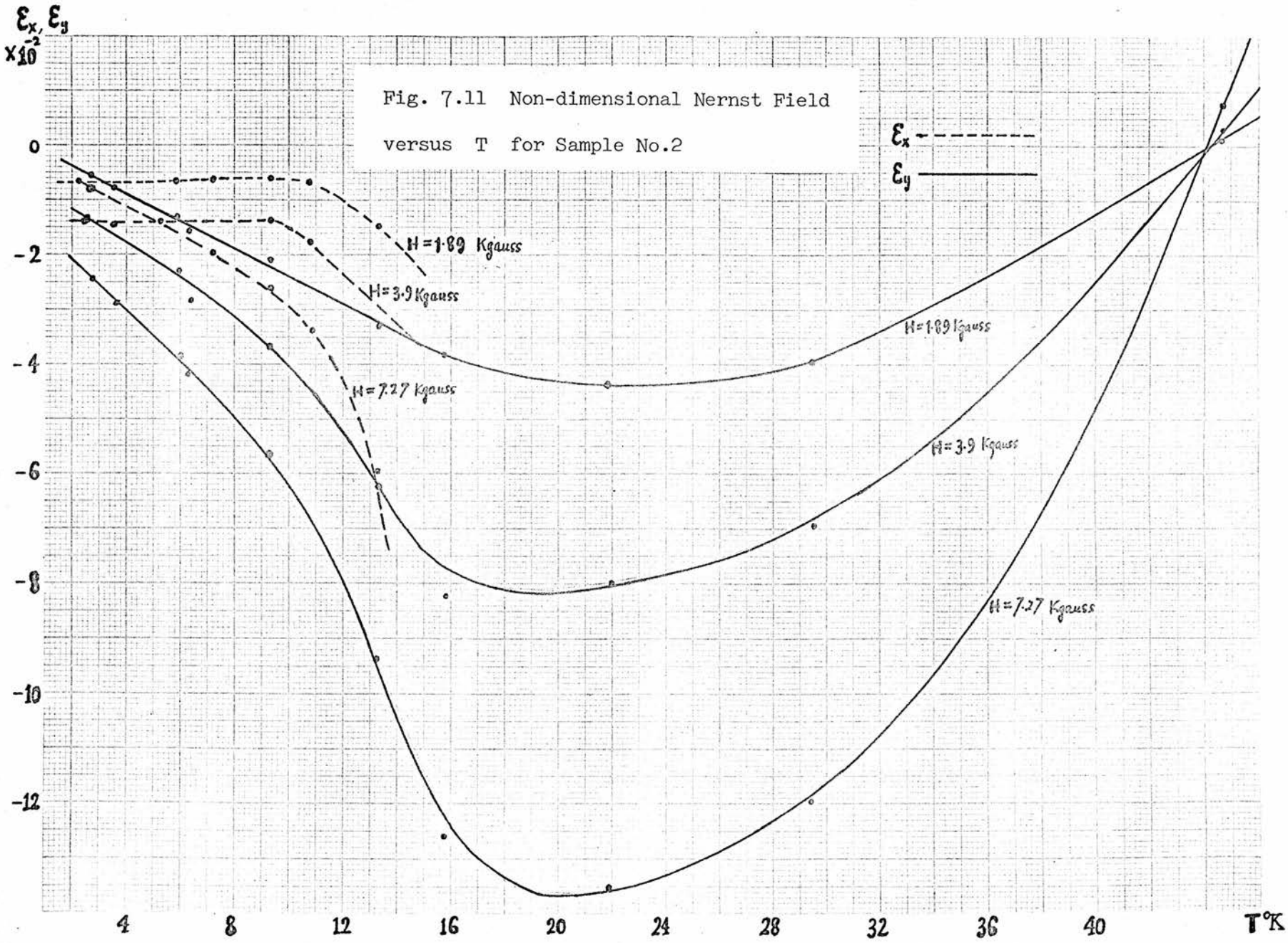

Fig. 7.11 Non-dimensional Nernst Field versus T for Sample No.2

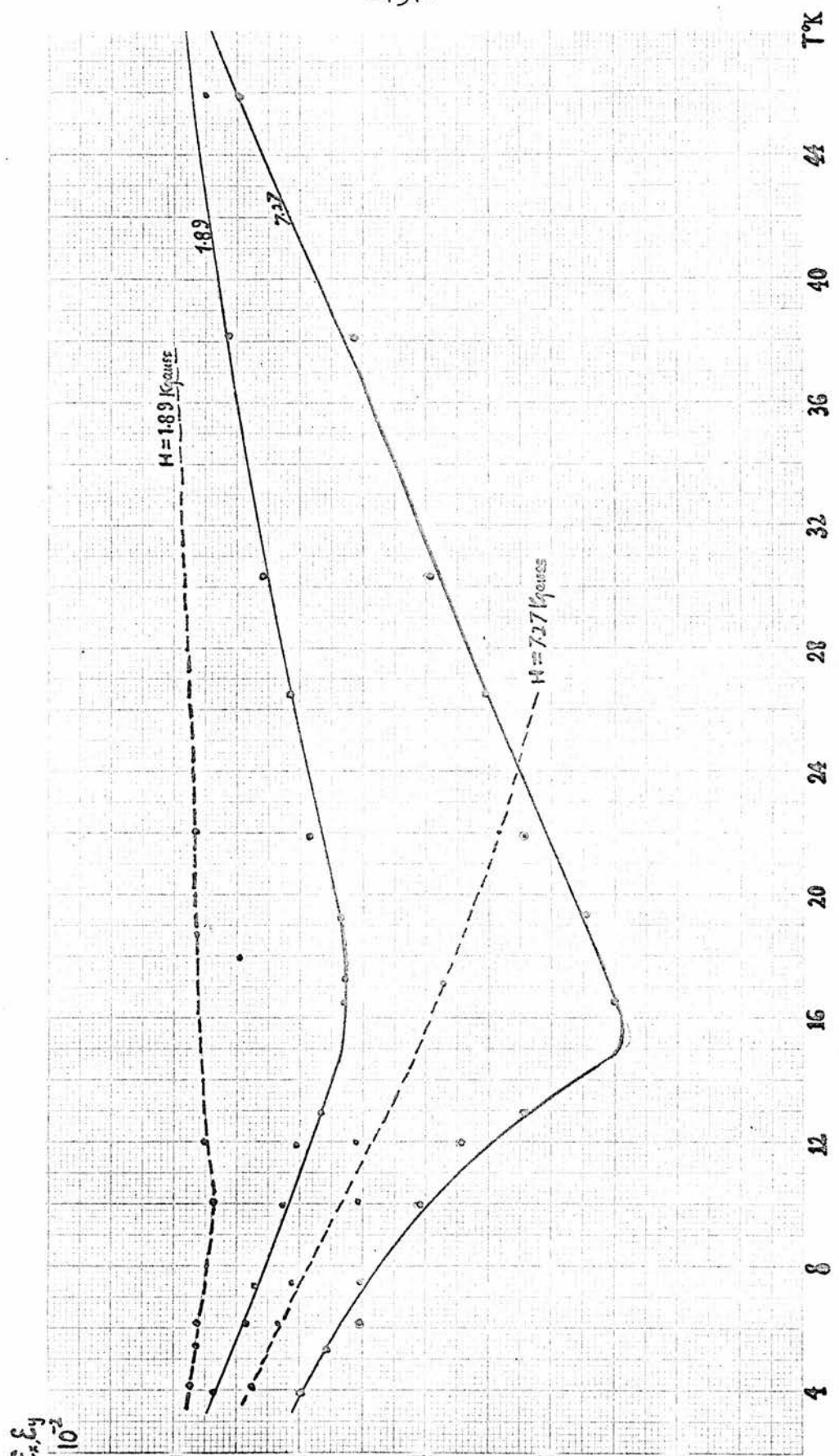

Fig. 7-12 Non-dimensional Nernst Field versus T for Sample No.3

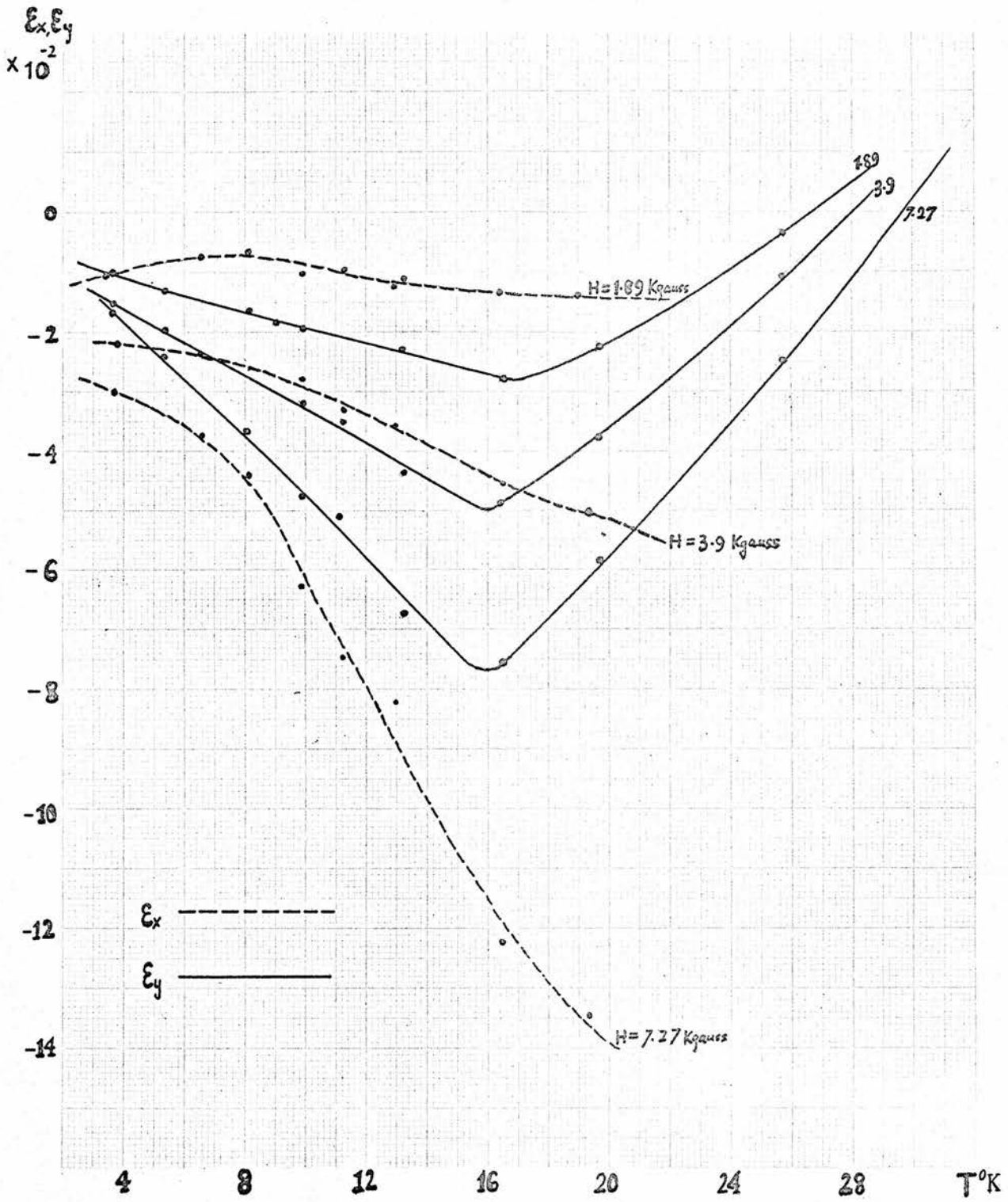

Fig. 7-13 Non-dimensional Nernst Field versus T for Sample No.4

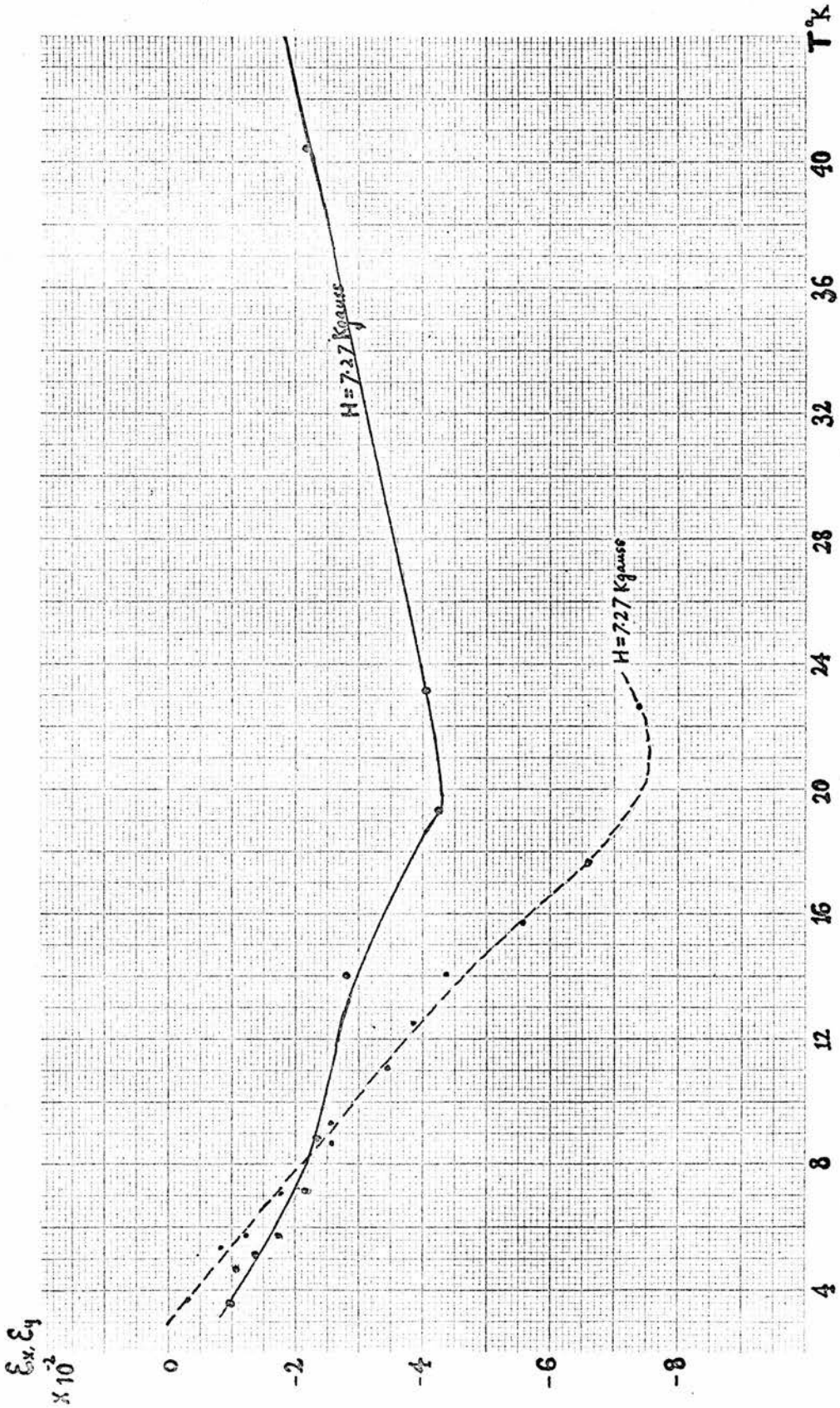

Fig. 7-14 Non-dimensional Nernst Field versus T for Sample No.5

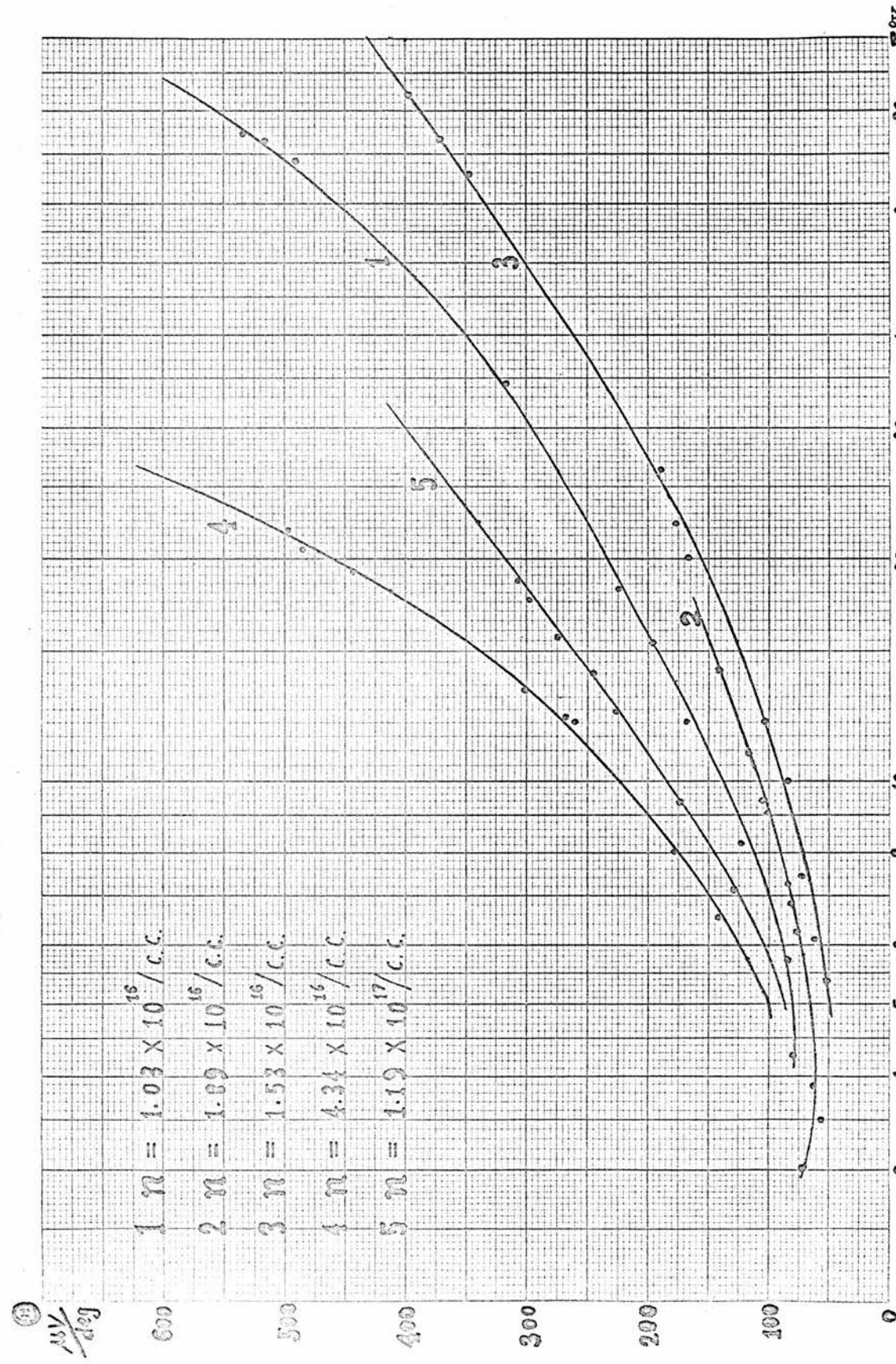

Fig. 7.15 Thermoelectric Power versus T

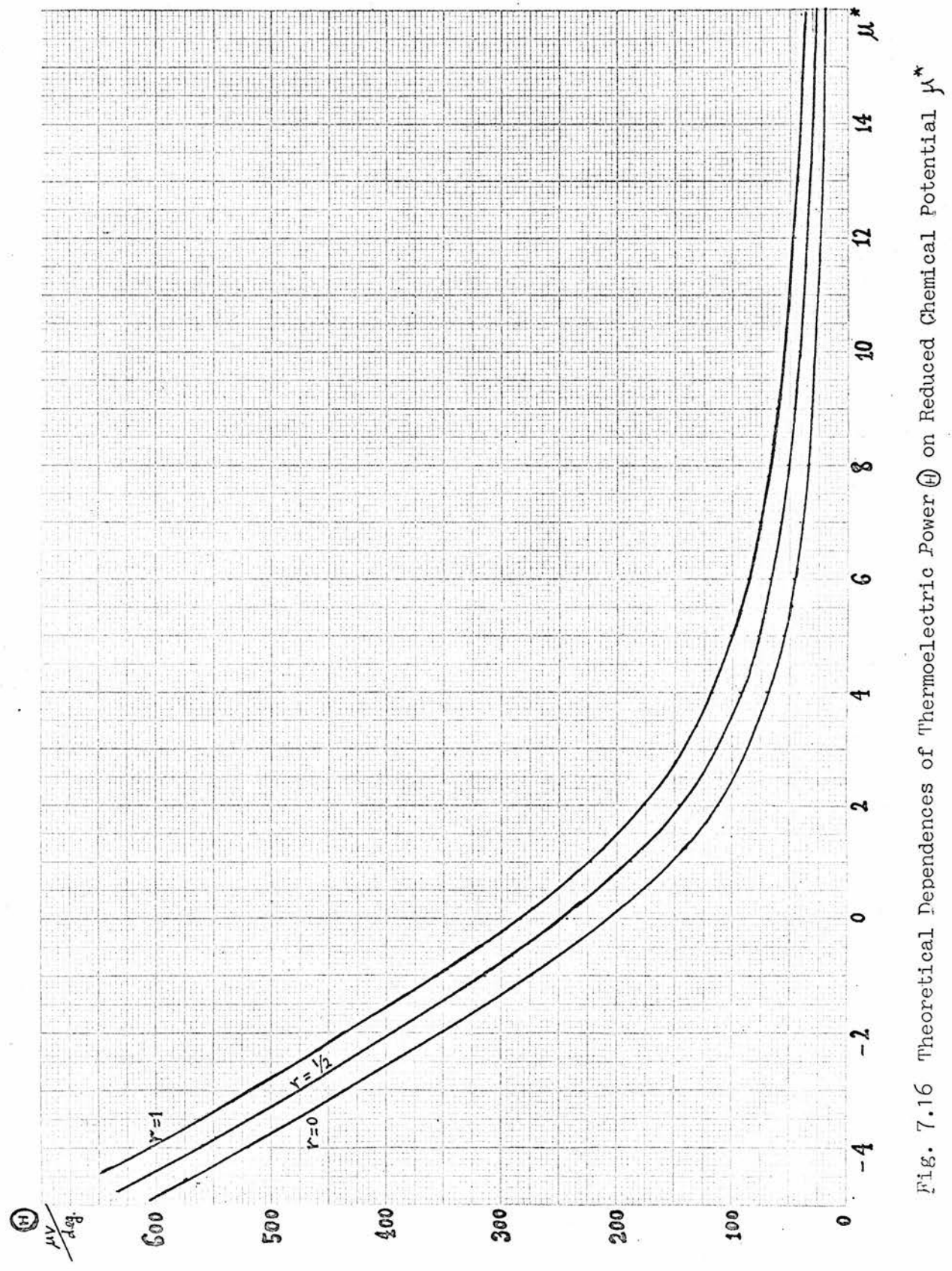

Fig. 7.16 Theoretical Dependences of Thermoelectric Power Θ on Reduced Chemical Potential μ^*

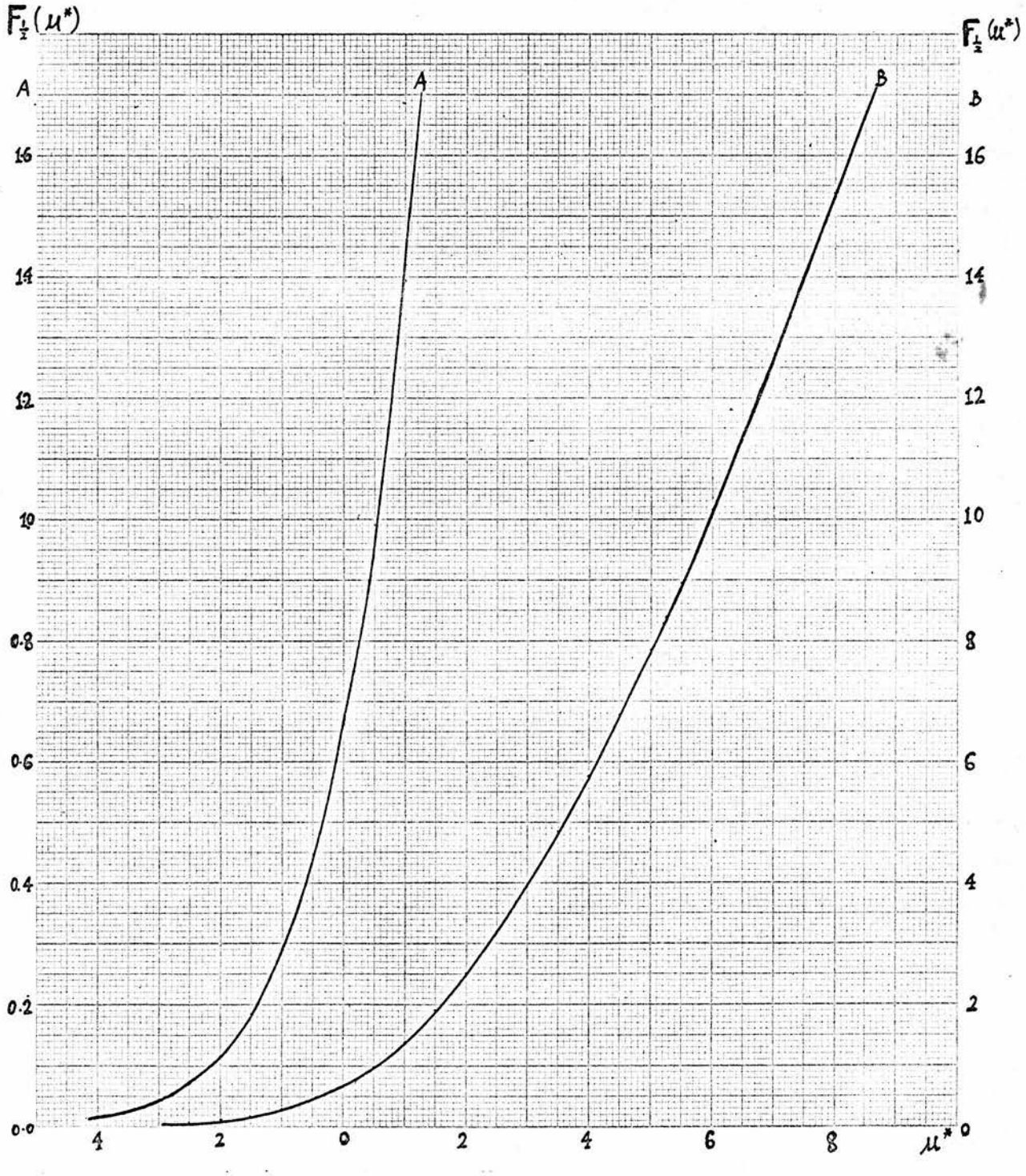

Fig. 7.17 Fermi Integral $F_{\frac{1}{2}}(\mu^*)$ versus μ^*

CHAPTER VIII

Suggestions for Future Research

We have studied the scattering mechanism for PbS from electrical, thermomagnetic and thermoelectric measurements mainly in temperature range between 4°K and 80°K. There is still plenty of room for further investigation. We suggest the following:

1. Measurement should be made of the resistivity at the lowest possible temperature. The H^{3-4} dilution refrigerator in the Department will enable measurements to be done down to 0.05°K. It was found that the slope of the resistivity - lnT plot below 3°K became less, but did not flatten out at the lowest temperature measured. It will be interesting to see whether this finite slope continues to lower temperatures. It provides a possibility of studying the bound state between the conduction electron spin and the localized spin at the Fermi surface suggested by Y. Nagaoka.

2. Some theoretical research is required to derive a rigorous formula based on Kondo's assumption for the spin-spin interaction generally valid for semiconductors.

3. Measurements of the transverse, longitudinal Nernst effects and the thermoelectric power should be extended below 4.2°K and an attempt made to develop a suitable theory.

4. Measurements could be made of the transverse and longitudinal effects with temperature gradient and magnetic field not perpendicular to each other. At the same time one could measure the longitudinal

transverse Nernst effect which is the appearance of an electric field along the z axis when temperature gradient is along x direction and magnetic field lying in the xz plane but not along z direction. (This is similar to the planar Hall effect.)

5. Measurements should be made of the thermal conductivity over a wide range of temperatures so as to observe the behaviour of the Wiedmann-Franz raio.

6. Since a phonon drag contribution has been found, it might be worth while investigating whether the Nernst effect and thermoelectric power is size dependent.

7. Similar measurements on the thermoelectric and thermomagnetic effects at low temperatures for other materials in the PbS group, such as PbSe, PbTe could be made.

8. A theoretical study of the contribution to the thermoelectric and thermomagnetic effects due to spin-spin interaction should be undertaken.

All these, together with the work already done should provide us with a clearer picture of the low temperature behaviour of this group of semiconductors.

REFERENCES

Anderson, P. W. Phys. Rev. (1961) 124, 41.

Anderson, P. W. Comments on Solid State Physics.

Akimova, K. A. Soviet Phys.-Solid State, 2, 459.

Bass, F. G. and Tsidil'kovskii, I. M., (1956) Soviet Phys. JETP, 4, 565.

Bashirov, R. I. and Daibov, A. Z. and Tsidil'kovskii, I. M. (1957)

Bashirov, R. I. and Tsidil'koskii, I. M. (1956) Soviet Phys.-Tech. Phys. p.2129 (Zhur. Tekh. Fiz. (USSR) 26, 2195 (1956)).

Berman, R. and Huntley, D. J. (1963) Cryogenics 3, 70.

Berman, R., Brock, J. C. F. and Huntley, D. J. (1964) Cryogenics 4, 233.

El-Saden, M. R. and Thomas, F. W. (1965) J. App. Phys. 36, 181.

Emel'yanenko, O. V., Kesamanly, F. P. and Nasledov, D. N. Soviet Phys.-Solid State 4, 397.

Emel'yanenko, O. V. and Nasledov, D. N. (1959) Soviet Phys.-Solid State 1, 902.

Emel'yanenko, O. V., Zolova, N. V. and Nasledov, D. N. (1959) Soviet Phys.-Solid State 1, 1711.

Farag, B. S., Smirnov, I. A. and Yousef, Y. L. (1965) Physica 31, 1673.

Finlayson, D. M. and Greig, D. (1956) Proc. Phys. Soc. 69B, 796.

Finlayson, D. M. and Mathewson, A. G. J. (1967) Phys. Chem. Phys. 28, 1501.

Finch, I. Temperature, its measurement and control in science and industry, Vol. 3. part 2, p.3 (Reinhold, New York, 1962).

Gershtein, T. S., Stavitskaia, T. S. and Stil'bans, L. S. Soviet Phys.-Tech. Phys. 2, 2302.

Greig, D. Ph.D. Thesis (1959) Aberdeen, unpublished, Phys.Rev.(1960)120,358.

Gurevich and Obraztsor (1957) Soviet Phys. JEPT 5,302.

Herring, C. Phys. Rev. (1954) 96, No. 5, 1163.

Herring, C., Gaballe, T. H. and Kunzler, J. E. Phys. Rev. (1958) 111, 36.

Johnson, V. A. Progress in Semiconductors Vol. 1 (1956)

Kasuya, T. Prog. Theor. Phys. (1956) 16, 45.

Katayama, Y. and Tanaka, S. Phys. Rev. Letters (1966) 16, 129.

Katayama, Y. and Tanaka, S. Phys. Rev. (1967) 153, 873.

Khosla, R. P. and Sladek, R. J. Phys. Rev. Letters (1965) 15, 521.

Kolomoets, N. V., Stavitskaia, T. S. and Stil'bans, L. S. Soviet Phys.-Tech. Phys. 2, 59.

Kondo, J. (1964) Prog. Theor. Phys. 32, 37.

Kos, J. F. and Lamarcho, J. L. G. (1967) Can. J. Phys. 45, 339.

Mathewson, A. G. Ph.D. Thesis (1967) Aberdeen, unpublished.

Matsubara, T. and Toyozawa, Y. (1961) Prog. Theor. Phys. 26, 1961.

Mochan, I. V. and Smirnova, T. V. (1959) Soviet Phys.-Solid State 1, 1016, (1962) 3, 1936.

Nakamura, A. and Kinoshita, N. (1969) J.Phys.Soc. Japan 27, 382.

Pearson, W. B. Phil. Mag. (1955) 46, 920.

Nagaoka, Y. Phys. Rev. 138, A1112.

Powell, R. L., Caywood, L. P., Jr., and Bunch, M. D. Temperature, its Measurement and Control in Science and Industry, Vol. 3, 65.

Powell, R. L. and Spark, L. L. LT11 (1968) (St. Andrews)

Putley, E. H. Proc. Phys. Soc. (1955) 68B, 22.

Putley, E. H. Materials used in Semiconductor Devices by Hogarth, C. A.

Rosenbaum, R. L. Rev. Sci. Instr. (1968) 39, 890.

Sarachik, M. P. Corenzwit, E. and Longinotti, L. D. Phys. Rev. (1964) 135, A1041.

Sarachik, M. P. Phys. Rev. (1964) 137, A659.

Smirnov, I. A., Moizhes, B. Ya. and Nensberg, E. D. Soviet Phys.-Solid State 2, 1793.

Sparks, L. L., Powell, R. L. and Hall, W. J. Progress on Cryogenic Thermocouples of N.B.S. (1968).

Sparks, L. L., Powell, R. L. and Hall, W. J. Cryogenic Engineering Conference, Ohio, August 1968.

Stavitskaia, T. S. and Stil'bans, L. S. Soviet Phys.-Tech. Phys. 3, 456.

Toyozawa, Y. (1962) J. Phys. Soc. Japan 17, 986.

Tsidil'kovskii, I. M. (1962) Thermomagnetic Effects in Semiconductors (Infosearch Ltd)

Woodhams, F. N. D.; Carlow, J. S. and Meads, R. E. J. Sci. Instrum. (1966) 43, 333.

Wright, R. W. Proc. Phys. Soc. (1951) A64, 984; A64, 350.

Zhuze, V. P. and Tsidil'kovskii, I. M. Soviet Phys.-Tech. Phys. 3, 2177.